The American Mineralogist

Journal of the Mineralogical Society of America

Vol. 33 SEPTEMBER-OCTOBER, 1948 Nos. 9 and 10

Contents

Published bi-monthly by the Society

The enlarged issues of this journal for 1948 are made possible by a grant from the Penrose Fund of the Geological Society of America.

The American Mineralogist—Journal of the Mineralogical Society of America

A journal containing articles on mineralogy, crystallography, petrography, and allied sciences, issued every two months. Contributions are invited from everyone.

Office of Publication, Mineralogical Laboratory, Ann Arbor, Mich.

The general conduct of the journal is in the hands of the Editor, Walter F. Hunt, Ann Arbor, Michigan. The council of the Mineralogical Society has appointed the following board of associate editors, to whom should be sent articles dealing with the special subjects indicated:

Michael Fleischer, U. S. Geological Survey, Washington, D.C., *New minerals.*
Samuel G. Gordon, Academy of Natural Science, Philadelphia, Pa., *Mineral museums.*
Esper S. Larsen, Harvard University, Cambridge, Mass., *Optical crystallography.*
Austin F. Rogers, Stanford University, California, *Geometrical crystallography.*
M. N. Short, University of Arizona, Tucson, Arizona, *Mineralography.*
George Tunell, University of California at Los Angeles, *Structural crystallography.*

Contributors of leading articles are given without charge 100 reprints (without covers) of their article. If additional reprints are desired these can be purchased at the following rates:

Pages	*1–4*	*5–8*	*9–12*	*13–16*	*17–20*	*21–24*	*25–28*	*29–32*	*Covers*
Copies									
25	$3.50	$5.00	$ 8.00	$ 9.50	$11.00	$13.00	$15.00	$16.00	$4.90
50	3.80	5.55	8.80	10.40	12.10	14.20	16.40	17.50	5.50
75	4.10	6.10	9.60	11.30	13.20	15.40	17.80	19.00	6.10
100	4.40	6.65	10.40	12.20	14.30	16.60	19.20	20.50	6.70
Addl. C's	1.20	2.20	3.20	3.60	4.40	4.80	5.60	6.00	2.40

Cover Composition $1.55.

Sent to all members and fellows of the Mineralogical Society of America. Subscription price, $3.00 per year (single copies of normal issues, 75¢ plus postage).

Entered as second class matter at the post office at Menasha Wis., under Act of March 3, 1879. Acceptance for mailing at the special rate of postage provided for in section 1103, Act of Oct. 3, 1917, paragraph 4 section 429 P. L. & R. authorized March 13, 1922.

Notices of change of address, orders, and remittances should be sent to Dr. Earl Ingerson, U.S. Geological Survey, Washington 25, D. C.

Printed by the George Banta Publishing Company, Menasha, Wisconsin

Now in Print!

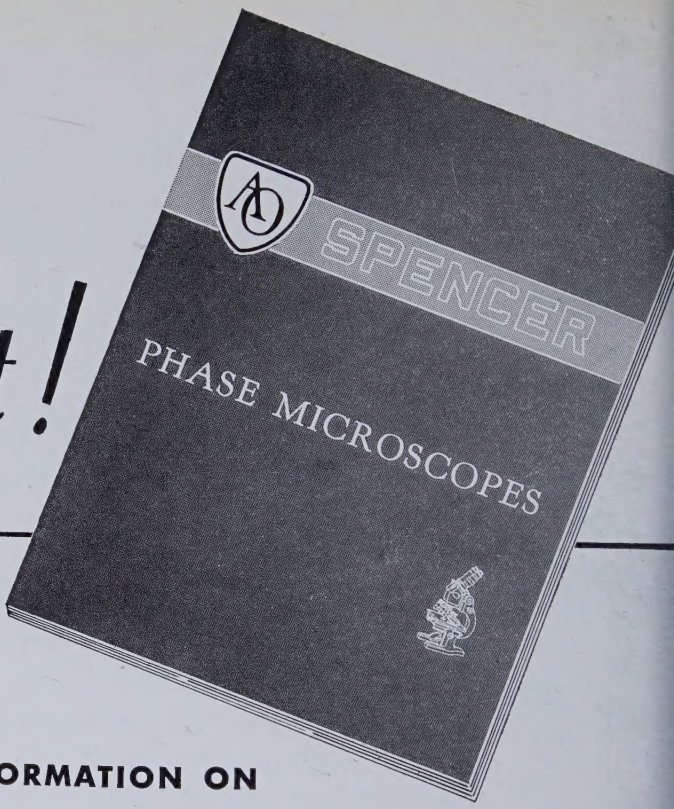

COMPLETE INFORMATION ON

Phase Microscope

EQUIPMENT AND APPLICATION

This new booklet includes:

- ★ A brief history of phase microscopy.
- ★ Schematic diagram of light path.
- ★ Non-mathematical explanation of theory.
- ★ Chart showing 68 tested applications for phase microscopy — and suitable objectives for each application.
- ★ List of Spencer phase objectives in dark, bright and B-minus contrast.
- ★ The two Spencer phase condensers—turret and single unit.
- ★ Spencer phase microscopes and suggested optical outfits.
- ★ Complete bibliography on phase microscopy.
- ★ Numerous photomicrographs and other illustrations.

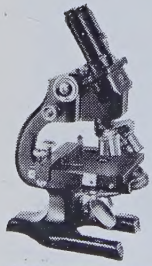

Phase Microscope No. 18 MLS

Much of this information has never been available before. For your free copy write Dept. J7.

Phase Microscope No. 18 MAV

American Optical
COMPANY
Scientific Instrument Division
Buffalo 15, New York

Manufacturers of the **SPENCER** *Scientific Instruments*

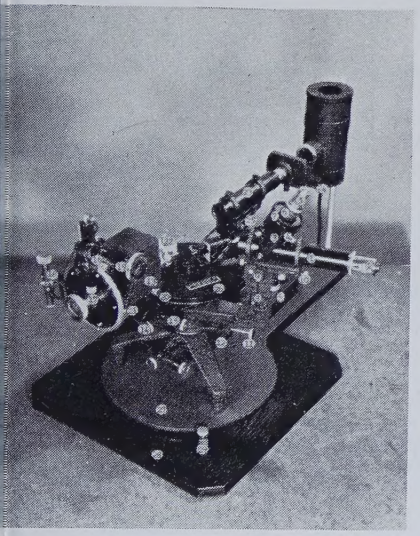

Grieger's

EXCITING *News*

ON SEPTEMBER 15TH WE RELEASED

The New 1948 Edition of our Encyclopedia and Super Catalog of the Lapidary & Jewelry Arts

THIS ENCYCLOPEDIA IS A HANDSOME VOLUME OF NEW AND VALUABLE INFORMATION INCLUDING MUCH THAT HAS NEVER BEFORE APPEARED IN PRINT.

• IT IS AN OUTSTANDING NEW BOOK - NOT A CATALOG • NEITHER TIME, COST OR RESEARCH HAVE BEEN SPARED TO MAINTAIN THE HIGHEST STANDARD OF USEFULNESS AND SCOPE. IT SUGGESTS THINGS TO DO - THE MOST APPROVED METHODS OF DOING THEM AND IS FILLED WITH ILLUSTRATIONS AND INSTRUCTIONS DESIGNED TO FULFILL YOUR EVERY REQUIREMENT.

HERE "IN A GEODE" IS WHAT THE ENCYCLOPEDIA CONTAINS. VERY IMPORTANT CONTRIBUTIONS ON ALL PHASES OF GEM CUTTING PROCEDURES BY SUCH NATIONALLY KNOWN AUTHORS AS - HOWARD - BAXTER - VAN LEUVEN - PEARL AND MERZ. YOU WILL FIND A COMPLETE ARRAY OF IMPORTANT INFORMATIVE BOOKS ON GEM CUTTING AND JEWELRYCRAFT WITH AN EXTENSIVE SECTION ON MINERAL SPECIMENS AND IDENTIFICATION. MATERIALS, TOOLS, SUPPLIES AND ALL THE MAJOR LINES OF LAPIDARY EQUIPMENT INCLUDING SUCH FAMOUS NAMES AS HILLQUIST - HIGHLAND PARK - VRECO - COVINGTON - ALLEN - FELKER - ORCUTT AND POLY PRODUCTS ARE DISPLAYED IN DETAIL.

WE SUPPLY RUF GEM MATERIAL AND PREFORMS
A GREAT CONVENIENCE AND SAVING TO THE GEM WORKER =

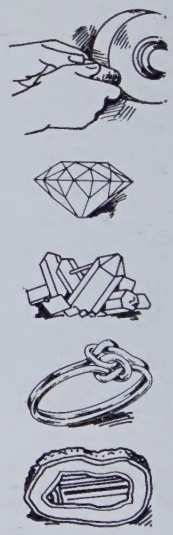

THE ENCYCLOPEDIA AND SUPER CATALOG IS 9"×12" IN SIZE, CONTAINS 160 PAGES AND HAS A SEWED BACK BINDING WITH A PLASTIC LAMINATED COVER. YOU HAVE NEVER BEEN ABLE TO BUY SO MUCH FOR A DOLLAR. OUR FIFTEENTH ANNIVERSARY CATALOG PUBLISHED IN SEPTEMBER 1947, TOGETHER WITH VARIOUS SUPPLEMENTS THAT COMPRISE 80 PAGES 9"×12", IS AVAILABLE FOR 35¢

IN CASE YOU ORDER THE ENCYCLOPEDIA DO NOT ORDER THE 35¢ CATALOG

Grieger's

1633 EAST WALNUT STREET
PASADENA 4, CALIFORNIA.
PHONE SY 6-6423

OPEN ON FRIDAY AND SATURDAY ONLY 8:30AM - 5:30 PM - MONDAY THRU THURSDAY OPEN BY APPOINTMENT ONLY

THE AMERICAN MINERALOGIST
JOURNAL OF THE MINERALOGICAL SOCIETY OF AMERICA

Vol. 33 SEPTEMBER-OCTOBER, 1948 Nos. 9 and 10

INFRARED LIGHT FOR MINERAL DETERMINATION

RENE BAILLY, *Washington University, Saint Louis, Missouri.*

ABSTRACT

Many minerals that are opaque to visible light are transparent to infrared light. By adapting photoelectric cells, sensitive to infrared, to different optical instruments used in mineralogy, it is possible to obtain the refractive indices, birefringence, absorption indices, etc. The variations of the intensity of the infrared light transmitted by the mineral can be converted by the cell into variations in electric current. It is a relatively simple task to interpret these values of the current which are recorded on a sensitive galvanometer.

Until quite recently opaque minerals were identified by various methods such as macroscopic study, chemical analysis, microchemical tests, and a study of the optical characters in reflected light with the microscope (9, 11, 14, 17, 19, 24, 31, 32). About 1930, Orcel, in France, improved the optical methods in reflected light by the use of a photoelectric ocular for measuring the reflecting power of polished sections (3, 24, 25, 26, 27, 28, 29).

In 1935, I showed that many minerals which are opaque in visible light are transparent in thin sections in infrared light (near 9000 Å).

The first investigations were made by means of photography using the polarizing microscope and special plates (Agfa 850). The mineral studied was wolframite. The thickness of the sections was about one tenth of a millimeter. Wolframite is very transparent in infrared light. It was possible with different exposures to obtain extinction angles and other optical properties. Molybdenite was also studied; the interference figure and the optical sign were obtained. However, this rather easy method is time consuming (1, 21).

The investigations are considerably simplified by making use of photoelectric cells sensitive to infrared light (5, 7, 10, 13, 25). A photoelectric cell placed at an appropriate height above the eyepiece of the microscope will, with the use of a sensitive galvanometer, indicate the intensity of light transmitted by the thin section. This may be obtained with ordinary as well as with polarized light. This method may also be applied to studies with a prism refractometer, a total reflection refrac-

tometer, the universal stage, etc. The observations will be qualitative in the determination of extinction angles, pleochroism, refractive indices, birefringence, and optical sign in convergent light, etc. They will be quantitative in the measurement of absorption, reflecting power, etc.

After several experiments, an apparatus suitable for the above mentioned investigations was built in the laboratories of the Institute of Mineralogy, University of Liège, Belgium (1, 2).

Description

The infrared light may be obtained from different sources according to the type of research (Fig. 1). When a high degree of intensity is required, a filament bulb is very useful. I used a 1000 watt bulb with 110

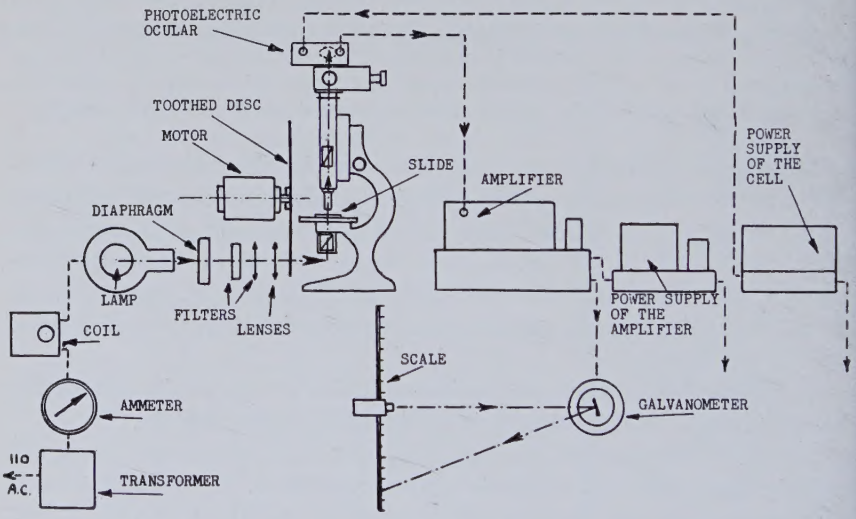

Fig. 1. Diagram of the apparatus.

volts A.C. Preferably the filament should be short and thick, giving a better calorific inertia. This type of filament diminishes the effect of the cyclic variation of current. Also a high degree of regularity may be obtained by the use of a voltage regulator with iron-hydrogen bulbs.

The light is concentrated by a set of lenses and a diaphragm, and is filtered. The filters are from the Jena Glass Works, Zeiss, or Reichert. The maximum intensity is attained near 8500 Å. When a low intensity suffices, a cesium arc lamp is recommended. With appropriate filters this lamp gives lines at 8521, 8761, 8943 Å. The principal line is at 8521 Å.

After passing through the lenses and filters and before entering the

microscope, the light is modulated to a constant frequency by a revolving toothed disc driven by a synchronized electric motor. The frequency of modulation is 166.66 . . . per second. Modulation is necessary if the current of the photocell is amplified.

The microscope used was a large field Leitz. The model with rotating nicols is more desirable because of its ease in centering. The light passes through the microscope and the thin section of the mineral, and enters the photoelectric ocular which replaces the visual eyepiece. The image of the mineral is projected on the anode of the photocell. A sliding prism permits visual examination by a lateral eyepiece (Fig. 2).

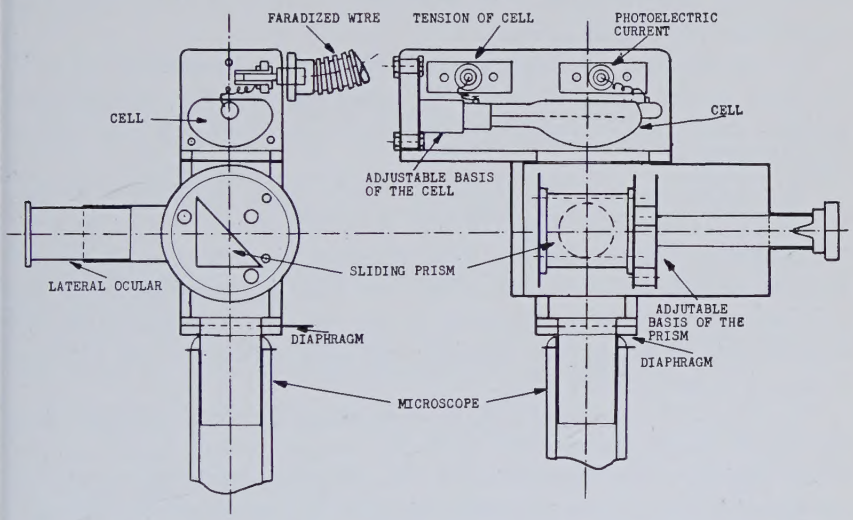

FIG. 2. Photoelectric ocular.

The photoelectric cell is carefully insulated and mounted in vibration-proof metallic box. It is also screened against electric perturbations. The photoelectric tubes (photoemissive model), are of two types: the gas tubes and the high vacuum tubes. The gas tubes are particularly suitable when a very high sensitivity is required, but they are not perfectly stable. The sensitivity of the 3535 Philips is about 160 microamperes per lumen with a cathode polarized at 100 volts; the spectral sensitivity is included between 5000 and 12000 Å with a maximum at about 7500 Å. The high vacuum cells are designed primarily for great stability and high precision. The tube M 122 Cesium special 1 Infram Pressler is sensitive between 5500 and 12000 Å. The power is 50 microamperes per lumen with 20 to 140 volts to the cathode. The variations of voltage on the cathode between these limits have no effects on the stability (5). Other models,

such as the 1P40 and 917 RCA, can be used. It would be particularly interesting to use an electron multiplier tube, because its power is about one ampere per lumen, but up to now only multipliers sensitive in visible light have been made.

The power supply of the cell can be a dry battery. I prefer to use a rectifier, the voltage of which is regulated by a neon tube. A divider gives all voltages between 0 and 360.

The current produced by the anode of the photoelectric cell is driven to the galvanometer, but generally it must be previously amplified. In that case the light must be modulated by the toothed revolving disc because the amplification of an undulatory current is easier than the amplification of a direct current.

The wire between cell and amplifier is well insulated and faradized; it is the same as that used in cameras for sound reproduction, but here experience shows that it is necessary to faradize the wire itself in a flexible metallic tube.

After many tests, a five push-pull triode stage amplifier was constructed (2). It is supplied by 110 volts A.C. The order of the tubes from the beginning to the end is: two 1H5, two 2A6, two 2A6, one 53, two 56 and one rectifier 5Z3. The first stage (two 1H5) is heated by a dry 1.3 volt battery for reducing the noise of the cathode. The others are 2.5 volt cathode tubes. As the amplifier was built during the war it was necessary to use ordinary tubes.

The resistance coupling is used between stages; however the third and the fourth stages are coupled by a low frequency coil tuned on the 166.66 periods of the modulation. So the amplification is increased and the parasitic frequencies are partly eliminated. The output transformer is also tuned to the modulation. The amplifier produces only a voltage amplification, therefore the output power is low.

The amplified current is rectified by a copper oxide Westinghouse unit and transmitted to the galvanometer. The galvanometer used is of the two sensitivities type, Hartman & Braun, with a maximum sensitivity of 0.3 10^{-9} ampere. The amplification factor is adjustable from zero to a maximum by potentiometers.

In addition, a loud speaker or a headphone is driven by a supplementary tube (2A3). It allows the sound of the modulation to be heard and, therefore, a first coarse adjustment can be made before the fine adjustment by means of the galvanometer.

Operations

1. *Microscope* (2). In parallel light, without analyzer and thin section, the amplifier is adjusted to give for example, the mark 1000 on the

scale of the galvanometer. For eliminating the absorption of the glass, a slide is previously put on the stage.

Different thin sections of a mineral, preferably cut in definite orientations, are successively placed on the stage. They will drive the spot of the galvonometer to different points on the scale. These values are proportionate to the values of light intensity.

The equation of absorption is (4,6)

$I = KI_0e^{-4\pi xz/\lambda}$ with K = coefficient of reflected light
I_0 = intensity without thin section
I = intensity with thin section
x = coefficient of absorption
z = thickness of the section
λ = wave length of the light
$e = 2.7182818$

By solving this equation for different values of I and z, it is possible to obtain K and x, and draw the calculated curve of absorption of the mineral. For the smallest thickness, the curve must be corrected because a part of the light is reflected on the lower and the upper faces of the section.

For $z = 0$ on the corrected curve, the intensity I shows the reflecting power R of the mineral.

Using R, measured by reflected light, and x, an approximate value of the refractive index n can be determined by the equation

$$R = \frac{(n-1)^2 + n^2x^2}{(n+1)^2 + n^2x^2}.$$

If the mineral is pleochroic, the measurements will be made in the directions of maximum and minimum absorptions.

On rotation between polarizer and analyzer, an anisotropic mineral will show four extinctions and four maxima of transmitted light. They appear as the minima and maxima on the galvanometer. Extinction angles are referred to a direction of cleavage or elongation seen in visible light. The precision of these determinations is very high.

Using the Fedorov stage, the measurements are exactly the same as with visible light, perhaps a little more complicated, but the determinations are more exact. The maxima and minima of the light intensity are determinated with a fine precision by the photoelectric cell.

In the case of a section perpendicular to the optic axis of a uniaxial mineral, if the refractive index ω is determined, it is easy to obtain the value of the birefringence. If one horizontal axis of the stage is fixed at 45° to the planes of polarization of the nicols, the intensity of light will show successively different maxima and minima according to the retardations $\lambda/2$, λ, $3\lambda/2$, 2λ, . . . , if the stage is inclined to that axis. The

angles β_1, β_2, β_3, . . . , are read on the vertical circle of the stage. Four types of measurements of the angles β can be read: two in the first position of the axis for the opposite inclinations of the stage, and two after a 90° rotation of the axis. The average of four values of the β angles gives sufficient precision (2,22).

If the mica test plate is introduced into the slot of the microscope, the same operation will show an increase of the values of the β angles for a direction of the rotating axis, and a decrease of β for the perpendicular direction. By the orientation of the mica and the differences in the values of β, the optic sign is clearly indicated. Exactly the same reasoning is used in convergent visible light where two black spots are observed after the introduction of the mica plate.

With the values of β, ω, z (thickness), λ, and the optic sign, the equations are

$$\frac{k\lambda}{z\omega} = \sqrt{1 - \frac{\sin^2\beta}{\epsilon^2}} - \sqrt{1 - \frac{\sin^2\beta}{\omega^2}} \quad \text{for a positive sign,}$$

$$\frac{k\lambda}{z\omega} = \sqrt{1 - \frac{\sin^2\beta}{\omega^2}} - \sqrt{1 - \frac{\sin^2\beta}{\epsilon^2}} \quad \text{for a negative sign.}$$

These equations are easily solved and give the value of the birefringence $B=\omega-\epsilon$ or $B=\epsilon-\omega$ (22).

2. *Refractometer.* The indices of opaque minerals are generally too high for the use of the total reflection refractometer. The prism method with a horizontal goniometer is the most useful. The normal incidence method is preferable to the minimum deviation method, because often one face of the prism is cut parallel to one of the principal crystallographic planes of the mineral. The method is the same as in visible light (2, 4, 6, 12) (Fig. 3).

The prism is oriented and its angle measured in white light. When the incident face is perpendicular to the axis of the collimator, the ocular of the telescope is replaced by a photoelectric ocular. In front of the cell, an adjustable slit replaces the cross-hair used in the visual eyepiece. By rotating the ocular around the crystal, the image of the collimator slit will be transmitted across the ocular slit for one position of the circle. If the mineral is birefringent the two refracted beams are identified by means of a rotating nicol in the collimator. In view of the high values of the refractive indices the angle of the prism is generally between 5° and 20°.

The measurements are particularly precise (in many cases, more precise than in visible light) because, when the image of the slit is diffuse, the slit of the photocell determines exactly the position of maximum intensity.

The edge of the prism must be made and polished with care. It is necessary to grind and polish one face of the mineral carefully and to attach that face onto a piece of glass with balsam. Then, the other face is ground and polished through the mineral and the glass. The curvature

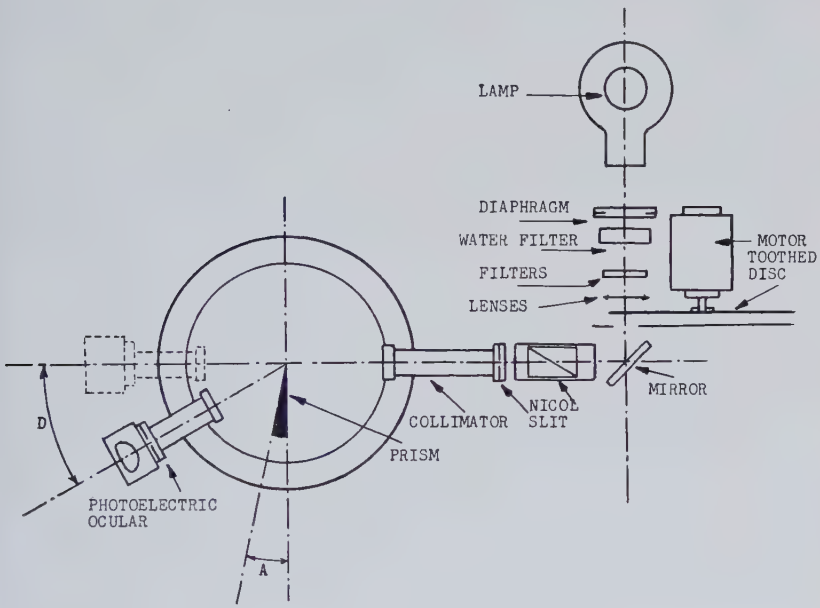

Fig. 3. Diagram of the photoelectric refractometer.

produced by polishing is then on the glass, and the edge of the prism is perfectly sharp and straight (Fig. 4). The prism is detached by solution of the balsam.

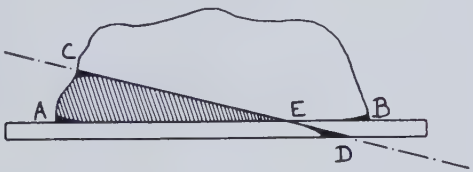

Fig. 4. Cutting of the prisms.

3. *Brewster angle* (6). The determination of the index by measurement of the Brewster angle by means of an horizontal goniometer is relatively precise.

4. *Reflected light.* The procedure of measuring reflecting power is the same as the Orcel method (3, 24, 25, 26, 27, 28, 29, 30).

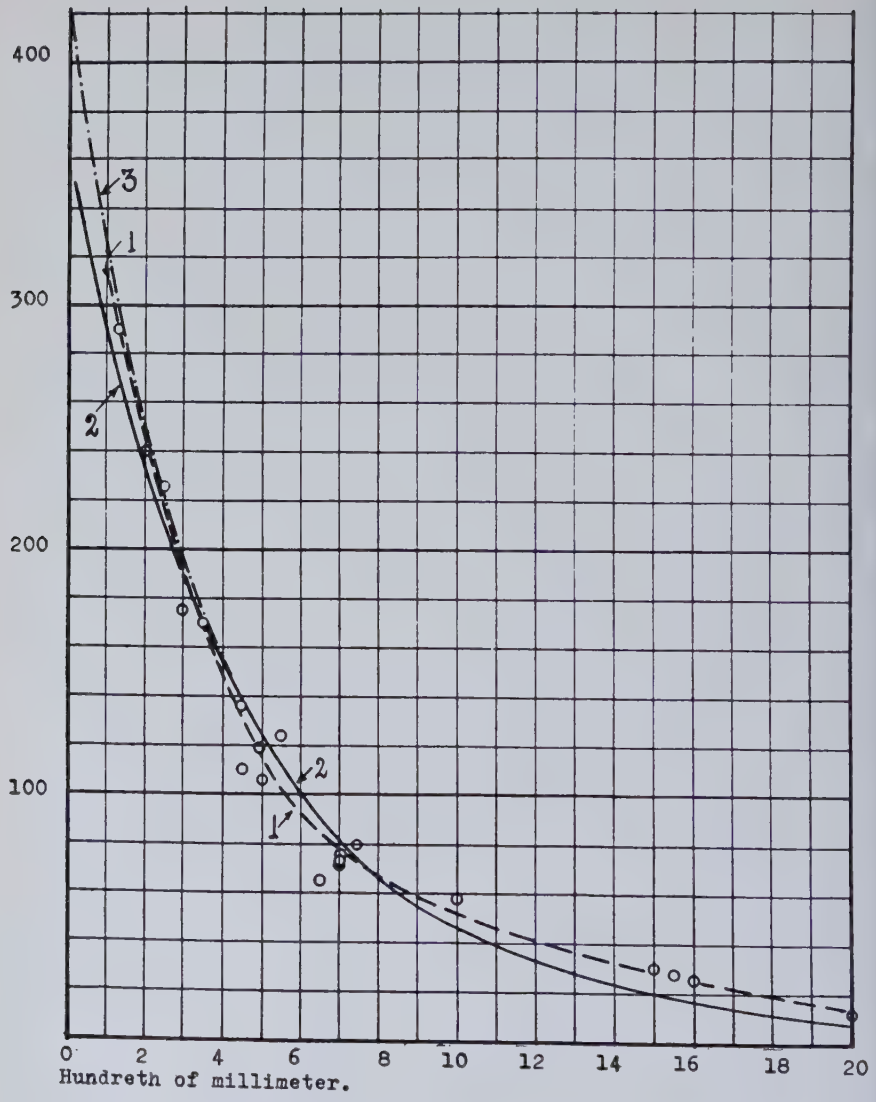

FIG. 5. Absorption of molybdenite. Curve 1, experimental curve. Curve 2, calculated curve. Curve 3, calculated and corrected curve.

Results

Stibnite. Very transparent in infrared light. (8521 Å) (2,15,18).

$\beta = 3.875$ parallel to (001):(100)
$\gamma = 4.137$ parallel to (001):(010)

Reflecting power, measured: $R_\beta = 0.354$
$R_\gamma = 0.374$
calculated: $R'_\beta = 0.348$
$R'_\gamma = 0.369$

Absorption coefficient: $x_\beta = 0.000065$
$x_\gamma = 0.000077$

Molybdenite. Very transparent.

Uniaxial negative (determination made by the use of universal stage and photography) (2, 21, 22).

Optic axis perpendicular to (0001).

Refractive index, $\omega = 4.336 \pm 0.007$
$\epsilon = 2.03$

Birefringence determined on the universal stage: $B = 2.301$

Reflecting power: measured $R_\omega = 0.400$
calculated $R'_\omega = 0.391$
calculated $R'_\epsilon = \pm 0.116$

Absorption: $x_\omega = 0.001489$ (Fig. 5)

Reflecting power calculated by the absorption: $R''_\omega = 0.398$

Hauerite (2). Isotropic. Very transparent.

Refractive index: $n = 2.634$

Tetrahedrite-tennantite (2). Isotropic. Variable transparency.

The refractive index, measured on 33 samples, is nearly constant from tetrahedrite to tennantite. The average is: $n = 3.014$.

The maximum is: $n = 3.128$; the minimum is: $n = 2.914$.

It seems that the index increases slightly with the Sb content.

The transparency decreases with the Fe content.

Bournonite (2). Very transparent. Biaxial, positive.

$\alpha = 3.141$ parallel to (001):(010).
$\beta = 3.166$ parallel to (001):(100).
$\gamma = 3.280$ parallel to (100):(010).
$2V = 52°$. $B = 0.139$.

Stephanite (2). Very transparent. Biaxial, negative.

$\alpha = 3.001$ parallel to (100):(010).
$\beta = 3.053$ parallel to (001):(100).
$\gamma = 3.077$ parallel to (001):(010).
$2V = 67°$. $B = 0.076$

Enargite (2). Transparent. Biaxial, positive.

Strong absorption parallel to (001):(100).
$\alpha = 3.081$ parallel to (001):(010).
$\beta = 3.089$ parallel to (001):(100).
$\gamma = 3.120$ parallel to (100):(010).
$2V = 54°$. $B = 0.039$.

Hematite (2, 18). Transparent. Uniaxial, negative.

1. Samples from Elba Island, Italy.

$\omega = 2.784$.

2. Sample from Saxony, Germany. Fibrous hematite.

$\epsilon = 2.690$ parallel to the fibers.

$\omega = 2.769$ perpendicular to the fibers.

Strong absorption parallel to ω.

Strong dispersion.

This hematite is slightly hydrated and loses 0.35% H_2O at 250° C.

Goethite (2, 8, 18, 23, 30). Transparent in visible and infrared light.

Sample from Restormel Mines, Lanlivery, Cornwall, England.

λ=9000 Å	α=2.170	β=2.277	γ=——	2V
8500	2.185	2.292	2.304	+36°
7000	2.234	2.344	2.356	+26°
6450	2.247	2.371	2.378	+17°
5890	2.275	2.409	2.415	−23°
5420	2.303	2.439	2.447	−25°

The goethite is uniaxial for $\lambda = \pm 6200$ Å (Fig. 6).

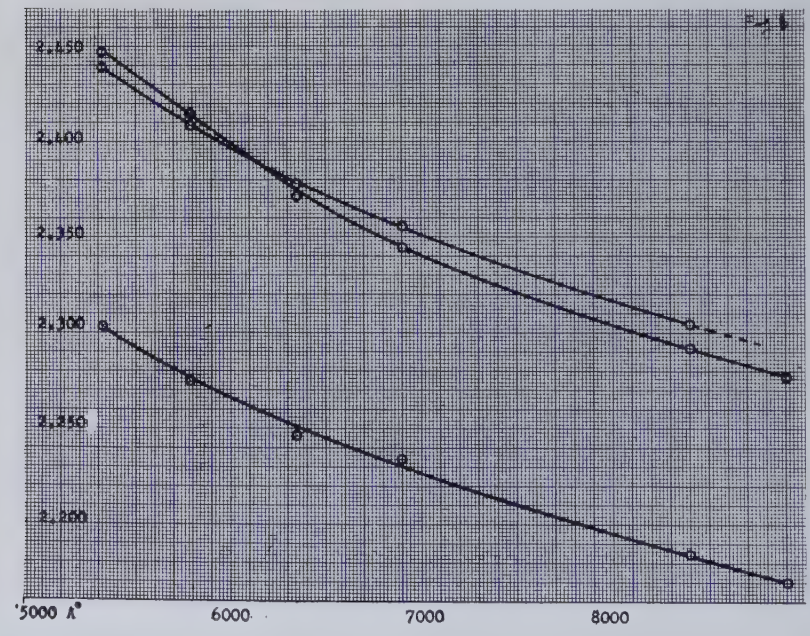

FIG. 6. Dispersion of goethite.

Chromite. Variable transparency. The absorption increases with the Fe to Cr ratio. The isomorphous mixture with magnetite produces the same effect.

The refractive index varies slightly with the Fe to Mg ratio.

Pure chromite, $FeO \cdot Cr_2O_3$, $n = 2.118$.

Picotite, $(Fe, Mg)O \cdot (Al, Cr)_2O_3$, $n = 2.078$.

Picrochromite, $MgO \cdot Cr_2O_3$, $n = 2.054$.

Different values were measured between these limits. The average is: $n = 2.07$.

Wo'framite (2, 14, 18, 32). Variable transparency. The absorption and the indices increase from huebnerite to ferberite.

Biaxial, positive. Axial plane perpendicular to (010).

$2V = \pm 75°$. Strong pleochroism.

Chemical analyses and measurements of refractive indices of 30 samples have permitted the drawing of a diagram showing the variations of the indices with composition. The dispersion of the points around the average curves is probably caused by scheelite $CaWO_4$ and an excess of FeO. The following values could be adopted: (Fig. 7).

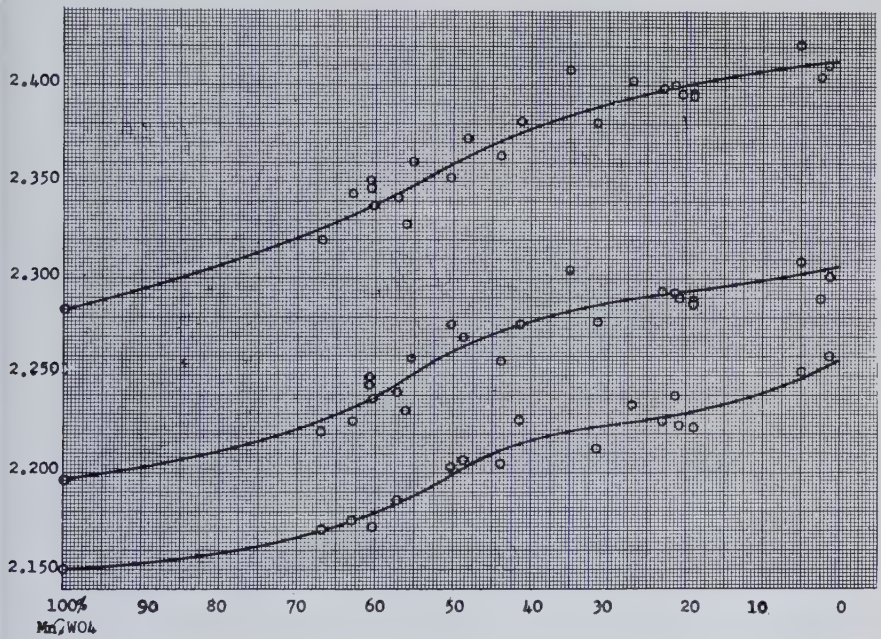

FIG. 7. Variation of the indices of wolframite according to the chemical composition.

Huebnerite	100% $MnWO_4$	$\alpha = 2.150$	$\beta = 2.195$	$\gamma = 2.283$
Wolframite	60% —	2.178	2.238	2.336
	50% —	2.200	2.263	2.360
	30% —	2.224	2.287	2.392
	20% —	2.229	2.291	2.400
Ferberite	0% —	2.255	2.305	2.414

REFERENCES

1. BAILLY, R., Emploi de l'infra-rouge dans l'étude des mineraux: *Bull. Acad. Roy. de Belg., Cl. Sc.*, no. 12 (1938).
2. BAILLY, R., Utilisation des radiations infra-rouges dans les recherches minéralogiques et en particulier pour la détermination des minéraux opaques: *Bull. Soc. Franç. de Miner.* Paris. (in press)
3. BERTHELOT, C., AND ORCEL, J. Les minerais. Paris. Baillères (1930).

4. Bouasse, Propagation de la lumière. Théorie de la réflexion vitreuse et métallique. Paris. Delagrave (1925).
5. Boutry, G. A., Les phénomènes photoélectriques et leurs applications. 1. Phénomènes photoémissifs. 2. Cellules photoémissives. 3. Photoconductivité. 4. Photométrie photoélectrique. 5. Photométrie photoélectrique, mesure des courants. 6. Photométrie photoélectrique, mesure des flux. *Actualités Scientifiques et Industrielles*. Paris. Herman. (1936).
6. Bruhat, Cours d'optique.
7. Case, F. W., Thalofide cell. A new photoelectric substance: *Phys. Rev.*, **E.15,** 239 (1920).
8. Cesaro, G., and Abraham, A., La goethite: *Bull. Acad. Roy. de Belg. Cl. Sc.* no. 2 (1903).
9. Dana, J. D., Descriptive Mineralogy. John Wiley and Sons. London.
10. Deribere, M., Les applications pratiques des rayons infra-rouges. Paris. Dunod (1944).
11. Doelter, C., *Handbuch der Mineralchemie*. Dresden und Leipzig. Theodor Steinkopf (1912–1931).
12. Duparc, L., and Pearce, F., Traité de Technique Minéralogique et Pétrographique. Leipzig. Veit (1907).
13. Freyman, R., Recherches sur le proche infra-rouge. Thèse présentée à la Faculté des Sciences de Paris. Paris. Masson (1933).
14. Hess, F. L., and Schaller, W. T., Colorado ferberite and the wolframite series: *U. S. Geol. Surv., Bull.* **583** (1914).
15. Hutchinson, A., Die optishen Eigenschaften des Antimonit: *Zeit. Kryst.*, **XLIII** (1907).
16. Koenigsberger, J., *Phys. Zeit.*, **4,** 495 (1903).
17. Lacroix, A., *Minéralogie de la France et de ses Colonies*. Paris. Caudry 1893–1895.
18. Larsen, E. S., and Berman, H., The Microscopic Determination of the Nonopaque Minerals: *U. S. Geol. Surv., Bulletin* **848** (1934).
19. Legraye, M., Tables déterminatives des minerais opaques en sections polies: *Rev. Univ. des Mines*. 7th série. no 4. Liège (1925).
20. Lecomte, J., Le spectre infra-rouge: Recueil des conférences-rapports de documentation sur la physique. Paris. Blanchard (1928).
21. Malmquist, D., Mikrophotographische Aufnahmen von Achsenbildern opaker Mineralien im Ultra-Rot: *Zentralb. Mineralogie* . . . Abt. **A** 209 (1935).
22. Melon, J., and Bailly, R., Détermination de la biréfringence d'un uniaxe en lumière convergente: *Mém. Acad. Roy. de Belg., Cl. Sc.* **XI** (1937).
23. Nuffield, E. W., and Peacock, M., Recrossing axial plane dispersion in goethite: *University of Toronto studies., Geol. Ser.*, **47** (1942).
24. Orcel, J., Les méthodes d'examen microscopique des minerais métalliques: *Bull. Soc. Franç. de Miner.*, **48** (1925).
25. Orcel, J., La mesure du pouvoir réflecteur des minéraux opaques à l'aide de la cellule photoélectrique et ses applications: *Livre Jubilaire du Cinquantenaire de la Soc. Franç. de Miner.* (1930).
26. Orcel, J., L'éclat des minéraux et la mesure de leur pouvoir réflecteur: *Archives du Muséum. Vol. du Tricenteraire. 6th serie.* **XII** (1935) Paris.
27. Orcel, J., Sur l'emploi de la pile photoélectiruque pour la mesure du pouvoir réflecteur des minéraux opaques: *C. R. Acad. Sc.*, **CXXXV** (1927) Paris.
28. Orcel, J., Remarques sur la mesure des pouvoirs réflecteurs des minéraux opaques et des minéraux transparents très réfringents: *C. R. Acad. Sc.*, **CLXXXVII**. Paris (1928).

29. Orcel, J., and Fastre, P., Courbes de dispersion de quelques étalons de pouvoir réllecteur utilisables dans l'étude microscopique des minerais métalliques: *C. R. Acad. Sc.*, **CC**. Paris (1935).
30. Peacock, M. A., Recrossing axial plane dispersion in goethite. An error: *Univ. of Toronto Studies, Geol. Ser.* **49** (1945).
31. Schneiderhohn, H., Anleitung zur mikroskopischen Bestimmung und Untersuchung von Erzen und Aufbereitungsprodukten besonders im auffallenden Licht. *Berlin* (1922).
32. Winchell, A. N., *Elements of Optical Mineralogy*. John Wiley and Sons. New York (1927).

THE STRUCTURE OF TOURMALINE

GABRIELLE E. HAMBURGER AND M. J. BUERGER,
Massachusetts Institute of Technology, Cambridge, Mass.

ABSTRACT

The structure of tourmaline is reported in this paper, but without extensive experimental details. The space group of tourmaline is $R3m$, and the cell of the colorless sodium, magnesium crystals from de Kalb has the dimensions $a=15.951$ Å, $c=7.24$ Å. This hexagonal cell has a volume of three primitive rhombohedral cells. The structure analysis shows that this kind of tourmaline has an ideal formula of $NaMg_3B_3Al_6Si_6O_{27}(OH)_4$. One such formula weight is contained in the primative rhombohedral cell, or three in the hexagonal cell whose dimensions are given.

Part of the structure of tourmaline may be described as a fragment of "Mg-kaolin." This part consists of a six-membered ring of silicon tetrahedra, each of which shares one free apex with a corner of a magnesium octahedron. The three magnesium octahedra constitute a small trigonal fragment of a brucite layer. The boron atoms occur in triangular coordination, each triangle sharing a common apex with two magnesium octahedra. This composite unit is knit to others like it by aluminum atoms, and its outer oxygen atoms are also atoms of the aluminum coordination octahedra. The alkali atoms occur sandwiched between the units along the c axis.

The structure not only provides excellent agreement between computed and observed diffraction intensities, but its electrostatic valence structures is very acceptable. The analyses of the tourmalines used, the coordinates of the atoms in the structure, computed and observed intensity comparison, interatomic distances, and the electrostatic bond structure are shown in tables.

INTRODUCTION

Tourmaline is one of the few common silicate crystals whose structure is not known. We have just succeeded in solving this structure, but it will be some time before our detailed account of the structure analysis can appear in print. In view of the unusual mineralogical interest in the results of our study, we thought it important to describe the structure immediately, giving sufficient intensity data to assure the critical reader that the structure is correct.

The cell and true space group of tourmaline were determined by Buerger and Parrish.[1] The space group is $R3m$. The cell edges of the Etta tourmaline on which that study was based, and referred to hexagonal axes are as follows:

$$a=15.96 \text{ Å}$$
$$c=\ 7.16 \text{ Å}$$

(The original cell edges were given in kX units. These have been converted to Ångstrom units in the pair given above.) This hexagonal cell

[1] Buerger, M. J., and Parrish, William, The unit cell and space group of tourmaline (an example of the inspective equi-inclination treatment of trigonal crystals): *Am. Mineral.*, **22**, 1139–1150 (1937).

contains 3 $\left|\begin{matrix}Na\\Ca\end{matrix}\right| B_3 \left|\begin{matrix}Mg\\Al\end{matrix}\right|_9 Si_6O_{27}(OH)_4$. This formula will be explained and corrected in subsequent discussion.

Material

For our structural study, we deliberately chose tourmalines of com-

Table 1. Analyses and Cell Dimensions of Tourmalines used in Structure Investigation

	Colorless, de Kalb, N. Y.*	Black, Andreasberg, Harz**
SiO_2	36.72%	34.01%
TiO_2	.05	.61
B_2O_3	10.81	10.89
Al_2O_3	29.86	28.80
Fe_2O_3	—	4.37
FeO	.22	13.57
MnO	—	.12
MgO	14.92	.42
CaO	3.49	.58
Na_2O	1.26	2.03
K_2O	.05	.20
Li_2O	—	.10
H_2O	2.98	2.92
F	.93	.71
Density	3.06–3.13	3.25
a	15.951 Å	16.01 Å
c	7.24 Å	7.18 Å

* Doelter, number 15, p. 751, Vol. 2, part 2. From: Penfield, S. L., and Foote, H. W., "Ueber die chemische Zusammensetzung des Turmalins": *Zeit. Krist.*, **31,** 332 (1899).

** Doelter, number 71, p. 758, Vol. 2, part 2. Analysis from Dittrich, M., and Noll, F., Inaug.-Diss., Heidelberg (**1913**) p. 22.

paratively simple compositions. One was the white magnesian tourmaline of de Kalb, and the other was the black iron tourmaline from Andreasberg. The analyses of these are quoted in Table 1, together with the cell dimensions of the respective tourmalines obtained by semi-precision methods. The *a* axis of the de Kalb tourmaline was obtained from a back-reflection Weissenberg photograph,[2] while the other data were determined

[2] Buerger, M. J., The precision determination of the linear and angular constants of single crystals: *Zeit. Krist.*, (A) **97,** 433–468 (1937).

with the aid of a special back-reflection, rotating-crystal camera of 10 cm. diameter.

Structure Analysis

Since our method of structure analysis will be discussed in considerable detail elsewhere, we merely outline the main features of our methods here. The locations of the dense cations were determined directly by implication methods.[3] Furthermore, the two tourmalines chosen for the structure study were deliberately selected so that their compositions were substantially identical except that one had three iron atoms where the other had three magnesium atoms. This was done so that the difference diagram[4] could be used to locate the positions of this particular replacement without any reference to the locations of the rest of the atoms.

Table 2. Coordinates of the Atoms in Tourmaline of Composition

$NaMg_3B_3Al_6Si_6O_{27}(OH)_4$
(Hexagonal Coordinates)

Atom	*Equipoint*	*x*	*y*	*z*
Na	3*a*	0	0	.770
Mg	9*b*	.133	.067	.255
B	9*b*	.117	.233	0
Al	18*c*	.050	.367	.825
Si	18*c*	.192	.192	.624
O_1=(OH)	3*a*	0	0	.403
O_2	9*b*	.058	.117	0
O_3=(OH)	9*b*	.233	.117	.032
O_4	9*b*	.142	.071	.624
O_5	9*b*	.102	.204	.742
O_6	18*c*	.200	.200	.403
O_7	18*c*	.279	.246	.758
O_8	18*c*	.058	.292	0

The rest of the structure (consisting chiefly of the locations of the oxygen atoms) was deduced from considerations of the usual coordinations of the metal atoms as well as space requirements, and supplemented by comparisons of observed intensities with those computed from trial oxygen locations. The parameters of the atoms found by these methods are shown in Table 2. That the structure they define is actually the

[3] Buerger, M. J., The interpretation of Harker syntheses: *Jour. Appl. Phys.*, **17**, 579–595 (1946).

[4] Buerger, M. J., A new Fourier series technique for crystal structure determination: *Proc. Nat. Acad. Sci.*, **28**, 281–285, esp. 283 (1942).

correct one for tourmaline is proved by the good agreement between observed and computed intensities, which is shown in Tables 3 and 4.

TABLE 3. COMPARISON OF OBSERVED AND COMPUTED INTENSITIES FOR TOURMALINE STRUCTURE

(F's for $hk \cdot 0$, arranged in order of decreasing observed F.)

$hk \cdot 0$	Observed F	Computed F	$hk \cdot 0$	Observed F	Computed F
5 5·0	139	109	11·5·0	22	20
2 2·0	94	78	9 6·0	20	22
10· 1·0	83	75	15·3·0	20	13
6 6·0	63	68	12·0·0	17	32
9 0·0	57	46	8 5·0	17	24
4 4·0	50	45	10·4·0	17	22
15· 0·0	50	33	8 8·0	17	19
7 4·0	42	50	11·2·0	10	18
3 0·0	41	51	9 9·0	10	10
9 3·0	41	47	7 1·0	10	10
4 1·0	41	39	3 3·0	10	10
10·10·0	41	40	5 2·0	10	8
8 2·0	35	38	11·8·0	10	5
16· 1·0	30	29	6 3·0	0	4
6 0·0	28	34	1 1·0	0	1
			7 7·0	0	1

TABLE 4. COMPARISON OF OBSERVED AND COMPUTED INTENSITIES FOR TOURMALINE STRUCTURE

(F's for $h0 \cdot \bar{l}$ and $0k \cdot \bar{l}$, arranged in order of decreasing observed F. Computed F's not corrected for temperature.)

$hk \cdot \bar{l}$	Observed F	Computed F	$hk \cdot \bar{l}$	Observed F	Computed F
5 0·1	146	136	3 0·3	33	32
0·10·1	116	110	0 1·4	32	35
6 0·3	100	89	2 0·1	32	28
0 0·6	87	81	6 0·0	28	31
0 0·3	76	78	7 0·2	20	26
1 0·2	59	59	2 0·4	20	22
9 0·0	57	47	4 0·2	17	17
0 6·3	50	59	0 7·1	17	17
15· 0·0	50	54	0 4·1	17	17
3 0·0	41	45	0 1·1	10	9
0 0·9	37	34	0 2·2	0	3
0 4·4	36	34	8 0·1	0	3
0 3·3	36	30			

Description of the Structure

In order to give a grasp of the main features of the tourmaline structure, it is presented in diagrammatic fashion in Figs. 1 and 2. In these illustrations the coordination polyhedrons of the silicon, magnesium, and

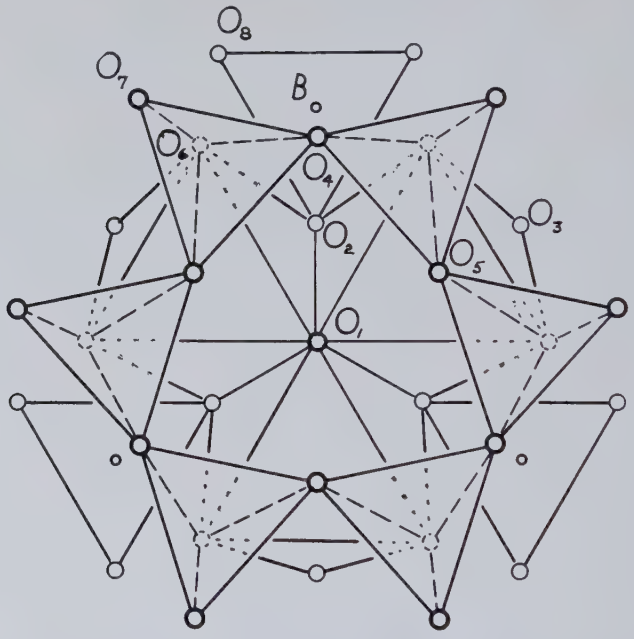

Fig. 1. "Central segment" of composition $Mg_3B_3Si_6O_{27}(OH)_4$, of the tourmaline structure, as seen looking down the c axis. The diagram shows the designations adopted for the oxygen atoms. All small rings represent oxygen locations, except the small ring labeled B, which represents a boron location. The silicon atoms are approximately in the centers of the tetrahedra, while the magnesium atoms are approximately in the centers of the octahedra.

boron atoms are emphasized. The characteristics of these polyhedra are tabulated in Table 6, and are discussed in the next paragraph. Figure 1 shows a central segment of the structure, without aluminum atoms, illustrating in some detail how the polyhedra surrounding silicon, boron, and magnesium are joined. Figure 2 shows how these central segments fit into the tourmaline structure, held together by aluminum atoms. In Fig. 2, only the bonding due to the upper set of aluminum atoms is shown.

The magnesium atoms are surrounded octahedrally by oxygen and (OH) ions, namely $O_1 = (OH)$, O_2, $O_3 = (OH)$, and O_6. The three octahedra immediately surround the 3-fold axis at the origin, and each octahedron

shares an edge with each of its two equivalent neighbors. The shared ions are $O_1 = (OH)$, and O_2. The magnesium atoms and their surrounding oxygen or (OH) ions thus constitute a small trigonal fragment of a brucite layer.

The six silicon atoms are surrounded tetrahedrally in the usual manner

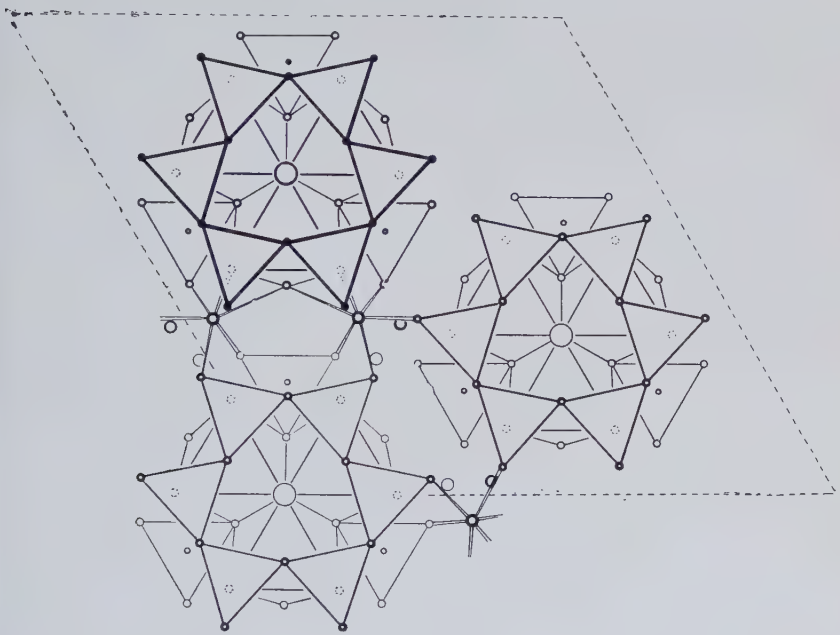

FIG. 2. Part of the tourmaline structure, as seen looking down the *c* axis. The diagram shows how three neighboring columns of "central segments" are held together by aluminum atoms. The bonding of only the uppermost aluminums is indicated. Sodium atoms are represented by the largest circles, and occur in the centers of the "central segments." The hexagonal unit cell is outlined in broken lines.

by four oxygen atoms. Each of the six tetrahedra share two of their points (O_4 and O_5) with neighboring tetrahedra to form a six-membered ring of composition Si_6O_{18}. This Si_6O_{18} ring differs from the beryl ring in not having an equatorial plane of symmetry. Instead, one of the two unshared points (O_7) is substantially in the same plane as the shared oxygens, and the other (O_6) points at right angles to this plane.

This last apical oxygen atom (O_6) is also an oxygen of the brucite fragment. The combined segment of the structure composed of the silicate ring and the brucite fragment comprises three layers of oxygen atoms in approximately cubic close-packed array, and has the formula

$Mg_3(OH)_4Si_6O_{21}$. This central core of the tourmaline structure can also be regarded as a small trigonal fragment of a "Mg-kaolin" sheet. "Mg-kaolin" is also the structure proposed by Aruja[5] for crysotile, and is also similar to part of the structure proposed by Gruner[6] for amesite.

Table 5. Metal-Oxygen Distances in Tourmaline

Metal	Number of Oxygens	Oxygen Designation	Distance
Si	1	O_4	1.55 Å
	1	O_5	1.67
	1	O_6	1.60
	1	O_7	1.60
B	1	O_4	1.58
	2	O_8	1.58
Al	1	O_3	2.23
	1	O_6	2.01
	2	O_7	2.05
	2	O_8	1.85
Mg	1	O_1=(OH)	2.12
	2	O_2	2.10
	1	O_3=(OH)	2.12
	2	O_6	2.12
Na	1	O_1	2.32
	3	O_2	2.32

The aluminum, boron, and sodium atoms, in one manner or another, serve to cement together these "central cores." The three boron atoms are each surrounded by three oxygen atoms (O_2 and O_8) in plane triangular coordination. One corner of the triangle has an oxygen (O_2) shared by two magnesium atoms, while the other two corners (O_8) are oxygen atoms outside the central $Mg_3(OH)_4Si_6O_{21}$ segment, giving a larger complex segment of composition $Mg_3B_3(OH)_4Si_6O_{27}$. The six additional oxygen atoms are part of the cubic close-packed array of oxygen atoms on substantially three levels.

The aluminum atoms are coordinated to six oxygen atoms in somewhat

[5] Aruja, reported in "Summarized proceedings of conference on x-ray analysis—Oxford 1944": *Jour. Sci. Inst.*, **21**, 115–116 (1944).

[6] Gruner, John W., The kaolinite structure of amesite, $(OH)_8(Mg, Fe)_4Al_2(Si_2Al_2)O_{10}$, and additional data on chlorites: *Am. Mineral.*, **29**, 422–430 (1944).

irregular octahedral coordination, which are part of the enlarged boron-bearing unit just described. The aluminum octahedra share edges and spiral down the 3-fold screw axis. The oxygen atoms of the aluminum

TABLE 6. ELECTROSTATIC VALENCE BONDS IN TOURMALINE OF COMPOSITION $NaMg_3B_3Al_6Si_6O_{27}(OH)_4$

Bonds donated by	Bonds received by							
	O_1	O_2	O_3	O_4	O_5	O_6	O_7	O_8
Si				1+1	1+1	1	1	
B		1						1
Al			$\frac{1}{2}+\frac{1}{2}(-)$*			$\frac{1}{2}$	$\frac{1}{2}+\frac{1}{2}$	$\frac{1}{2}+\frac{1}{2}$
Mg	$\frac{1}{3}+\frac{1}{3}+\frac{1}{3}$	$\frac{1}{3}+\frac{1}{3}$	$\frac{1}{3}$			$\frac{1}{3}$		
Na		$\frac{1}{3}$						
Σ bonds received	1	2	$1\frac{1}{3}(-)$*	2	2	$1\frac{5}{6}$	2	2

* This Al-O bond has a length of 2.23 Å, which is greater than normal. Consequently the bond strength to be attributed to it is probably subnormal.

octahedra consist of (*a*) the points of two boron triangles, O_8, (*b*) the points of two silicon tetrahedra, O_7, and two oxygen atoms of the magnesium octahedron, O_3 and O_6. The aluminum and magnesium octahedra, therefore, share the edge O_3O_6.

The sodium atoms occur on the three-fold axis, sandwiched between the central $Mg_3(OH)_4Si_6O_{21}$ segments, which are repeated in translation-equivalent fashion along the *c* axis. The sodium has an immediate coordination of three oxygen atoms and one hydroxyl ion in tetrahedral coordination.

THE COMPOSITION OF TOURMALINE

The description given above of the tourmaline structure has been arranged to bring out the geometry of the structure. In order to consider the composition of tourmaline and its variation, it is desirable to recast the description into another form.

The strengths of the bonds in a tourmaline of composition $NaMg_3B_3Al_6Si_6O_{27}(OH)_4$ decrease in the following order:

	electrostatic bond strength
Si-O, B-O	1
Al-O	$\frac{1}{2}$
Mg-O, (OH)	$\frac{1}{3}$
Na-O, (OH)	$\frac{1}{9}$ or less

The bonds between the first three cations in the list, with oxygen, may be thought of as forming the frame of the structure within which there exist central pockets, which occur along the 3-fold axes. The variability of the composition of tourmaline tends not to occur in this frame. Thus, the number of silicon atoms in tourmaline closely approximates six, the number of borons is almost always exactly three, and the number of aluminums is usually $6+x$. The number x represents the number of additional aluminum atoms which may proxy for magnesium on occasion. If any variability does occur in this frame, it is chiefly in respect to a variability in aluminum. This is to be expected because the aluminum-oxygen bond strength is only $\frac{1}{2}$ as against 1 for Si-O and B-O.

The chief variability in the composition comes from the manner in which the central pocket is filled with weakly bonded cations. Since the electrostatic fields in the pocket are weak, any stray field is more or less inconsequential, and, therefore, the particular cations which enter this part of the structure are not of great importance. However, the sum of them should neutralize the interior of the pocket. Thus, the extreme center may be occupied by sodium (rarely potassium, since it is too large for the small available interstitial space) or calcium, while the three cations in the next zone must have octahedral coordination and compensate for sodium versus calcium. They may be either the monovalent lithium, divalent magnesium or iron, trivalent aluminum, iron, manganese, chromium, etc., in such a collection that the contents of the central pocket remains a self-neutralizing collection.

Finally, we wish to point out that the electrostatic valence rule is satisfied in the structure of tourmaline. This is shown in Table 6.

THE DARK-FIELD COLOR IMMERSION METHOD

Nelson B. Dodge, *Bausch and Lomb Optical Co., Rochester, New York.*

Abstract

With dark-field illumination, color criteria provide an alternative to the usual methods for comparing index of crushed grains with immersion media. Since organic immersion liquids have steeper dispersion curves than inorganic solids, spectrum colors are produced from white light by refraction at interfaces of grains and liquid. With ordinary illumination, when the dispersion curves intersect in the yellow, the oblique illumination test produces colored grain borders as explained by F. E. Wright and others. Dark-field colors appear in bright contrast to a dark background, affect grains everywhere in the microscope field, and require no changing of focus.

Most microscopes can be adapted for dark-field illumination, which requires a hollow cone of light from the condenser, focused on the preparation, having a greater aperture than the objective. The field of view is dark, except where refraction and reflection in the preparation send light to the eye. When solid and liquid indices differ widely, grains appear white against a dark background. When indices differ by a few units in the second decimal place, or less, grains are yellow if higher and blue if lower in index than liquid. At equality of sodium index, $\pm .001$, grains appear purplish blue with a scattering of deep red borders.

The colors can be explained as a result of the Christiansen effect. They are due to the subtraction of the lost transmitted wavelengths from white light.

Introduction

The dark-field color immersion method may be used for obtaining refractive indices of crushed minerals. The essential feature of this method is the employment of low-grade dark-field illumination with white light to produce colors indicative of relative sodium index of grains and immersion liquid. Many possibilities and difficulties remain to be explored, but it is evident that in many cases this method may be used with advantage to supplement the standard procedures in current use, namely the Becke line—central illumination method and the oblique illumination method (2, 4).

In both of these standard methods, when used with white light, colors are seen, due to the Christiansen effect, when the refractive indices of mineral grains and surrounding immersion liquid are near equality. Most familiar is probably the appearance of blue and orange-red on opposite sides of grains in the oblique illumination method. Less used but often seen are the differences in color between borders and interiors with central illumination. These phenomena have been known since the 1870's, when both the current methods were discovered. F. E. Wright in 1911 summarized earlier work and evaluated the methods based on color from white light due to relative dispersion, finding that an accuracy of better than $\pm .002$ is not to be expected of them (5). A serious disadvantage of

such methods is that colors appear over a comparatively short range of index difference between solid and liquid.

This appearance of color in normally colorless mineral fragments results from the difference in dispersion of minerals and the liquids used for immersion media. In the great majority of cases, organic immersion liquids have steeper dispersion curves than inorganic solids lying in the same general index range. Differential refraction of light crossing liquid-solid interfaces at other than right angles produces spectral colors. The range of index difference over which colors appear varies with the amount by which the dispersion of the liquid exceeds that of the solid material. These same fundamental causes are believed to underlie the colors observed in dark-field illumination. In dark-field, however, the colors are much more brilliant, and are useful as criteria over a greater range of index difference between liquid and solid.

The use of dark-field colors to determine refractive index was suggested by Mr. G. C. Crossmon of the Bausch and Lomb Chemical Laboratory (1).

Dark-field Illumination

Dark-field conditions may be produced by placing an opaque central

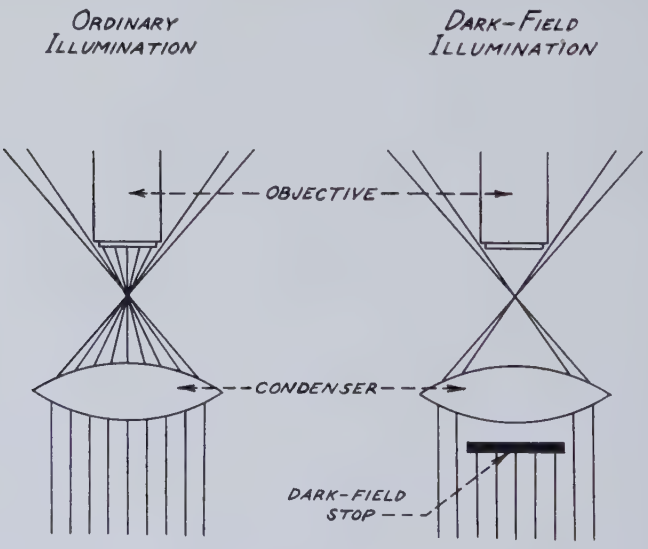

Fig. 1

stop below the substage condenser. This results in a hollow cone of light which is focused on the object slide. Biological microscopes are usually

designed to permit dark-field work. Petrographic microscopes ordinarily require some adaptation, as explained in a later section. The essential condition is that the inside angle of the cone of light must slightly exceed the angular aperture of the objective. With nothing on the stage, all light is lost, and the field of view is dark (Fig. 1).

When a preparation of grains in an immersion liquid is placed on the stage, the grains reflect and refract light into the aperture of the objective. This causes the grains to appear luminous against a dark background. If solid and liquid are far apart in index the grains appear white. When the sodium indices of solid and liquid differ by a few units in the second decimal place, or less, the grains appear colored.

Color Phenomena in Dark-field

With reference to crushed grains in immersion fluids, Fig. 2, top row, shows dispersion curves for solid and liquid. Three cases are shown:

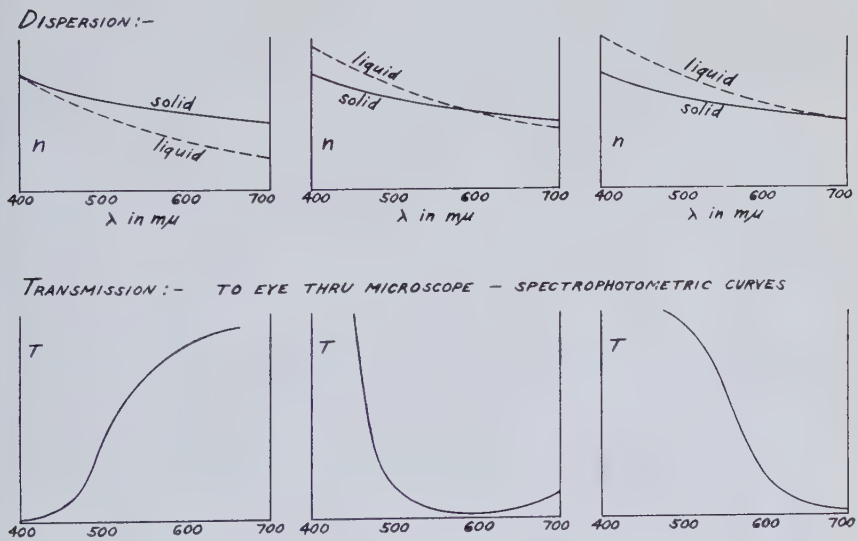

Fig. 2

On the left, solid is greater than liquid in index of refraction for sodium light (589.3 mμ); in the middle they are equal; and on the right the liquid is greater in n_D. The corresponding transmission curves (Fig. 2, bottom row) were determined by spectrophotometric measurement of the colored light transmitted through the microscope, using crushed glass in three different liquids. The transmission scale is relative and differs from one

figure to another. These spectrophotometric curves were determined by Mr. W. G. Kirchgessner of this Laboratory, assisted by the writer.

With intersection of the dispersion curves at the violet end of the visible spectrum, the mineral will appear yellow against a dark background. The yellow color is at first faint, mixed with much white; with increasing index of the liquid the color intensifies. The origin of the yellow color is as follows: Where the dispersion curves intersect, liquid and solid are equal in index; light of that wave-length is not deviated by the grains, so it passes straight through the preparation, misses the objective, and is lost. On either side of this wave-length, where the dispersion curves are close together, light is not deviated enough to enter the objective. Toward the red end, the separation of curves is greater, and light of these longer wave-lengths is refracted enough to reach the eye through the objective (Fig. 2, top, left). Thus, in terms of the transmission curve (Fig. 2, bottom, left), a band of some width with center at the intersection is subtracted from the original white light. This results in a transmission to the eye which would register as yellow.

If the liquid index is raised further, the intersection of dispersion curves moves to the right, and with it goes the band of subtracted wave-lengths. The result of this changing subtraction is that first some violet comes in along with the yellow; the yellow changes gradually to orange and then red; while the violet becomes more bluish and relatively more intense. Red and blue-violet are seen about equally when the liquid is a few points in the third decimal place below the solid in n_D, when using the more common immersion fluids.

Figure 2, middle, top and bottom, shows the situation when grains and liquid are equal in index for sodium light. Grains will now appear mostly blue, or bluish violet, with scattered touches of red here and there. Many grains will show no red.

At the right of Fig. 2 the dispersion curves intersect in the red. The transmission curve indicates a sensation of blue. Blue is the only color shown when solid n_D is less than liquid n_D.

Some of the color criteria are illustrated on the accompanying color plate, from Kodachrome.

The color sequence as described holds good for various mixtures of such organic liquids as Government oil, butyl carbitol, α-chlornaphthalene (or Halowax oil), α-bromnaphthalene, and methylene iodide. If cinnamic aldehyde, having an unusually high relative dispersion, is used as one component, extremely brilliant colors are produced and they extend over a much longer range of index difference, but the detection of the match point for sodium index is rendered less exact. In choosing liquids one must keep in mind that accuracy of match will vary inversely

with total range of criteria. Solids tested include corundum, quartz, halite, topaz, sucrose, and a variety of optical glasses of difference indices and dispersions.*

Media for making permanent mounts such as balsam, Aroclor 4465, and naphthalene formaldehyde resin also show the characteristic colors with minerals of appropriate index. However, such media usually require purification as they are likely to be full of extraneous suspended matter of widely differing indices which becomes all too visible in dark-field illumination.

The fact that a match of liquid and solid indices for sodium light is

Table 1. Summary of Color Criteria for Relative Index (n_D) of Grains and Liquid in Dark-field

Grains Greater	*Grains = Liquid*	*Liquid Greater*
Yellow	Blue or blue-violet with very little red or none.	Blue
Yellow and violet		
Orange and violet		
Red and blue-violet		

indicated by the vanishing point of the red color and the transition of violet to blue has so far not been explained as anything but a fortunate coincidence resulting from the constancy of the relative shapes of the solid and liquid dispersion curves.

Equipment

The colors described above were obtained with a research type petrographic microscope using a standard 10 × (16 mm.) 0.25 N.A. strain-free achromatic objective, and a standard 0.28 N.A. condenser (upper element swung out). The opaque stop used is 14 mm. in diameter and mounted so as to swing in and out readily between the polarizer and the bottom of the condenser. It is quickly and easily centered with one hand; centering is observed by inserting the Bertrand lens. The best illumination is obtained with the condenser slightly lowered. Owing to the small diameter of the standard calcite polarizer, light was not passed around the stop to make the hollow cone; this was remedied by replacing the calcite with polaroid mounted in an interchangeable tube (a standard item from a student model instrument can be used). There seems no objection to having polaroid in the substage and calcite in the analyzer.

* For the highly unusual case in which the dispersion of the solid is greater than that of the liquid of the same index, the color sequence is reversed. The only such case so far actually observed is sylvite in a mixture of Government oil and Nevillite oil.

The same set-up is quite satisfactory for the 6× (22.7 mm.) and the 4× (32 mm.) objectives.

A simpler arrangement, also for use with the 10×, 6×, and 4× objectives, is to use a standard 13 mm. dark-field stop, with a condenser N.A. of 0.28. For higher powers, such as the 20× and 45× objectives, the standard petrographic type condenser may be too small in diameter to pass light around the larger opaque stop which is needed. In such cases a different condenser can be substituted.

Directions for setting up dark-field illumination by simple modifications which the user can perform himself without instrument machine shop facilities are so specific for different makes and models of microscopes that it is suggested that the manufacturer be consulted for detailed instructions. These arrangements need not interfere with a quick return to ordinary bright-field illumination whenever desired. Ordinarily only minor items of additional equipment are needed.

When no petrographic microscope is available a great deal of useful work may be done with a biological microscope (1).

Strong illumination is needed for dark-field, such as can be obtained from a 100-watt lamp. Suitable filters are needed to cut down glare and to reduce excess of longer wave-length light from the tungsten filament. The above-described colors were obtained while using a daylight blue glass, polished on both sides. A neutral ground glass or a second daylight blue may be added to regulate the light. Obviously the exact nature of the colors will be affected by differences in filters used. A condensing lens on the lamp was focused to produce nearly parallel light. A diaphragm on the lamp is useful to help in darkening the background.

When working with the 4 mm. objective the illumination becomes decidedly more critical. Satisfactory results will be obtained by using the 6-volt 108-watt ribbon filament lamp, with a Corning Daylite blue filter,

Upper left: Sample of commercial talc for use as filler. Talc (blue), lower index, and tremolite (yellow), higher index, in liquid having $n_D = 1.588$. White grains: Unidentified impurity.

Upper right: Crushed topaz (white and yellow), higher index, and quartz (blue), lower index, in liquid having $n_D = 1.556$.

Lower left: Crushed topaz in pure cinnamaldehyde ($n_D = 1.619$). Grains equal to or greater than liquid in index, depending on their orientation with respect to polarizer.

Lower right: Crushed quartz (yellow) and chalcedony (blue-violet with red) in liquid having $n_D = 1.536$. n_D of chalcedony = 1.539.

All 100×, using petrographic microscope with polaroid in substage. 14 mm. dark-field stop placed just below condenser of N.A. = 0.28. Liquids except lower left, are mixtures of α-chlornaphthalene and butyl carbitol.

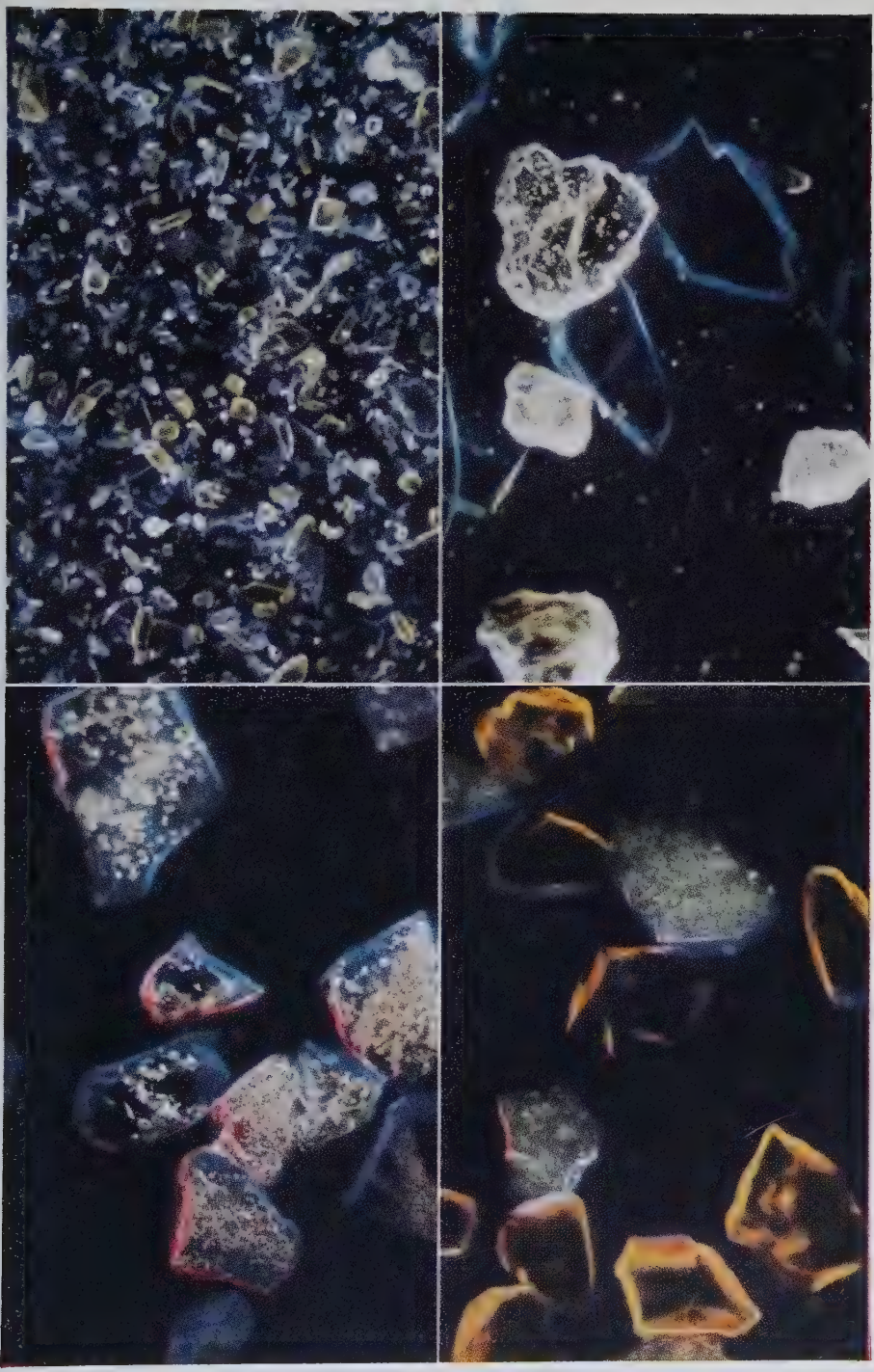

polished on both sides (no ground glass). Careful adjustment of the illuminator, the mirror, centering of the dark-field stop, and position of the substage makes a great difference in the intensity of the colors produced.

Scrupulously clean slides and cover glasses, free from scratches, cracks, or other defects must be used, and the immersion liquids should not contain suspended matter, as all such things show up in brilliant white in dark-field. In addition to obscuring the view of grains under observation, they scatter white light, reducing contrast by lightening the background. Tiny spots on the cover glass, being out of focus, blur out into larger white circular patches of light.

Accuracy

The dark-field color method with white light has been checked many times against the Becke line—central illumination method with the sodium arc, both with and without a temperature-controlled stage cell. An accuracy of $\pm .001$ may be attained with the dark-field method under favorable conditions, such as by using a set of liquids with an index interval of .002 in an air-conditioned room or where temperature changes are slow enough that correction curves can safely be applied. With an index interval between liquids in the set of .004 or .005, the accuracy would about $\pm .002$. With index variation methods involving changing of temperature or varying of composition of liquid, the dark-field method can be made practically exact in the third decimal place.

With monochromatic light, the Becke line—central illumination method, the oblique illumination method, and the double diaphragm method* of Saylor (3) (the method of two-fold oblique illumination of Wright, 6) are all inherently more exact than the dark-field color method. Therefore it is not suggested as a substitute for them in such fundamental studies as the determination of the indices of the end-members of systems, or other analyzed materials where the highest accuracy is desired. However, for most ordinary work, such as identification, the dark-field method can be used quite safely.

For materials of high birefringence, the dark-field method will probably suffer a loss in accuracy.** This has not been investigated, but seems to follow inescapably from the calculations of F. E. Wright (7) and the experimental work of C. P. Saylor (3), on other methods involving oblique incidence of light. Due to the symmetrical character of the illumination in the present case, it is possible that this error may be somewhat less

* Discovered by F. E. Wright, this method was improved by C. P. Saylor who placed the upper diaphragm just above the upper element of the objective.

** As pointed out by Dr. Horace Winchell and Dr. Chester B. Slawson during discussion of this paper.

than in those methods involving unilateral oblique illumination. In any event, from Saylor's work it seems apparent that the error is relatively small with low aperture objectives (32 mm. and 16 mm.).

Special Applications

One of the most obvious and striking uses of the dark-field color method is for detecting impurities in various powdered materials. By selecting an appropriate immersion liquid the substance to be checked can be shown in color, while impurities will appear white or a different color. The impurities will almost always contrast strongly with the desired material, so that a glance at a field gives an immediate estimate of the situation, and grain counts and measurements are facilitated.

When grains are heavily loaded with inclusions, the outer Becke line may be obscured by many internal Becke lines due to the inclusions. Even though inclusions are more conspicuous and more clearly observed in dark-field, the color criteria for the host mineral are unaffected. The inclusions are seen in brilliant white in colored grains.

If routine testing work is to be done by semi-skilled technicians this method has obvious advantages.

For photographic record purposes this method, with color photography, is not subject to the possible confusion of other methods, such as uncertainty as to whether a Becke line was photographed above or below focus, or whether the proper orientation was maintained with oblique illumination.

For very fine-grained material, requiring high-power objectives, dark-field illumination permits more reliable observations than ordinary illumination, as pointed out by F. E. Wright (8). In such cases, more accurate determinations may be made by half-shadowing the field, using monochromatic light, as advised by Wright (9), but sufficient accuracy for identification work may be had by observing the dark-field colors with white light, as proposed by Crossmon (1) and in the present paper.

Summary

A microscopic immersion method for refractive index, based on dark-field illumination, has been presented in the hope that petrographers may find it useful. Some special applications in which it affords advantages have been pointed out. Necessary optical conditions have been described; these are subject to improvement and simplification particularly for high power objectives. Accuracy about equal to that of methods in current use is attainable for most work. The color criteria are so striking and clear cut that this method is really a pleasure to use.

References

1. Crossmon, G. C., (*a*) Optical staining of tissue: *Jour. Opt. Soc. Am.*, **38,** 417 (1948). (*b*) Microscopical distinction of corundum among its natural and artificial associates: Analytical Chemistry, in press.
2. Larsen, E. S., and Berman, H., The microscopic determination of the nonopaque minerals, 2nd Ed.: *U. S. Geol. Surv., Bull.* **848** (1934).
3. Saylor, C. P., Accuracy of microscopical methods for determining refractive index by immersion: *J. Research NBS*, **15,** 277–294 (1935).
4. Wright, F. E., The methods of petrographic-microscopic research: *Carnegie Institution of Washington, Publication No.* **158,** 92–98 (1911).
5. Wright, F. E., *Op. cit.*, 85–87 (1911).
6. Wright, F. E., The determination of the relative refringence of mineral grains under the petrographic microscope: *Jour. Wash. Ac. Sc.*, **4,** 389–392 (1914).
7. Wright, F. E., The accurate measurement of the refractive indices of minute crystal grains under the petrographic microscope: *Jour. Wash. Ac. Sc.*, **5,** 101–107 (1915).
8. Wright, F. E., The methods of petrographic-microscopic research: *Carnegie Institution of Washington, Publication No.* **158,** 53, 94–95 (1911).
9. Wright, F. E., *Op. cit.*, 87 (1911).

PEGMATITES OF EIGHT MILE PARK, FREMONT COUNTY, COLORADO

E. Wm. Heinrich, Department of Mineralogy, University of Michigan, Ann Arbor, Michigan.

(*Continued from p. 448, Vol. 33, Nos. 7–8*)

TABLE OF CONTENTS

MINERALOGY

General Features

On the basis of occurrence the pegmatite minerals may be divided into three groups:

1. The common rock-forming minerals, which constitute the bulk of the material of the zones.
2. The rarer minerals which occur chiefly in the secondary units.
3. The products of supergene alteration.

The mineralogy of the zones and of undifferentiated pegmatites is simple and is characterized by strong development of primary rock-forming minerals: quartz, microcline, muscovite, and biotite. Other subordinate constituents are oligoclase, garnet, schorl, magnetite, and chlorite.

The rarer constituents are restricted to the secondary units, wherein the dominant minerals are sodic plagioclase, quartz, and muscovite. Other important minerals are tourmaline, garnet, apatite, beryl, lepidolite, triplite, and chalcocite. Other, still rarer, constituents also may be present. Vugs are very rare, and, if present at all, are small. In the School Section pegmatite 1- to 6-inch vugs containing minute cleavelandite and sericite crystals were observed. Vugs with very small quartz crystals were found on the Mica Lode dumps. A few 1- to $1\frac{1}{2}$-inch vugs were noted in the Van Buskirk deposit.

Calcite, kaolinite, limonite, and manganese oxide are the chief products of weathering.

The complete list of mineral species found in the pegmatites is given in Table 5.

Table 5. List of Minerals of the Pegmatite Bodies

Quartz	Apatite	Malachite
Microcline	Triplite	Azurite
Andesine	Fremontite	Chrysocolla
Oligoclase	Cerussite(?)	Beyerite
Albite	Columbite	Bismutite
Muscovite	Torbernite(?)	Limonite
Biotite	Magnetite	Manganese oxide
Chlorite	Hematite	Calcite
Lepidolite	Chalcocite	Kaolinite
Garnet	Native silver	Chalcedony
Beryl	Native bismuth(?)	
Tourmaline	Covellite	

Description of Minerals

Quartz

Quartz occurs in all zones and in secondary units as well. Fine-grained granitic intergrowths with microcline are characteristic of wall zones,

and subgraphic to graphic intergrowths with microcline, and intergrowths with small muscovite flakes occur in intermediate zones. Quartz-muscovite aggregates also form border zones. Massive white quartz in pods as much as 30 feet long occurs in cores. In secondary units quartz forms a granular intergrowth with plagioclase; occurs in veinlets with albite, muscovite, and less commonly biotite; and less commonly is intergrown in a subgraphic pattern with either garnet or black tourmaline.

The color ranges from clear to milky white to light gray. In a few deposits limonite colors the mineral many shades of red and brown. In the McMullin Lease No. 2 pegmatite the core quartz is banded by alternating milky and clear layers about one inch thick. In many deposits post-crystallization fracturing has shattered the quartz. In the Mica Lode tiny flattened quartz crystals have formed along such fractures. On the dumps from this quarry were found several specimens with small vugs containing $\frac{1}{8}$-inch quartz crystals coated by manganese oxide.

Microcline

The chief feldspar is perthitic microcline which occurs intergrown with quartz in wall zones, as euhedral phenocrysts and irregular masses with graphically intergrown quartz in intermediate zones, and as 6-inch to 6-foot, quartz-free crystals in cores.

The color ranges from pink to dark red. The reddish color is characteristic for the area, not only for microcline in pegmatites but in Pikes Peak granite and aplite as well. That part of the red color was formed after crystallization is shown by borders of darker color along minute fractures. Microcline associated with abundant biotite is generally somewhat darker in color. Mottled white and pink microcline occurs locally in the Meyers Quarry pegmatite. In the Rim pegmatite phenocrysts of red microcline with intergrown quartz are set in a matrix containing white microcline. Coarse white microcline also occurs in a small pegmatite pod on the Meyers Quarry property, but in general the white color is atypical. Specimens of brown and gray microcline were noted in the Van Buskirk deposit.

Microcline is altered to sericite, kaolinite, or calcite. Replacement commonly proceeds outward from along perthite lamellae and cleavage traces.

In addition to the usual cleavages, some of the microcline at the Meyers Quarry has an unusual "cross ripple," which consists of minute grooves roughly parallel to the perthitic structure. These grooves may represent slickensides. A similar structure, formed by minute, sharply defined ridges, occurs in the microcline of graphic granite in the Van Buskirk pegmatite.

Graphic Granite

Sub-graphic and graphic intergrowths of quartz and microcline are common in intermediate zones and locally in wall zones. All gradations from irregular granular to well-defined graphic textures are present. At the Van Buskirk deposit this gradation is well illustrated by the following varieties:

1. Granular intergrowth of quartz and microcline; neither mineral is host.
2. Irregular blebs and pods of quartz in dominant microcline. The microcline host is not a single crystal and the quartz units may lie across the feldspar grain boundaries.
3. Irregular tabular quartz bodies, with lateral projections and apophyses, generally in a single host crystal of microcline.
4. Typical graphic individuals of quartz in single crystals of microcline; i.e., ideally developed graphic granite.
5. Minute, parallel lenses of quartz set in a rough en echelon pattern in single microcline crystals.

Landes (1935, p. 330) states his belief in a hydrothermal replacement origin of graphic granite. The writer favors the theory of simultaneous crystallization to explain the formation of these variable intergrowths. This also is supported by the phenocrysts of sub-graphic to graphic granite in a matrix of typically granular quartz and microcline. The origin of such a combination is difficult to explain by replacement of microcline by quartz, for only the phenocrysts are graphic in texture.

Plagioclase

Four varieties of plagioclase occur in the pegmatites. The most calcic, andesine, is restricted to several interior pegmatites that transect xenoliths of gabbro in Pikes Peak granite. The plagioclase of the other interior pegmatites is invariably white oligoclase.

The three generations of plagioclase that occur in secondary units are, from oldest to youngest:

1. Fine- to medium-grained plagioclase which ranges in composition from oligoclase to albite. The color is generally light red or pink but may be white, light gray, or grayish lilac.
2. Fine-grained, sugary, white albite.
3. White to light red cleavelandite, which occurs associated with small vugs, in large radiating masses, and in bands marked by comb structure.

Type 1 occurs in a granitic intergrowth with quartz and forms the bulk of the feldspar in replacement units. The unusual gray variety corrodes altered triplite, and the color may result from the breakdown of the phosphate. This plagioclase is veined by black tourmaline.

White sugary albite (Type 2) replaces pink plagioclase (Type 1), microcline, quartz, beryl, apatite, and tourmaline, and is cut by garnet vein-

lets. Thin films of fine-grained albite also coat fracture surfaces in the shattered quartz of the Mica Lode core.

In the Meyers Quarry pegmatite, cleavelandite (Type 3) occurs only in association with lepidolite and corrodes earlier pink plagioclase (Type 1), quartz, and beryl. In the School Section deposit cleavelandite, commonly coated by bright green sericite, is arranged in rosette structure marginal to small vugs. Minute crystals project into cavities. Here cleavelandite also replaces black tourmaline.

Muscovite

Primary muscovite is found in all zones except the core. With quartz it forms fine-grained border zones, where it may occur as a selvage of small books normal to the walls. In wall zones it occurs with microcline and quartz, and in intermediate zones it is intergrown with quartz in sub-parallel plumose aggregates of $\frac{1}{2}$- to $1\frac{1}{2}$-inch flakes. The origin of these dendritic growths is obscure. There is little evidence to indicate that the muscovite is much later than the quartz.

The large blades and books of muscovite and the masses of tightly interlocking flakes ("ball" mica) form fracture-controlled units or irregular replacement bodies. These bodies commonly occur along the footwall sides or in the footwall parts of core pods. In the Mica Lode, replacement of the footwall half of the core has been intense and irregular. Here muscovite occurs as follows:

1. Veins of fracture filling. These are thin and contain flattened garnet crystals and muscovite flakes parallel with the walls.
2. Tabular and pod-like masses that have the original fracture as in (1) but are distinguished by extremely coarse blades of muscovite arranged in comb or rosette structure, generally on the hanging-wall side of the fractures. Some of the wedge-shaped blades are as much as two feet long. These bodies are very abundant and may be 20 feet long and 10 feet wide.
3. Irregular masses and pods of "ball" mica with subordinate intergrown plagioclase (Type 1). Some of these pods may be rimmed by a border of bladed mica. Masses 25×30 feet in section, containing 60–90% muscovite have been mined. The individual flakes vary from 1/16 to 1 inch across.

Very little muscovite occurs in well-formed, flat books. The large blades are wedge-shaped, minutely fractured, and marked by heavy fishtail structure. In a few places incipient replacement around small core pods in the Meyers Quarry has led to the development of minor plagioclase and scattered flat muscovite books as much as 6 inches across. Some of these have A-structure and others are broken by reeves. Many contain heavy central inclusions of magnetite films. Similar books with similar defects occur locally around core pods in the School Section pegmatite.

The color varies from gray green to silvery green to bright green. Stain-

ing by red iron oxide and black manganese oxide is common in the aggregates of wedge blades.

Muscovite also occurs in long narrow strips intergrown with biotite. This intergrowth, called "tanglefoot," consists of a central strip of biotite and borders of muscovite. The laths are as much as six feet long, eight inches wide, and one inch thick. They are common in the wall zone of the School Section pegmatite, where they tend to be normal to the hanging-wall contact. They are certainly among the last components to crystallize, for they cut sharply across the fabric of the zone. Muscovite rimmed by lepidolite is found in the replacement units in the west end of the Meyers Quarry. The cleavage is uninterrupted by the transition, and contacts between the two are sharp.

TABLE 6. VARIATIONS IN γ INDICES OF THE MUSCOVITES

Occurrence	Color	Range in γ	Mean γ
1. Primary muscovite of the zones	Gray green to bright green	1.602–1.612	1.605
2. Bladed muscovite and "ball" mica in secondary units	Light silvery green	1.602–1.604	1.603
3. Muscovite associated with the cleavelandite-lepidolite replacement phase	Colorless	1.594–1.600	1.597
4. Sericite	Yellow, green, gray	1.580–1.590	1.585

Fine-grained, flaky, fibrous, or massive sericite is common. The color is yellow to bright green. It is one of the latest minerals to form and replaces microcline, beryl, tourmaline, cleavelandite, and fremontite.

Table 6 shows the variation in color and γ indices of refraction of the muscovites with respect to their paragenetic position. The younger muscovites have slightly lower indices.

Biotite

Biotite is widely distributed in wall zones as small books and flakes and as large blades of "tanglefoot." Locally it becomes very abundant, especially in the marginal pegmatites. At the Border Feldspar No. 1 deposit biotite occurs abundantly with quartz and red oligoclase in late veins that cut across the core. Blades as much as 6 feet long and $1\frac{1}{2}$ feet across lie parallel with the walls of the veins and appear to have formed along fractures in the quartz and plagioclase. Biotite also occurs

in the Magnusson pegmatite in a dendritic intergrowth. The central axis of the branch is 10 feet long with regular offshoots 2 feet long at 65-degree angles. Much biotite has been altered to gray-green chlorite.

Chlorite

Primary chlorite occurs only in a few pegmatites of the injection gneiss, where it forms $\frac{1}{2}$-inch, fibrous aggregates. Secondary chlorite formed by the supergene alteration of biotite is especially abundant in the School Section pegmatite.

Lepidolite

Lepidolite was found only in the core-margin replacement units of the Meyers Quarry pegmatite. A single specimen of lepidolite replacing beryl was obtained from the No. 4 Cut dumps, but all the rest of the mineral was found in the replacement pods near the western end of the deposit. Associated with it are beryl, garnet, abundant cleavelandite, muscovite, black, red, and green tourmaline, and rarely, fremontite and columbite. Three varieties were noted:

1. Flaky, fine-grained, deep purple lepidolite.
2. Pale lilac rims of lepidolite bordering muscovite books.
3. Large flat books of very pale lilac lepidolite.

The fine-grained type, which is most abundant, commonly is associated with rubellite. It replaces quartz and cleavelandite, and in association with quartz cuts across plagioclase (Type 1) in thin veinlets. It appears to corrode fremontite slightly. A little dark purple lepidolite also occurs in quartz in curved, 2×1-inch plates marked by closely spaced reeves.

The narrow rims of pale lepidolite around 1- to 3-inch muscovite books are not common. The books of very pale lepidolite, which occur with the older green tourmaline, appear to have formed somewhat later than the fine-grained darker lepidolite. The γ indices of refraction of the three types are as follows:

Fine-grained	*Rims*	*Pale books*
1.561–1.566	1.564	1.577–1.588

Garnet

Light-brown to clove-brown garnet is locally abundant in a few pegmatites. Although scattered crystals occur in wall zones and intermediate zones, the bulk of the mineral is found in the secondary units within or at the margin of cores.

Well-formed crystals, $\frac{1}{2}$ inch to 1 inch in diameter, are the rule, but small patches of a subgraphic intergrowth of garnet and quartz also occur.

There may be two generations of garnet. The earlier (?) is dark-brown spessarite, which is associated with black tourmaline, muscovite, and red oligoclase (Type 1). Cleavelandite (Type 3) strongly corrodes aggregates of this variety. The second (?) generation is reddish brown in color and occurs in finely granular aggregates and veinlets that transect and replace large crystals of gray-green apatite and white sugary albite (Type 2). Masses of spessartite as much as six feet across have been reported from the Mica Lode pegmatite. A large pod of intergrown garnet and chalcocite occurs in blocky microcline of the core, and irregular veinlets of spessartite cut across margins of quartz pods in the Mica Lode core. Much of the garnet alters readily to manganese oxide; some of it is replaced by light green sericite.

Beryl

Scattered crystals of beryl are widespread in secondary units, but local strong concentrations also occur there. An irregular mass of plagioclase-muscovite-beryl rock replaces part of the footwall side of the Mica Lode core. A similar but smaller unit occurs along the margin of the core pod in the No. 4 Cut at the Meyers Quarry. Scattered crystals occur in many other deposits.

The most common color is a pale blue-green, but deep blue, pale blue, light green, and lemon yellow also occur. Specimens of white to pale orange beryl were found on the Mica Lode dumps, and light red beryl was obtained at the Border Feldspar No. 2 deposit. Much of the beryl associated with triplite at the Mica Lode is stained black by manganese oxide from the altered phosphate. The texture of the mineral varies from chalky to glassy; small parts of a few crystals are of gem quality.

Many crystals show zoning, which may be expressed in one of three ways:

1. A core of beryl that contains numerous minute inclusions of muscovite separated from an outer inclusion-free zone by a film of muscovite or feldspar. The two zones are the same color.
2. A core of albite and quartz bordered by an unaltered outer shell of beryl (Fig. 12).
3. A deep-red core and an outer white shell: found only at the border Feldspar No. 2 pegmatite.

The crystals are commonly sheathed by small muscovite flakes or by fine needles of black tourmaline. Veinlets of quartz and tourmaline transect them normal to the length. Some crystals have cores and "inclusions" of quartz and albite (Type 2) ("shell" beryl) (Fig. 12).

Both tapering and non-tapering crystals may have such features. Shaub (1937, p. 1051) believes that the "beryl-albite intergrowths . . . are shown to be of such a nature that an origin through the processes of

replacement is most unlikely, while on the other hand their relationship and other features clearly indicates (sic) a comtemporaneous (sic) crystallization."

This origin seems untenable for several reasons: (1) Beryl in the Eight Mile Park pegmatites is restricted to secondary pegmatite units and is

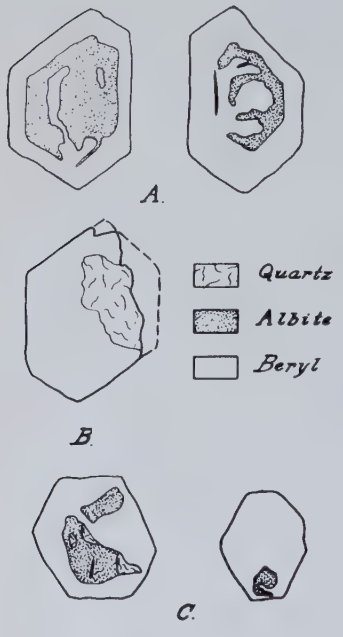

Fig. 12

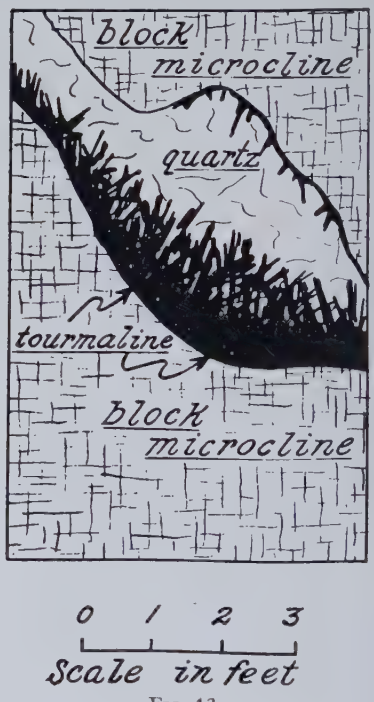

Fig. 13

Fig. 12. Cross sections of "shell" beryl crystals, School Section deposit.

Fig. 13. Preferential replacement of quartz by tourmaline, core of Border Feldspar No. 2 pegmatite.

itself of hydrothermal origin. (2) Much of the albite (Type 2) is clearly later than the tourmaline, which veins and coats the beryl crystals. (3) Moreover, the beryl crystals show considerable variation in their refractive indices from core to margin and also from the small end to the large end of tapered crystals. This indicates a zonal variation in their alkali content. (4) The intergrown quartz and albite commonly occur in cores or platy masses whose sides are parallel with prism faces of the beryl (Fig. 12). In fact, Shaub (p. 1046) notes this crystallographic control of the beryl on the albite and states, "The beryl at the large ends

consists of plate- or blade-like masses usually having their sides parallel to the first or second order prisms. In addition, other forms as pyramids and pinacoid were noted."[1] The writer believes these data offer strong support for origin of the intergrowths through the replacement of selected zones within beryl by albite and quartz. Analogies in other minerals are common, as for example, the zonal replacement of plagioclase by sericite; tourmaline by quartz, damourite, or cookeite (Frondel, 1935A, p. 856); pyrite by chalcocite and pyromorphite by galena (Schouten, 1934); plagioclase by epidote (Grimsley, 1894), and actinolite by talc (Phillips and Hess, 1936).

Many beryl crystals are very soft and crumbly. Microscopic examination reveals that they have been replaced by sericite.[2] The altered crystals also may be heavily stained by limonite and veined by manganese dendrites.

Some of the beryl crystals are markedly tapering, a structure characteristic of beryl from many pegmatites in south-central Colorado. Both zoned and unzoned crystals taper. The tapering crystals are commonly oriented nearly normal to the contact between unreplaced core rock and secondary muscovite-plagioclase pegmatite, with the larger end at the core side. These relations were observed for tapered crystals in the No. 4 Cut of the Meyers Quarry, at the Mica Lode, at the School Section deposit, and at the Suzana No. 3 pit. Beryl crystals normal to the contact between cores and adjoining pegmatite are shown by Johnston (1945, p. 1034) and by de Almeida et al. (1944).

The beryl associated with the lepidolite-cleavelandite type of mineralization differs somewhat from that found in the muscovite-plagioclase replacement units in its lemon-yellow color, porcelanoid texture, lack of taper and zoning, and freedom from alteration.

The ω indices of refraction of the green and blue beryls range from 1.576 to 1.587, with a mean of 1.581. The orange to white variety found on the Mica Lode dump has $\omega = 1.595$ and appears to be high in the alkali elements.

Tourmaline

The tourmaline is of two types, the common schorl, and the brightly colored varieties. Schorl occurs as a minor constituent of wall and intermediate zones, but is concentrated in core-margin replacement pods that are rich in muscovite and red plagioclase (Type 1). In the marginal pegmatites, fine-grained tourmaline occurs in narrow crosscutting veinlets.

[1] See also Johnston (1945, p. 1033).

[2] Checked by x-ray powder photograph.

Abundant black tourmaline has been found in the School Section pegmatite where it forms suns as much as four feet in diameter. Individual crystals may reach three inches in diameter and eight inches in length. In some the prismatic striations are bent.

Tourmaline prefers to replace quartz, if possible. This selectivity is particularly well illustrated in the Border Feldspar No. 2 open cut where individual quartz pods within the core have been strongly replaced by tourmaline, and the surrounding blocky microcline is completely free of the mineral (Fig. 13). This phenomenon also occurs in the School Section deposit. Similar relations, on a smaller scale, were observed in the Suzana No. 1 body, where quartz in a fine-grained, subgraphic intergrowth of quartz and microcline has been replaced selectively by black tourmaline. Tourmaline crystals formed in quartz commonly are well developed, with sharply-defined faces, whereas those which replace microcline are flattened, irregular, dull, and tend to occur not as single crystals but in matted clusters and narrow veinlets.

At the School Section quarry black tourmaline replaces quartz and microcline and appears to be contemporaneous with garnet. It is older than a little of the red plagioclase (Type 1), cleavelandite (Type 3), and a second generation of quartz. Quartz and plagioclase (Type 1) veinlets normal to the length are common. Many crystals have been offset along these filled fractures. Around the sides of small vugs black tourmaline is intensely replaced by cleavelandite, which is coated by bright yellow-green sericite.

Some crystals contain a poorly defined zonal structure with a core speckled by abundant small muscovite flakes and an outer muscovite-free layer (incipient selective replacement?). Other crystals are completely coated by fine-grained muscovite. "Shell" tourmaline crystals at the Colfelco No. 12 prospect have central parts selectively replaced by quartz and muscovite.

The colored tourmalines occur only in the cleavelandite-lepidolite replacement units in the western part of the Meyers Quarry pegmatite. The red, light green, and blue-black varieties occur as single-color crystals, but most of the crystals are color zoned with the following combinations:

Core	*Border*
1. Blue-black	Dark green
2. Dark green	Pink
3. Dark green	Light green
4. Light green	Yellow
5. Red	Yellow
6. Light green	Red

From these relationships the sequence of types, from oldest to youngest, is: (1) blue-black, (2) dark green, (3) light green, (4) pink, (5) red, and (6) yellow.

The colored tourmalines are veined by quartz and albite and may have the outer zone partly replaced by albite. They are closely associated with lepidolite: the green variety with flat books of pale lilac lepidolite, and the rubellite with masses of fine-grained purple lepidolite. Two crystals of green tourmaline may form a V with pale lepidolite between the arms. A few green crystals occur in radiating groups. Minute rubellite crystals form coatings on fremontite crystals.

Apatite

Apatite is unusually abundant in the core-margin replacement units of the School Section pegmatite, where it forms blocky crystals as much as eight inches across. The color varies from a dull gray-green to an iridescent dark purple. The mineral is veined by white sugary albite (Type 2) and by garnet. Veinlets of albite may be so numerous as to form a replacement breccia of the larger crystals. Fine-grained blue apatite occurs sparingly in the Van Buskirk, Suzana No. 4, and the Meyers Quarry pegmatites. At the last it replaces quartz and microcline.

An unusual dark brown apatite was found on the Mica Lode dumps. It resembles triplite with which it is closely associated. Under the microscope the mineral is seen to contain very abundant dark brown to black inclusions. Identification was confirmed by *x*-ray powder photograph. Like the associated triplite, the mineral is corroded by gray albite and muscovite. Possibly it formed by the supergene alteration of triplite by calcium carbonate waters. Associated are crusts of limonite and manganese oxide.

Triplite

Triplite was found only in the Mica Lode and School Section pegmatitites. In both bodies it is associated closely with beryl-muscovite mineralization. The occurrence and crystallography have been described in detail (Wolfe and Heinrich, 1947).

The mineral occurs chiefly in gray albite and small flakes of light-colored muscovite, which may sheath the masses. Less commonly both minerals corrode and vein triplite. In the School Section pegmatite fine-grained black tourmaline replaces triplite.

Fremontite

Fremontite was first described by Schaller (1911, 1912) from Eight

Mile Park under the name of natramblygonite. This was later withdrawn because of certain etymological objections (Schaller, 1914, 1916). The mineral also has been reported from Jeclov, near Jihlava, Moravia, in Czechoslovakia (Sekanina, 1933).

The description of this rare species follows:

Triclinic, with two cleavages, the better parallel to $\{001\}$, the other parallel to $\{100\}$; occurs in cleavable masses or crystals with rough faces; forms noted are $c\{001\}$, $b\{010\}$, $a\{100\}$, $z\{1\bar{2}0\}$, $e\{0\bar{2}1\}$, and $h\{\bar{1}01\}$; the angles agree with the corresponding angles on amblygonite; under the microscope two directions of polysynthetic twinning appear; $H=5.5$; $G=3.01$–3.06; color grayish to white; translucent to opaque; luster vitreous to greasy but approaches chalky upon weathering; optically positive; X nearly normal to $\{001\}$; $\alpha=1.594$, $\beta=1.603$; $\gamma=1.615$; 2V is large; before the blowpipe easily fusible with slight intumescence to an opaque white enamel.

Formula—(Na, Li) $AlPO_4$ (OH, F)

Analysis (by Schaller):

P_2O_5 =	44.35
Al_2O_3 =	33.59
Li_2O =	3.21
Na_2O =	11.23
K_2O =	0.14
H_2O =	4.78
F =	5.63
	102.93
$O=F_2$ =	2.37
	100.56

The type crystals and masses examined by Schaller are now part of the Holden collection at Harvard University and were restudied by the writer. The crystals are coated by thin films of yellow sericite and transected by quartz veinlets normal to the *c* axis. Small blebs of rubellite also form a coating and corrode the crystals. Lepidolite corrodes and replaces fremontite. The crystals are rough and did not form in vugs but were surrounded on all sides by pegmatite.

Several small fragments of fremontite were collected from the western part of the Meyers Quarry pegmatite. The mineral is restricted in its occurrence to the core margin replacement pods of cleavelandite-lepidolite rock, and it was found only at the easternmost of these.

A cerussite pseudomorph after fremontite has been reported by Frondel (1935B) from near Canon City. The association with quartz, lepidolite, and pink feldspar indicates that the specimen probably was obtained from the Meyers Quarry pegmatite. An attempt to locate the specimen (*Amer. Mus.* 18064) for further study was unsuccessful.

Columbite

Although columbite is a relatively common mineral in many pegmatites of south-central Colorado, it is rare in the pegmatites of Eight Mile Park. Headden (1905) has described the mineral from this locality and reports that it occurs in masses as heavy as 600 pounds, associated with red, green, and black tourmaline. This association clearly indicates that his material was found in the cleavelandite-lepidolite rock in the western part of the Meyers Quarry pegmatite. The analysis by Headden follows:

Cb_2O_5 = 56.48	
Ta_2O_5 = 22.12	
WO_3 = 0.45	
SnO_2 = 0.11	G = 5.6608
FeO = 8.07	
MnO = 12.45	
IgO = 0.15	
99.83	

Small specimens of columbite were found at the Meyers Quarry, Mica Lode, and School Section quarry. Sterrett (1923) in his description of the Mica Lode (Mica Hill) states (p. 56), "In small openings lower down rough crystals of beryl from an inch to a foot in diameter and columbite in masses weighing 2 or 3 pounds were found." At the School Section quarry a $\frac{3}{4}$-inch crystal was found in the eastern part of the Shipley Cut where it occurs in the plagioclase-muscovite replacement pod and is associated with beryl, triplite, and abundant black tourmaline.

Torbernite (?)

Associated with the rubellite, lepidolite, and fremontite of the Meyers Quarry are exceedingly minute flakes of a grass green uranium mineral, probably torbernite. The flakes tend to occur along contacts between rubellite or fremontite crystals and quartz-lepidolite matrix.

Magnetite

Magnetite is a very abundant constituent of pegmatites in the injection gneiss. Exterior pegmatites near the injection gneiss contacts also contain it, but interior marginal and other exterior pegmatites carry it but rarely. In some exterior pegmatites it occurs only in thin films, included in muscovite.

An unusual magnetite-bearing pegmatite occurs in the SW. $\frac{1}{4}$, NE. $\frac{1}{4}$, Sec. 22 overlooking Overshot Gulch (Fig. 2), on the McMullin Lease. The deposit is a sill which strikes N. 62° E. and dips 85° NW. It is very

poorly zoned with medium-grained margins of red microcline and quartz and a slightly coarser core of the same minerals. Biotite occurs sparingly. Magnetite, which is very abundant, occurs in "streaks" and clusters of crystals throughout most of the mass. The crystals range in size from $\frac{1}{4}$ inch to $2\frac{1}{2}$ inches. Most of them are faced, partly by rounded, striated octahedral faces and partly by flat, well-formed octahedral faces. The mineral appears to be primary in origin and probably crystallized early.

The crystals weather out and are concentrated in the debris below the outcrop. Somewhat similar pegmatites have been described by Ball (Spurr, Garrey, and Ball, 1908, p. 61), who states, "Magnetite is a widely distributed constituent, and in some places forms over one-third of the pegmatite mass, which in consequence becomes a lean iron ore. Magnetite occurs in crystals which solidified prior to the other constituents of the pegmatite or in irregular aggregates which solidified practically at the same time as quartz and orthoclase. The crystals, which are octahedrons or octahedrons modified by the faces of the cube, reach a maximum diameter of 4 inches, and some of the aggregates are 6 inches across."

Hematite

Hematite occurs as an alteration of the magnetite crystals and of the magnetite inclusions in muscovite. Coatings of specular hematite occur along fractures in massive quartz in the Suzana No. 3 pegmatite. Veinlets of fine-grained hematite are common in many pegmatites in injection gneiss.

Chalcocite

Chalcocite intergrown with spessartite garnet was found in a 6-foot pod in the Mica Lode quarry, and other large masses have been mined in the past.[1] The pod is rimmed by coarse blades of muscovite. The mineral is steely blue in color and transects and replaces microcline and associated muscovite. In polished section there appear minute, bronze-colored inclusions that may be native bismuth. The pod and the surrounding muscovite and microcline are heavily stained by manganese oxide from the decomposed garnet and by malachite from the altered chalcocite.

Chalcocite also occurs at the School Section deposit. Associated with it are minute patches of secondary covellite and copper carbonates. Only a few 1-inch pods of the material were found in a matrix of plagioclase and muscovite.

[1] Personal communication from Mr. Robert Shipley.

Native Silver

A polished section of the School Section chalcocite disclosed extremely minute blebs of a soft white mineral in grains too small to identify by etch test methods. Professor L. C. Graton kindly instructed the writer in the use of the microdrill (Harcourt, 1937) by means of which the tiny grains were drilled out. The powder was then collected in a capillary tube. An *x*-ray powder photograph of the material gave the correct lines and spacings for native silver. The native silver, native bismuth (?), chalcocite, and bismuth carbonates may be secondary minerals formed by the decomposition of a primary copper-bismuth-silver sulfosalt.

Malachite, Azurite, and Chrysocolla

Malachite is the chief alteration production of chalcocite both at the School Section quarry and at the Mica Lode. A little malachite also stains feldspar in the Main Cut of the Meyers Quarry. Azurite occurs sparingly at the School Section associated with minor chrysocolla and is locally abundant in the Mica Lode core where it forms thick crusts with malachite on dark red microcline.

Bismutite

Bismutite occurs as a secondary mineral at the Meyers Quarry, Mica Lode, Border Feldspar No. 1, and School Section pegmatites. Commonly it occurs as thin light green to gray crusts in fractured quartz. At the School Section and Mica Lode deposits an intergrowth of bismutite and beyerite forms 2-inch earthy pods. Bismutite is a common accessory mineral of many pegmatites in south-central Colorado and northern New Mexico (Heinrich, 1946).

Beyerite

The rare calcium-bismuth carbonate, beyerite, was found at the School Section deposit closely intergrown with bismutite, and at the Mica Lode quarry in relatively pure masses. The detailed mineralogy has been described (Heinrich, 1947).

Limonite and Manganese Oxide

Limonite and manganese oxide, which form by the weathering of triplite, commonly stain the surrounding minerals, microcline, quartz, plagioclase, beryl, and muscovite. Manganese oxide also results from the decomposition of spessartite garnet and stains the associated microcline and muscovite.

Kaolinite

Kaolinite forms as an alteration production of microcline and plagioclase. Less commonly it also replaces beryl, as in the Mica Lode and Meyers Quarry pegmatite. The color varies from olive-green, to gray, to light red.

Calcite and Chalcedony

Botryoidal crusts of earthy, cream colored calcite are very common in pegmatite at the very crest of the School Section hill. It replaces microcline along fractures and cleavage planes. Although no limestone remnants now cap the hill, it seems clear that there has been relatively little erosion of the knob since the cover of sediments was stripped away, and the secondary calcite probably was derived from Morrison limestone.

Veinlets of gray chalcedony occur in the Colfelco No. 12 pegmatite, which lies near the Morrison contact. Similar veinlets occur in pegmatites of the injection gneiss along the Morrison contact near the south edge of the area. Because of the close association with the sedimentary rocks, it appears likely that the silica was derived from them and deposited in fractures in the pegmatite bodies which these rocks formerly covered.

DESCRIPTIONS OF SELECTED DEPOSITS

History

One of the earliest references to mica deposits in Fremont County is found in Williams (1883), but the deposits of Eight Mile Park are not specifically mentioned. Holmes (1899) lists seven mica deposits in Colorado, but none in Fremont County.

It is reported that the first mining in Eight Mile Park was done by a Mr. Boyle of Canon City, probably shortly before 1900.[1] According to Sterrett (1923), the deposits have been prospected or worked at different times, but mica mining in Fremont County was most active from about 1904 to 1907. During this period the United States Mica Co., of Chicago, Ill., operated the mines of the Micanite region, and the Canon City Mica Mining & Mills Co. operated the Mica Hill (Mica Lode) mine. The United States Mica Co. had an elaborate trimming plant and a dry grinding mill near the mines. The Canon City Mining & Mills Co. had a dry grinding mill and an experimental plant in Canon City to develop uses for the product. None of the mines was in operation in 1908 and 1913.

[1] Personal communication from Mr. J. E. Meyers.

In 1928 Mr. J. E. Meyers of Canon City located a claim on the Mica Lode and operated it alone for a year and then with a partner, Mr. B. O. Halstead. Mr. Meyers sold his half interest in 1930, and shortly thereafter the property came under the control of the Western Feldspar Company (now Magnusson and Sons) of Denver. In 1939, after several years of litigation, the deposit was acquired by the Colorado Feldspar Company of Canon City (a subsidiary of the Consolidated Feldspar Corporation of Trenton, N. J.). It has been leased for many years to Robert Shipley of Canon City who constructed a small crushing and screening plant for mica separation.

The Meyers Quarry pegmatite (also known as Meyers-Halstead Quarry) was prospected in 1929 by Mr. Meyers and was operated intermittently until 1945 by the Colorado Feldspar Company. Seven claims, belonging to the company, cover the outcrop of the pegmatite belt along the schist-granite contact from the sedimentary hogbacks as far west as the Mica Lode. Since 1945 several contractors have mined the deposit for short periods.

The land on which the School Section pegmatite crops out is the property of the State of Colorado. It was leased first to Mr. Shipley, who began work in 1929 and continued until 1931. From 1931 to 1935 it was operated by the Western Feldspar Company, after which it lay idle for nearly four years. In 1939 the Colorado Feldspar Company reopened operations which were continued until 1945. A picking belt, constructed in 1944, was used for about a year. In 1945 and 1946 J. E. Meyers worked the deposit.

The Suzana Nos. 1, 3, 4, and 5 pegmatites were prospected by the Colorado Feldspar Company between 1940 and 1943. In 1945 the company explored the enormous Colfelco deposit in order to outline pegmatite reserves for the feldspar flotation mill that it constructed at Gorgemore and placed into operation in late 1947.

Smaller deposits operated and prospected by Mr. Meyers include the Meyers-McMullin, Ring, and Lorain. Magnusson and Sons have prospected the Van Buskirk, Magnusson, and Magnusson Crosscuts deposits. The two Border Feldspar deposits have been worked by Mr. Shipley. Most of the small cuts and pits in the western extension of the School Section pegmatite were made by Mr. Cal Dell of Canon City.

It is estimated that from 1928 to 1946 there have been produced from the district 235,000 tons of feldspar, 30,000 tons of muscovite (chiefly grinding mica), and about 40 tons of beryl.

Marginal Pegmatites

Colfelco

The Colfelco pegmatite, by far the largest in the district, occupies much of the northern half of Sec. 20 and continues westward into Sec. 19, where it is covered by Mesozoic sediments. The sheet-like deposit, which is one mile long and $\frac{1}{4}$ mile wide, trends N. 65° E. and probably has a general element of dip to the southeast. Its sheet-like nature is clearly shown by isolated patches of overlying granite and exposures of granite in footwall "windows." Locally it may be as much as 200 feet thick. In size it compares favorably with a pegmatite in the Georgetown Quadrangle, south of Duck Lake (Spurr, Garrey, and Ball, 1908), which is 1.7 miles long and 0.6 mile in width.

Like most of the marginal pegmatites it is very poorly differentiated, but several distinct rock types can be recognized:

1. The most common contains abundant euhedral graphic granite phenocrysts, 2 inches to 2 feet on edge, in a fine-grained matrix of microcline, quartz, and biotite. Locally muscovite supplants biotite. The phenocrysts comprise 10–80% of the rock.
2. The matrix of type 1 without the blocky graphic granite.
3. A rock composed chiefly of graphic granite (rare).
4. Near some core masses Type 1 grades into a two phase pegmatite composed of quartz-muscovite and quartz-microcline rock.
5. A border phase of fine-grained quartz, microcline, sericite, and magnetite.
6. Rare core pods as much as 50×20 feet in plan, composed of predominant quartz and subordinate microcline in crystals 4 feet or less on edge. In general quartz-free microcline is very rare in the deposit.
7. Along the footwall side of one of the larger core pods near the southwest corner of the mass plagioclase pegmatite has been developed. It contains abundant 6-inch masses of garnet and 3-inch books of muscovite.

Diabase dikes cut the sheet in several places. This relationship is particularly well shown on the south wall of the Gorge where the floor of the pegmatite body is clearly exposed.

The deposit has been prospected by means of a dozen small pits that constitute the recent assessment work by the Colorado Feldspar Company. Most of the outcrop is covered by 22 claims staked by the company who is quarrying the deposit as a source of feldspar-rich pegmatite for its flotation mill at Gorgemore. It is estimated that this deposit contains a minimum of 400,000,000 cubic feet or 32,000,000 tons of pegmatite.

School Section

The School Section pegmatite is the most extensively mined marginal pegmatite. It also appears to be the only marginal pegmatite that has

been markedly affected by hydrothermal replacement. The deposit, which is in the southeast corner of Sec. 16, has been mined from two large open cuts (the Meyers and Shipley Cuts), and from ten smaller cuts and pits (Fig. 14). The northwest-trending Meyers Cut is 300 feet long, 75 to 135 feet wide and 50 feet deep. A bench, 15 feet below the rim has been made at the west end. The Shipley Cut, which trends northeast, is 320 feet long, as much as 160 feet wide, and 25 feet deep. A level, 10 feet below the cut floor, was begun from the southeast.

The pegmatite, which trends N. 73° W., is an irregular sheet-like body that splits northwestward into several flat-lying arms. The exposed length is about $\frac{1}{2}$ mile, the maximum width is 500 feet, and the maximum thickness appears to be about 75 feet. In the southeast the general dip is 5–20° SW. but northwestward the dip changes to 10°–15° NE. The sheet-like form of the deposit is well shown by the granite exposed in several footwall "windows" (Fig. 14, Section B-B′) and by the gently dipping hanging-wall contact exposed on the northeast side of the Meyers Cut (Fig. 14, Projection A-A′). Moreover, the shallow gulch northwest of the Meyers Cut has cut through the upper part of the deposit.

Sixteen core pods were mapped, but it is probable that several more have been mined out completely. The pods, which range in length from several feet to nearly 200 feet, are flat-lying shallow masses that parallel the general pegmatite structure. The larger ones contain important concentrations of blocky feldspar, but many of the smaller are composed only of massive quartz.

Underlying, or less commonly partly surrounding, most of the core pods are replacement units of quartz-sodic plagioclase pegmatite in which garnet, muscovite, beryl, black tourmaline, cleavelandite, apatite, and sericite occur in varying quantities. Rarer constituents are columbite, triplite, chalcocite, beyerite, and bismutite. Rosette cleavelandite, black tourmaline, and apatite are especially abundant near the northeast entrance of the Shipley Cut. Triplite is also common there and likewise at the mouth of the Meyers Cut. No concentrations of beryl were noted, but scattered crystals, many of which have cores selectively replaced by albite and quartz, are widespread in these units.

The intermediate-zone rock is typically of two phases: (1) graphic granite and (2) quartz-muscovite pegmatite. Locally graphic granite predominates, and northwest of the Meyers Cut biotite in small flakes and in "tanglefoot" laths becomes an important constituent. In the Meyers Cut many of these laths tend to be normal to the hanging-wall contact. Where biotite is abundant, microcline is dark red. Secondary calcite is common near the crest of the knob.

FIG. 14. School Section pegmatite

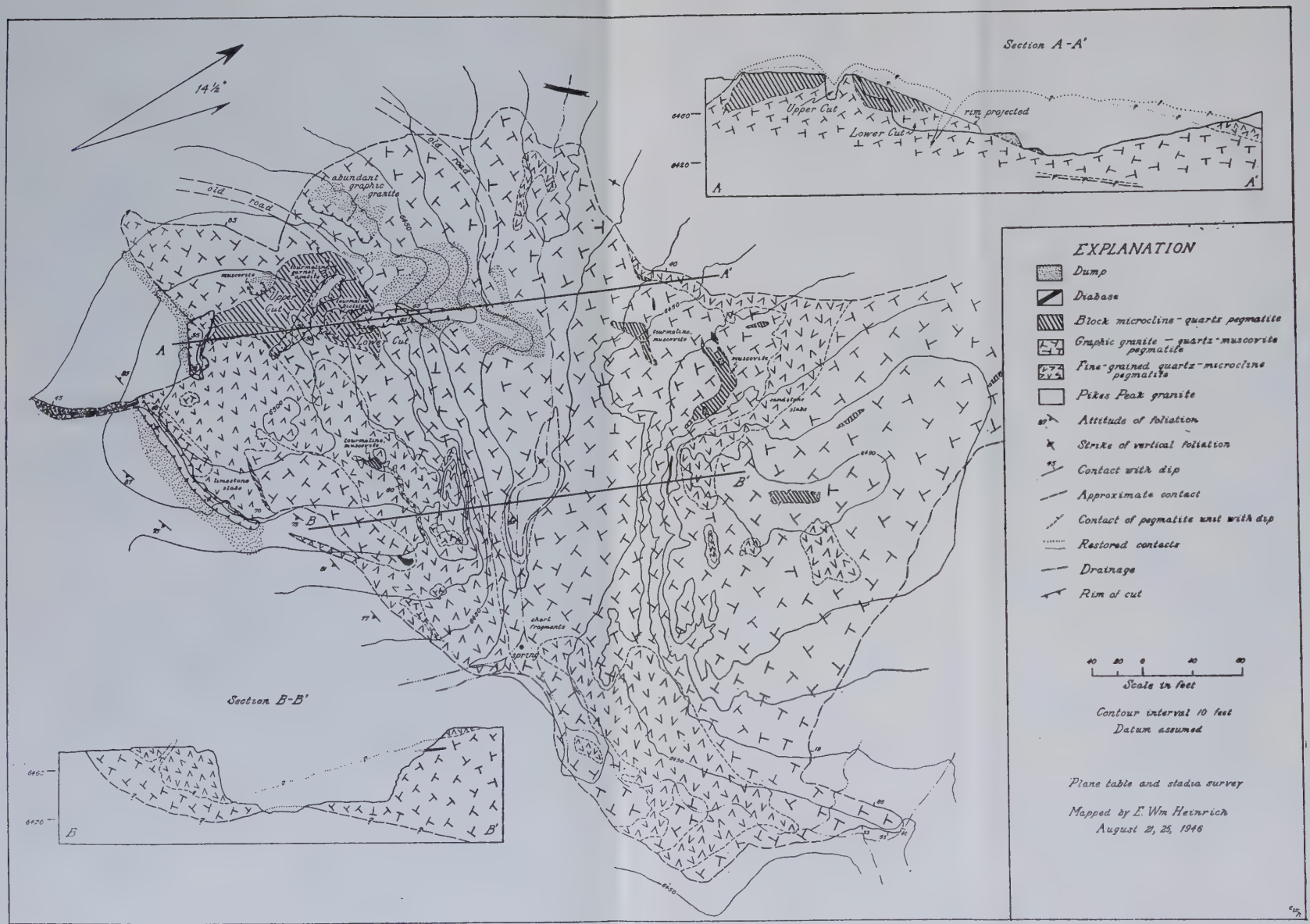

FIG. 15 Van Buskirk pegmatite.

The wall zone, which remains only on the footwall side, probably has been stripped from the hanging wall. It contains graphic granite phenocrysts in a groundmass of fine-grained quartz, microcline, and muscovite. The phenocrysts range in size from 6 inches to 3 feet, and are more resistant to weathering than the matrix. The zone crops out as a ledge with a knobby, irregular surface. Biotite occurs locally. In some parts of the zone phenocrysts are absent and the rock is a fine- to medium-grained quartz-microcline intergrowth.

Although much feldspar has been secured in the past, mining has always been difficult owing to the discontinuous nature of the core pods. Mineable quantities of feldspar are exposed on the northeast side of the Meyers Cut, but many of the other large concentrations appear to be exhausted. The pegmatite has yielded 25,000 tons of feldspar, 200 tons of grinding mica, and several tons of beryl.

Van Buskirk

The Van Buskirk body, which is in the NE $\frac{1}{4}$, SE. $\frac{1}{4}$, Sec. 15 is perhaps the type example of the marginal pegmatites. Only a few small pits have been made in the northern part of the deposit, but the southern third has been explored by means of 2 long cuts, 3 trenches, and a pit (Fig. 15). A gulch cuts across the general north trend of the body to reveal the footwall granite (Fig. 15, Section B-B′). Several roof pendants of granite are exposed in the two main cuts (Fig. 15, Section A-A′).

Three flat-lying pegmatite units are present. Along the hanging wall and footwall are discontinuous zones of fine-grained quartz and microcline with muscovite or biotite or both. The chief rock type is composed of phenocrysts of graphic granite in a fine-grained quartz-microcline groundmass, which grades into rock composed of graphic granite and quartz-muscovite intergrowth. The nearly horizontal core pods, which are generally small, consist of massive quartz and blocky microcline. Commonly they are bordered by scattered crystals of black tourmaline or muscovite. The largest core unit, which is exposed in the southwest corner of the deposit, has been mined from the two main cuts. It is rich in coarse microcline but contains in addition much biotite in blades 4 feet long and 6 inches wide. Along the footwall side is a concentration of red sodic plagioclase in which occur small patches of fine-grained muscovite, abundant black tourmaline, and a little blue apatite.

Exterior Pegmatites

Lorain

One of the most unusual deposits in the area is the Lorain pegmatite in the northern part of Sec. 29. The dike, which ranges in thickness from 5

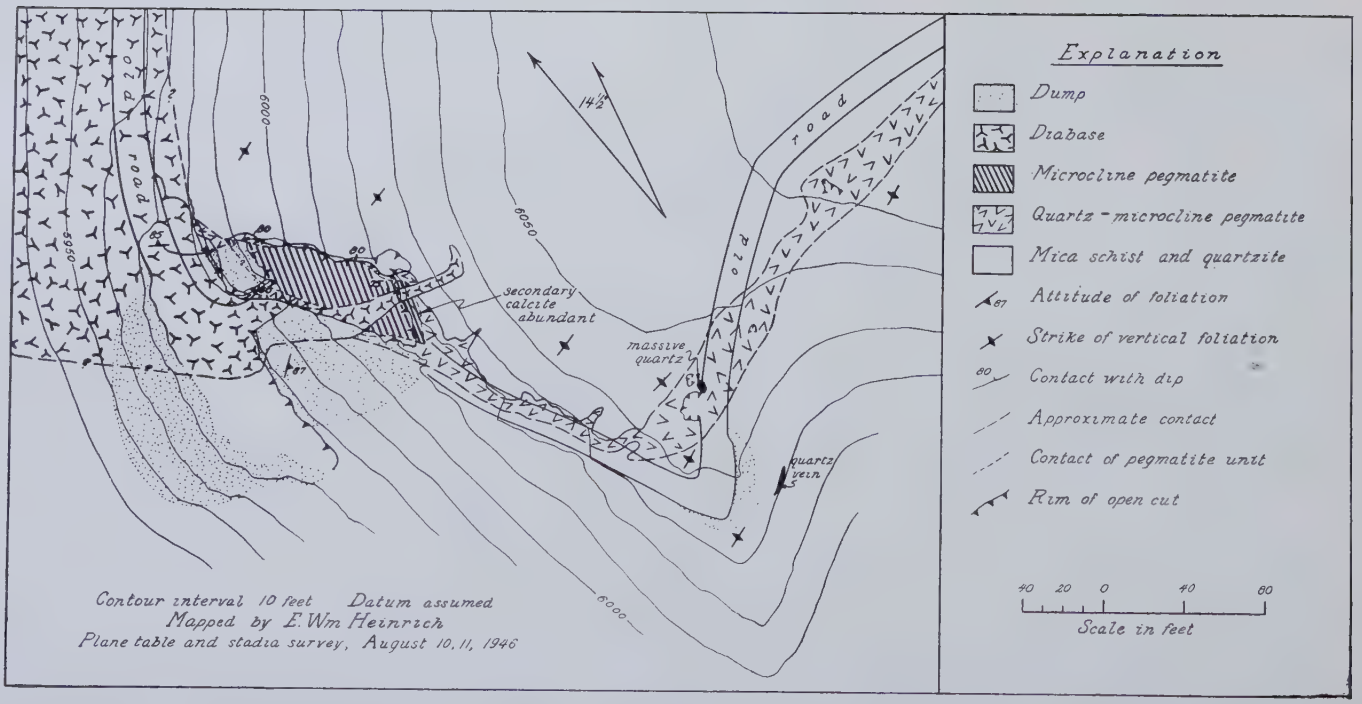

FIG. 16. Lorain pegmatite.

to 35 feet, is L-shaped in plan (Fig. 16). The eastern part, a vertical sill along the metamorphic foliation, strikes N. 80° E., but the crosscutting western arm strikes N. 25° W. and dips 80° NE. The western arm is 250 feet long, and the eastern branch continues for nearly $\frac{1}{4}$ mile. Near the northwestern end a large dike of diabase cuts sharply across the pegmatite.

The thicker western part has been mined from an open cut, 60 feet long, 30 feet wide, and as much as 45 feet deep, which marks the former site of a thick microcline core. Very little quartz was present. The microcline is transected by quartz-plagioclase veinlets on a very minute scale and is replaced by sericite. The core is flanked by thin zones of medium-grained microcline rock with uncommon 1-inch quartz blebs and traces of sericite and garnet. Southeast and east of the cut the dike consists of a fine- to medium-grained aggregate of quartz, microcline, graphic granite and a little muscovite and biotite. A small pod of massive white quartz occurs near the pit in the bend of the dike. Calcite derived from the weathered diabase coats pegmatite in the cut.

Border Feldspar No. 1

The Border Feldspar No. 1 pegmatite, which lies in the SW. $\frac{1}{4}$, NW. $\frac{1}{4}$, Sec. 22, has been mined from a quarry, 100 feet long and 50 feet wide. The floor level is 35 feet below the rim, and a bench lies 8 feet above the floor. The pegmatite body is extremely irregular in shape with numerous roof pendants of schist and many flat rolls in the hanging-wall. In section the body approaches that of a saucer (Fig. 17, Section A-A′). It has a maximum thickness of 50 feet.

The flat-lying, highly shattered core of dark red microcline and subordinate quartz is 10 to 30 feet thick. Fracture-filling biotite in parallel blades 6 feet long, $1\frac{1}{2}$ feet wide, and 4 to 5 inches thick, cuts across the core minerals. Red sodic plagioclase occurs between the blades. In addition 6-inch flat-lying veins of quartz and parallel biotite books transect the core. A moderate amount of feldspar remains to be mined from the core but the dark red color and the abundant biotite considerably reduce its value. Fine-grained plagioclase-quartz pegmatite with minor beryl, garnet, black tourmaline, sericite, and bismutite lies along the footwall side of the core, replacing the medium-grained quartz-microcline-graphic granite rock of the wall zones. Coarse muscovite is uncommon in the deposit.

The country rock is a fine-grained quartz-biotite-garnet schist, one of the few examples of garnet-bearing rocks in the area. The foliation strikes N. 65° E. and dips 75° NW. and the lineation formed by alignment of garnet crystals on the planes of schistosity plunges 60° NE.

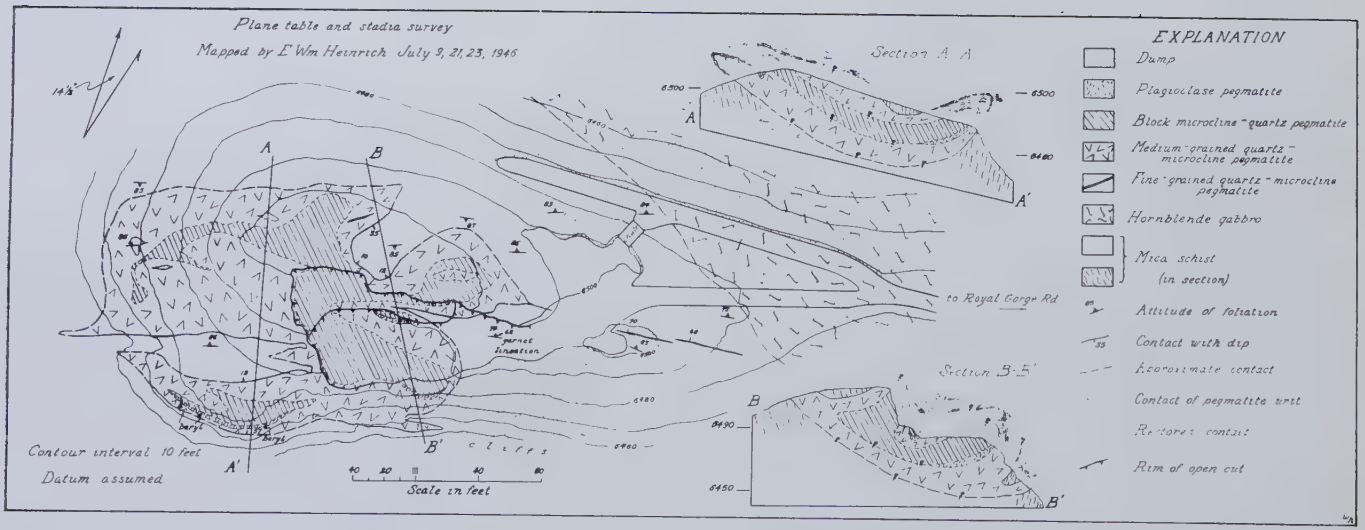

FIG. 17. Border Feldspar No. 1 pegmatite.

Magnusson Crosscut

The Magnusson crosscut is on the south side of the west end of Rattlesnake Ridge in the SW. $\frac{1}{4}$, SE. $\frac{1}{4}$, Sec. 14. It is the only pegmatite in the area developed by underground methods. The crosscut, which is 80 feet long, is opened by a 45-foot entry cut (Fig. 18). The pegmatite body, which is 60 feet thick, strikes N. 78° W. and dips 65–80° SW. On the footwall side the foliation of the muscovite schist strikes on the average N. 70° E. and dipps 44–58° NW., but on the hanging-wall the structure strikes east-west and dips 35° S. Thus the pegmatite appears to have been emplaced along the crest of an anticlinal fold or along a fault.

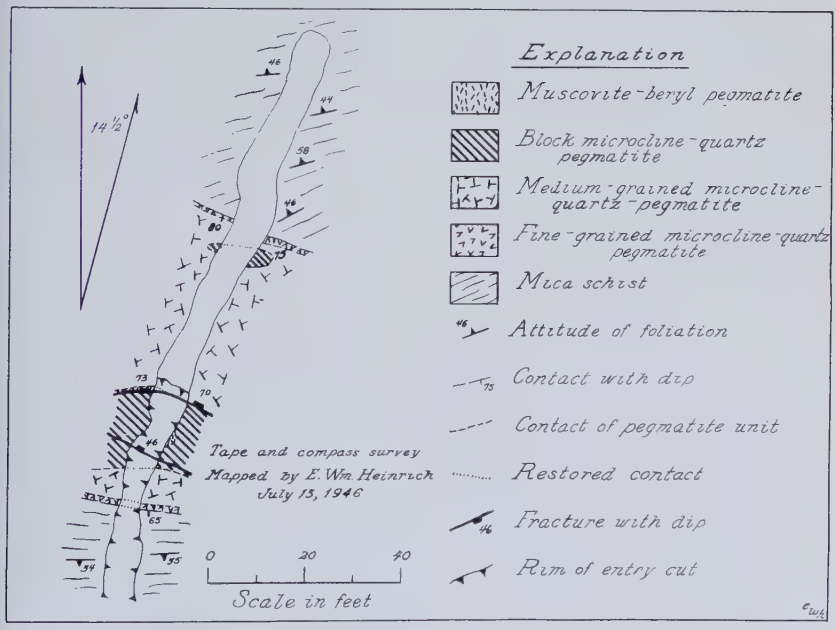

Fig. 18. Magnusson Crosscut pegmatite.

Along both contacts is a thin zone of fine-grained quartz and microcline. The intermediate zone is a medium-grained aggregate of quartz and microcline with abundant graphic granite. The core, which is 15 feet thick, lies near the hanging wall and consists of blocky microcline and coarse quartz partly replaced by plagioclase, "ball" mica, and beryl. On the east side of the entry cut is exposed a beryl crystal 2 feet in diameter and $3\frac{1}{2}$ feet long. Both the core and the replacement pegmatite are cut by several fractures that trend parallel with the core and dip moderately to steeply northwest.

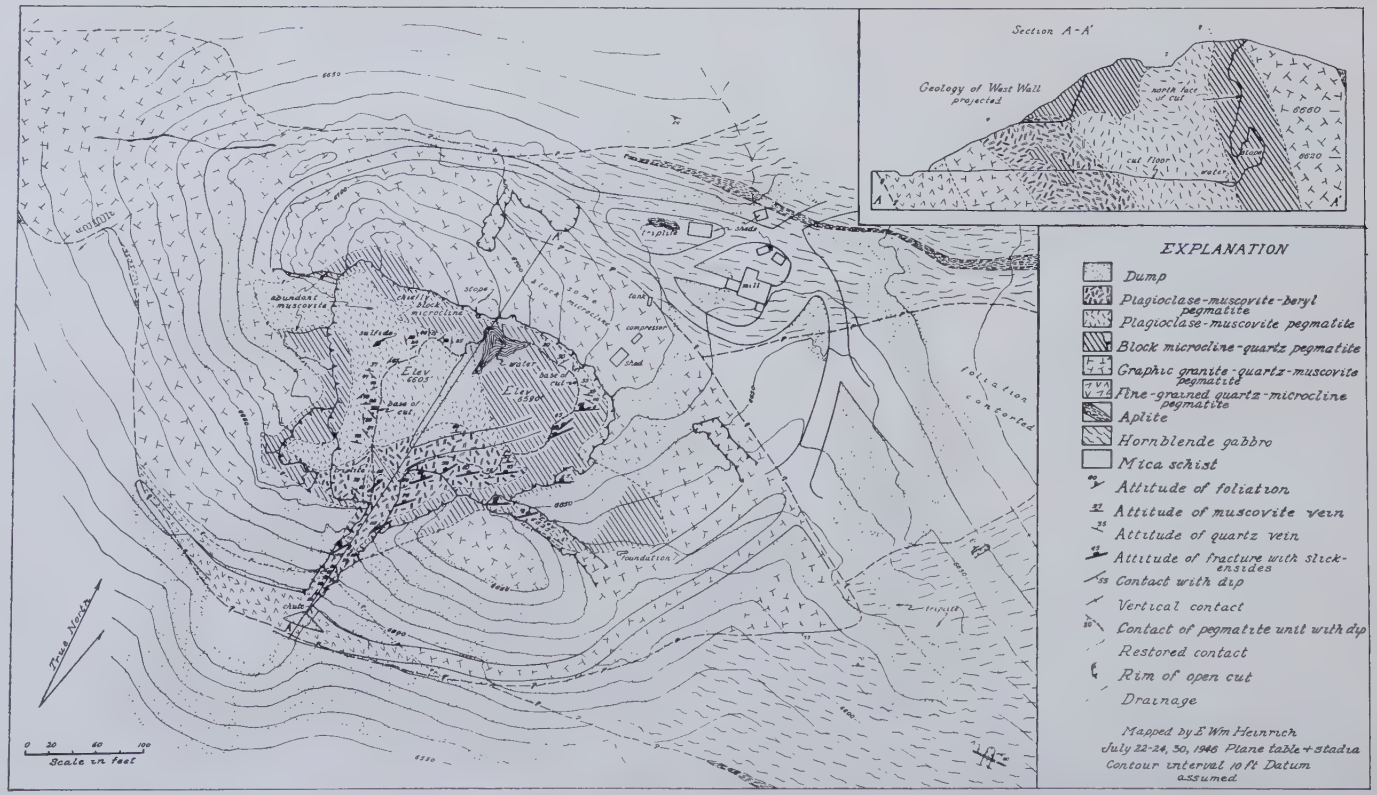

FIG. 19. Eastern part of Mica Lode pegmatite.

Mica Lode

The Mica Lode pegmatite, which is in the NE. $\frac{1}{4}$, SW. $\frac{1}{4}$, Sec. 14, is a lens-like sill, about 1300 feet long and as much as 450 feet wide, that strikes and dips moderately to steeply northeastward. Although the contacts are somewhat obscured by dumps, the offshoots that are so typical of the Meyers Quarry body appear to be largely absent in this deposit. Schist and gabbro alternate along the walls.

The deposit has been mined from an open cut which is 200×280 feet in plan and as much as 150 feet deep at the north face. An irregular stope, 35 feet long and 35 feet high, has been driven into the north face at floor level. Several small benches have been developed at levels 15, 35, and 85 feet above the floor. Two long and narrow entryways lead into the quarry. The one from the east is no longer used and has been left hanging 40 feet above the floor. In addition to the main quarry, four prospect trenches have been dug.

Border zones were not observed, and wall zones are poorly developed and poorly exposed. The stronger development of wall zone rock is on the footwall side. It consists of fine-grained quartz and microcline, with a little muscovite. A few veinlets of muscovite cut across the aggregate. The intermediate zones are very similar in mineralogy and texture to those of the Meyers Quarry pegmatite (see below) and likewise constitute the single largest unit of the deposit.

The core is a single central unit, 400 feet long and as much as 230 feet thick, that dips steeply to the northwest. It is composed of massive pods of white quartz as much as 30 feet long and crystals of red microcline six feet or less on edge. Quartz is somewhat more abundant near the footwall side where a prominent shear zone that trends N. 14–60° E. and dips 43–80° NW., has shattered the rock. The north face of the quarry, which lies near the hanging-wall side of the core, is unusually rich in microcline of very good quality.

Much of the footwall and central parts of the core has been replaced by plagioclase-muscovite pegmatite. This replacement unit is Y-shaped in section with an unreplaced mass of core rock lying between the two arms (Fig. 19, Section A-A′). On the basis of mineralogy two subdivisions are recognized: the southern part, which contains beryl and triplite in addition to the usual muscovite and plagioclase, and the larger northern part which is beryl-free and richer in coarse muscovite.

Muscovite is strongly developed and occurs in spectacular veins and fracture-controlled replacement bodies, 2 to 6 feet thick, and 6 to 20 feet long. The 1- to 3-foot wedge blades are arranged in rosette and comb structures. In addition, abundant masses of "ball" mica, as much as 25 ×30 feet in section, also have been found. The rest of the unit consists of

FIG. 20. Central part of Meyers Quarry pegmatite.

interstitial red sodic plagioclase and quartz, unreplaced remnants of coarse microcline and massive quartz, veinlets of garnet, late veinlets of quartz and albite, rare pods of chalcocite, and garnet.

The fractures that controlled the replacement are abundant. Many are curving and irregular in attitude. Northwest strikes and northeast strikes are almost equally abundant, but dips are more common to the northeast and northwest. Dips to the south are rare. Minor minerals in the beryl-bearing rock are schorl, triplite, apatite, and columbite. Muscovite is less abundant in this lower replacement unit.

The shearing along the southeastern side of the cut probably came close to the end of the period of hydrothermal mineralization, for beryl crystals and muscovite books are also fractured and broken. Some of the fracture planes are coated by white albite and by small flattened quartz crystals. In the small cut in the western nose of the pegmatite a shear zone, similar in strike but dipping 60° SE., fractures medium-grained quartz-microcline pegmatite.

The Mica Lode is the only deposit in the district in which there remain moderate to large reserves of quartz-free feldspar and mica. It is estimated that 175,000 tons of feldspar, 30,000 tons of grinding mica and 30 tons of beryl were obtained from the deposit between 1928 and 1946.

Meyers Quarry

The Meyers Quarry pegmatite is about $\frac{1}{2}$ mile long and as much as 300 feet thick. The main workings, which are in the NW. $\frac{1}{4}$, SE. $\frac{1}{4}$, Sec. 14, include three large open cuts, 15 smaller cuts and trenches, and about a dozen small pits. The Main Cut, the largest, is 100×150 feet in plan and 50 feet deep at the face. The No. 4 Cut to the west, which is 100×50 feet in plan and 55 feet deep, is opened by a deep curving entrance way (Fig. 21). Part of the southwest face is overhanging. The West Cut, 100 feet long and 50 feet wide, contains a bench 20 feet below the rim and the floor 13 feet lower.

The pegmatite is very irregular in shape; it pinches and swells and sends off irregular branches and long apophyses (Fig. 20). The general trend, which is N. 75° E., is parallel with the strike of the country rock structure. It dips on the average moderately to steeply northwest. On the northwest side the wall rock is hornblende gabbro, but on the southeast the chief rock is mica schist. The intrusion appears to have been guided by the contact between the two.

The pegmatite is well differentiated. An incompletely developed 1- to 2-foot border zone consists chiefly of $\frac{1}{4}$- to $\frac{1}{2}$-inch muscovite flakes in a gray quartz matrix. Microcline is generally absent. In a few places, as around the roof pendant of gabbro exposed in the northeast corner of the

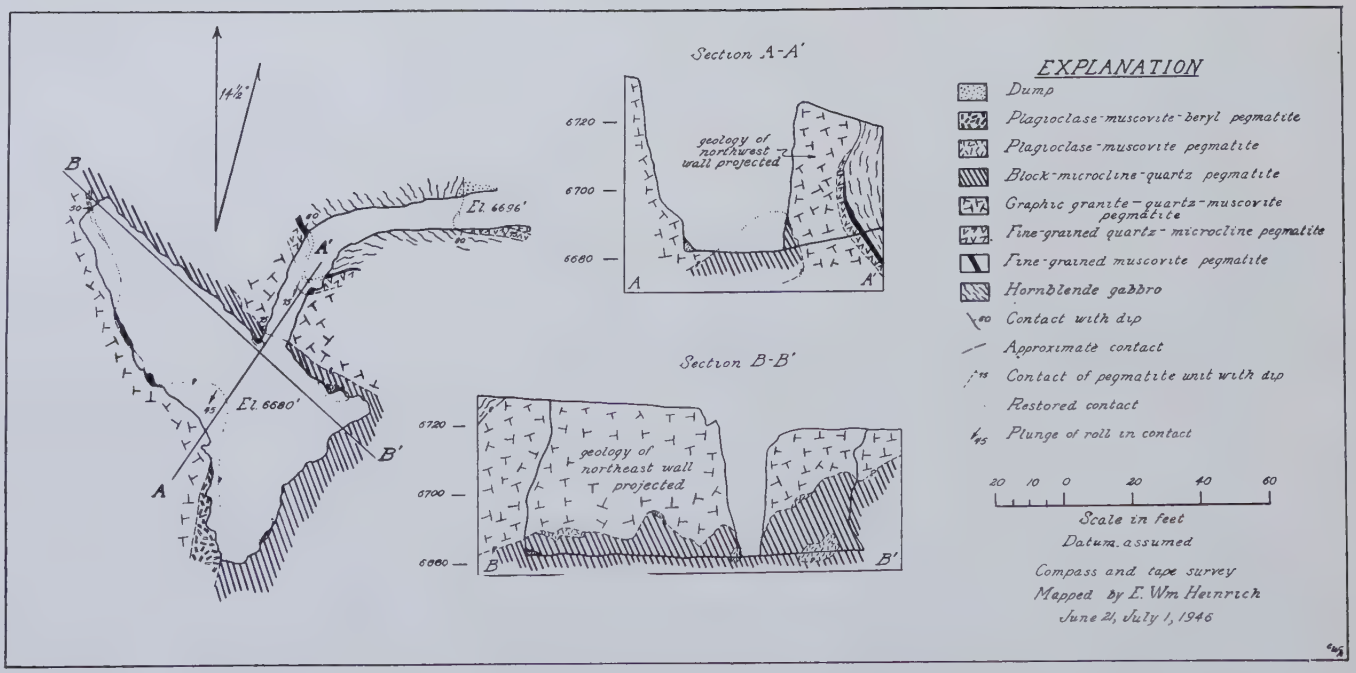

FIG. 21. No. 4 Cut, Meyers Quarry pegmatite.

Main Cut (Fig. 20), there is a thin selvage of muscovite books, $\frac{1}{2}$ to $1\frac{1}{2}$ inches in size, which tend to be normal to the contact.

The wall zone is generally discontinuous and somewhat more strongly developed along the footwall side. The rather uniformly fine-grained rock consists of quartz, microcline, and muscovite. Locally occur streaks and lenticular patches of somewhat coarser quartz and microcline as much as one foot wide and five feet long, parallel with the walls. The zone, which weathers to a pebbly surface, is resistant to erosion, and where well developed tends to crop out as a rib, four to five feet above the flanking schist and intermediate-zone pegmatite. The contact with the intermediate zone is not always easy to define, and commonly a gradation exists.

The intermediate zone, which forms the largest part of the body, is characterized by two petrologic phases: (1) a subgraphic to graphic microcline-quartz rock and (2) a quartz-muscovite rock. Locally graphic granite ("corduroy spar") becomes dominant and may grade into small masses of quartz-free microcline ("embryonic" cores). Other variations include a few scattered blocks of quartz-free microcline generally less than a foot on edge, small clusters of muscovite books four to five inches wide, a few crystals of black tourmaline and garnet, and uncommon blades of "tanglefoot."

The core, which is not a single continuous unit but a number of isolated pods of varying size, contains only massive quartz and crystals of microcline as much as four feet on edge. The largest of these core pods has been mined in the Main Cut and reportedly was unusually rich in microcline. It is a tabular lens whose hanging-wall contact dips 15–20° north and whose footwall dips 50° northward but flattens with depth. According to Mr. Meyers the lens was mined out downward and to the north. Below it lies pegmatite rich in "ball" mica and plagioclase, a footwall replacement unit. Part of this unit is exposed on the walls of the cut.

Another large core pod, somewhat more irregular in shape, was quarried in the No. 4 Cut (Fig. 21). Much good quality microcline remains on the southeast side of this cut, but overhanging walls would make its removal hazardous. Along the west side of the core is a large mass of "ball" mica and sodic plagioclase that dips beneath the core. On the core side of this unit, tapering beryl crystals, as much as 12 inches long and five inches across, are abundant. They tend to lie normal to the contact between the two rock types, with the larger end embedded in the core.

On the crest of the ridge between the No. 4 and the West Cuts another core pod crops out, but it has not been prospected, although some coarse microcline is exposed. A number of smaller core pods occur both east and west of the three main openings. Those to the east are quartz-rich, and those in the western part are very small but are important because they overlie and have localized cleavelandite-lepidolite pegmatite (Fig. 22).

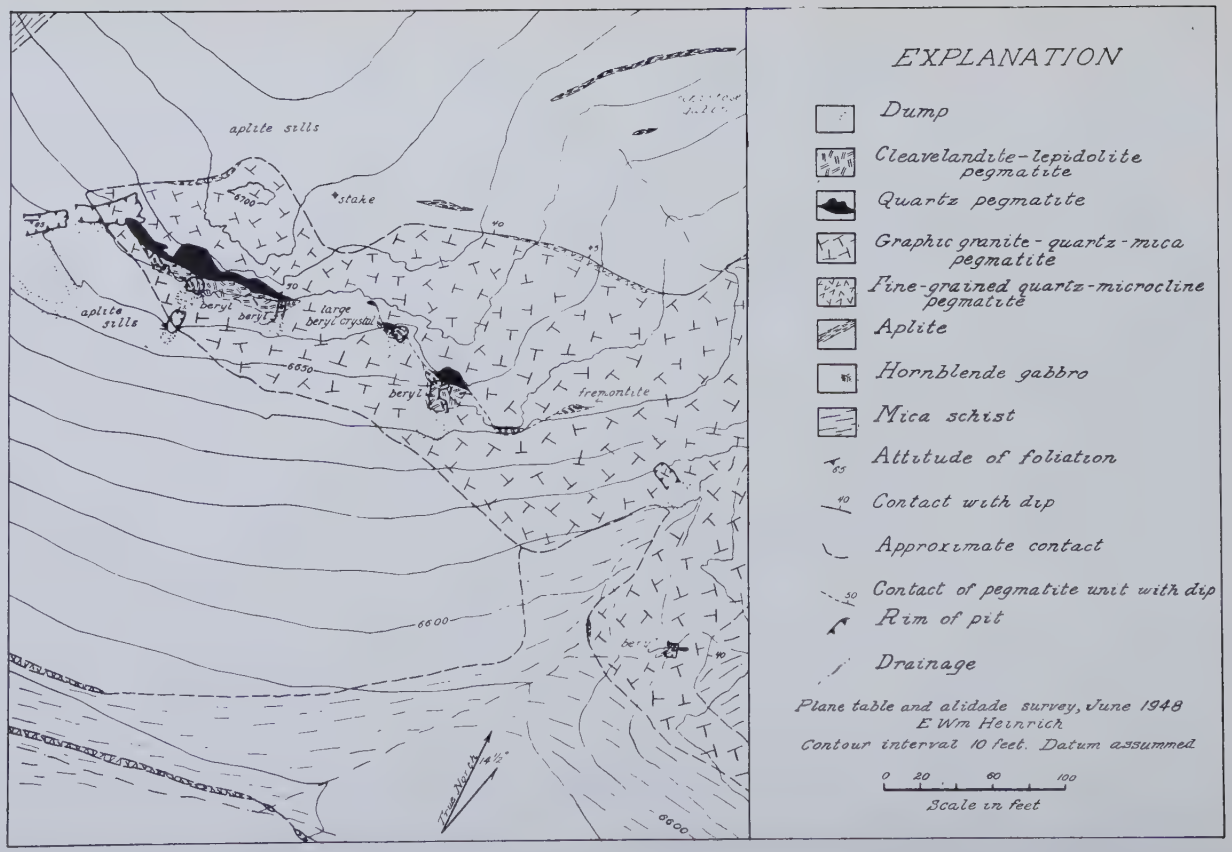

FIG. 22. Western part of Meyers Quarry pegmatite.

These pods dip moderately northwestward in conformity to the general pegmatite dip.

The footwall core-margin units in the Main and No. 4 Cuts consist chiefly of red oligoclase and muscovite. The latter mineral occurs most abundantly in unoriented flaky aggregates ("ball" mica), but tabular bodies of large wedge-shaped blades in comb structure are also common, especially directly along the core contacts. Locally within the cores, microcline has been replaced by small irregular masses of "ball" mica. Plagioclase-muscovite pegmatite is not confined to the footwall sides of cores but is developed only slightly along the hanging-wall contacts. Other minerals found in the units include: in the Main Cut, black tourmaline, garnet, and bismutite; in the No. 4 Cut, apatite, columbite (on dump), tourmaline, and garnet.

Lepidolite-cleavelandite pegmatite is restricted to the footwall margins of the small cores in the western part of the pegmatite. Pale pink to white cleavelandite, the chief mineral, occurs in curved bands and radiating clusters. Most of the lepidolite is in fine-grained flaky aggregates intergrown with quartz and albite. Locally garnet is very abundant, as are black tourmaline, muscovite, and beryl. Beryl occurs in crystals as much as $1\frac{1}{2}$ feet in diameter. Rarer constituents are the colored tourmalines and fremontite. Columbite and cerussite are reported. The replacement unit localized along the schist contact in the gulch (Fig. 22) is distinctly banded with layers of cleavelandite and of quartz and lepidolite.

CONCLUSIONS

The pegmatites are related in position, mineralogy, age, and origin to the batholith of Pikes Peak granite. They are granitic in composition, and red microcline is characteristic of both granite and pegmatite. The pegmatites are younger than the granite and the associated alplite dikes, but are older than the diabase dikes. Both aplites and pegmatites appear to have been intruded relatively shortly after the crystallization of the Pikes Peak magma. It is believed that they are late differentiates of this magma.

The pegmatites occur as three different types: interior, marginal, and exterior. Each type has its own characteristic shape, attitude, and internal structure. Interior and marginal pegmatites are generally lacking in hydrothermal mineralization, which reaches a peak in the larger exterior pegmatites.

The internal structural elements of the pegmatites are divisible into two groups: zones and secondary units. Zones, which formed first, resulted from the crystallization of the pegmatite magma in successive stages inward from the contacts. Slower cooling and consequent coarser texture attended the formation of the inner zones. The development of

the larger crystals also may have been aided by a concentration of volatiles in the central parts of the bodies. Closed system conditions appear to have prevailed during this stage.

Superimposed on this zonal structure are secondary units of several

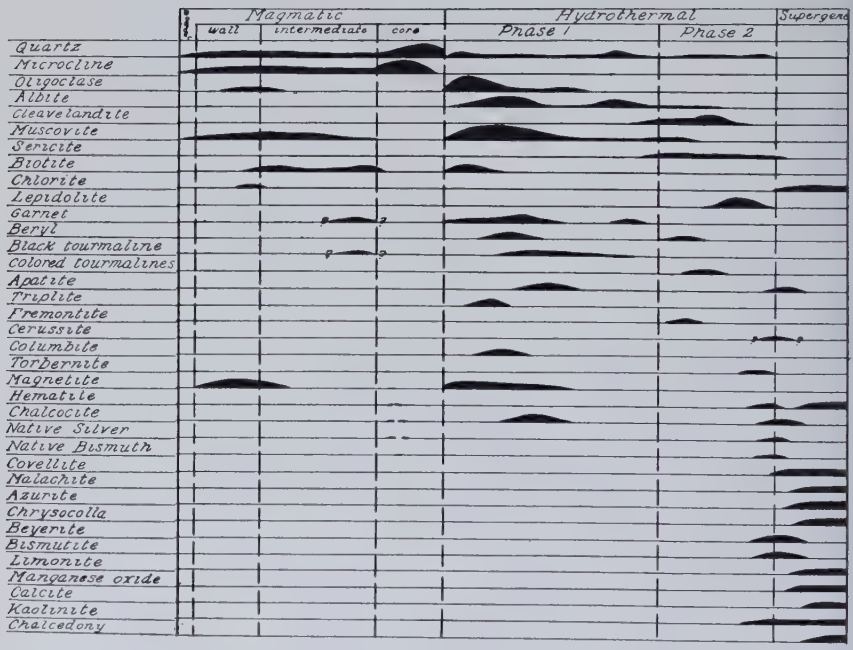

FIG. 23. Paragenesis of the pegmatite minerals.

types: fracture-filled veins, and fracture-controlled and zone contact-controlled replacement bodies. These units transect the zonal structure, cutting one or more zones and replacing parts of a single zone or of several zones. In many cases the guiding fissures can still be discerned; in others only a vague suggestion of fracture control remains. Replacement along the footwall contacts of cores is particularly extensive. Secondary structural units are believed to have formed by the replacement of crystallized zonal pegmatite by material carried by hydrothermal solutions. These solutions may represent further additions to the pegmatite from the original magmatic source (open system conditions) or they may be merely the offspring of the pegmatite magma itself, accumulated as residual, volatile-rich material during the development of the zones. The total amount of pegmatite formed by hydrothermal processes is very small, of the order of 1% of the total volume of pegmatite exposed in the district.

Two distinct hydrothermal phases are present. The earlier is characterized by abundant muscovite and red plagioclase (oligoclase-albite), and by less abundant garnet and black tourmaline. In its more intense aspects apatite, triplite, and beryl are common. Phase 2, which apparently is later, is almost entirely restricted to the western part of the Meyers Quarry pegmatite. It characteristically contains lepidolite, cleavelandite, and the colored tourmalines. Black tourmaline, garnet, and muscovite, which are more typical of the older phase, are corroded and partly replaced. The paragenetic sequence of the minerals is shown diagrammatically in Figure 23.

BIBLIOGRAPHY

Bannerman, H. M. (1943), Structural and economic features of some New Hampshire pegmatites: *New Hampshire State Planning and Dev. Comm., Min. Res. Surv.*, Part VII.

Bastin, E. S. (1911), Geology of the pegmatites and associated rocks of Maine, including feldspar, quartz, mica, and gem deposits: *U. S. Geol. Surv., Bull.* **445.**

Blake, W. P. (1884), Tin ore in the Black Hills of South Dakota: *U. S. Geol. Surv., Min. Res.* **1883,** 602–613.

Blum, Victor J. (1944), A magnetic survey of the Canon City area: *Am. Geophys. Union, Trans.* **1944,** Part IV, 556–558.

——, (1945), The magnetic field over igneous pipes: *Geophysics,* **10,** 368–375.

——, (1946), Geology of the Canon City, Colorado, area: Abst. *Bull., Geol. Soc. Am.*, **57,** No. 2, 1263.

Boos, M. F., and Boos, C. M. (1934), Granites of the Front Range—The Longs Peak-St. Vrain batholith: *Bull., Geol. Soc. Am.*, **45,** No. 2, 303–332.

— — and Aberdeen, Esther (1940), Granites of the Front Range, Colorado: the Indian Creek plutons. *Bull., Geol. Soc. Am.*, **51,** 695–730.

Cameron, E. N., Jahns, R. H., McNair, A. H., and Page, L. R. (1946), Internal structure of granitic pegmatites: Abstr. *Am. Mineral.*, **31,** 191.

——, Larrabee, D. M., McNair, A. H., Page, J. J., Shainin, V. E., and Stewart, G. W. (1945), Structural and economic characteristics of New England mica deposits: *Econ. Geol.*, **40,** 369–393.

—— and Shainin, V. E. (1947), The beryl resources of Connecticut: *Econ. Geol.*, **42,** 353–367.

Campbell, Ian (1937), Types of pegmatites in the Archean at Grand Canyon, Arizona: *Am. Mineral.*, **22,** 436–445.

Campbell, Marius R. (1922), Guidebook of the Western United States, Part E. The Denver and Rio Grande Western Route: *U. S. Geol. Surv., Bull.* **707.**

Cross, Whitman (1894A), Geologic Atlas of the United States, Pikes Peak Folio, Colorado, (No. **7**): *U. S. Geol. Surv.*

——, (1894B), Geologic Atlas of the United States, Crested Butte Folio, Colorado, (No. **9**): *U. S. Geol. Surv.*

Darton, N. H. (1906), Geology and underground waters of the Arkansas Valley in eastern Colorado: *U. S. Geol. Surv., Prof. Paper* **52.**

de Almeida, S. C., Johnston, W. D., Jr., Leonardoes, O. H., and Scorza, E. P. (1944), The beryl-tantalite-cassiterite pegmatites of Paraiba and Rio Grand do Norte, Northeastern Brazil: *Econ. Geol.*, **39,** 206–223.

Finlay, G. I. (1916), Geologic Atlas of the United States, Colorado Springs Folio, Colorado, (No. **203**): *U. S. Geol. Surv.*

Frondel, Clifford (1935A), Vectorial chemical alterations of crystals: *Am. Mineral.*, **20,** 852–862.

——, (1935B), Catalogue of mineral pseudomorphs in the American Museum: *Bull. Am. Mus. Nat. Hist.*, **67,** 389–426.

Fuller, Margaret B. (1926), Contact metamorphism in the Big Thompson schist of north central Colorado: *Am. Jour. Sci.*, **11,** 194–200.

Gevers, T. W. (1936), Phases of mineralisation in Namaqualand pegmatites: *Trans., Geol. Soc. South Africa,* **39,** 331–378.

Griffitts, W. R., Heinrich, E. Wm., Jahns, R. H., Olson, J. C., and Parker, J. M. III, (1946), Occurrence of mica-bearing pegmatites in the southeastern states: Abstr. *Am. Mineral.*, **31,** 194.

Grimsley, G. P. (1894), The granites in Cecil County in northeastern Maryland: *Jour. Cincinnati Soc. Nat. Hist.*, April and July, **1894,** 19.

Harcourt, G. Alan (1937), The distinction between enargite and famatinite (luzonite): *Am. Mineral.*, **22,** 517–525.

Headden, W. P. (1905), Mineralogic notes, No. 11: *Proc., Colo. Sci. Soc.*, **8,** 57–58.

Heinrich, E. Wm. (1946), Bismuth minerals in Colorado and New Mexico pegmatite Abstr. *Am. Mineral.*, **31,** 198.

——, (1947), Beyerite from Colorado: *Am. Mineral.*, **32,** 660–669.

——, (1948), Fluorite—rare earth mineral pegmatites of Chaffee and Fremont Counties, Colorado: *Am. Mineral.*, **33,** 64–75.

Hess, Frank L. (1933), The pegmatites of the western states: Ore Deposits of the Western States (Lindgren Volume) 526–536. *Amer. Inst. Min. Met. Eng.*

Hitchcock, Edward (1933), Report on the geology, mineralogy, botany, and zoology of Massachusetts: *Mass. Geol. Survey.*

Holmes, J. A. (1899), Mica deposits in the United States: *U. S. Geol. Survey, 20th Ann. Rept.*, Part 6 (cont.).

Holmquist, P. J. (1910), The Archean geology of the coast regions of Stockholm: *Geol. Fören. Förh.*, **32,** 789–911.

Jahns, Richard H. (1946), Mica deposits of the Petaca District, Rio Arriba County, New Mexico: *New Mexico Bureau of Mines and Min. Res., Bull.* **25.**

Johnston, W. D., Jr. (1945), Beryl-tantalite pegmatites of northeastern Brazil: *Bull., Geol. Soc. Am.*, **56,** 1015–1070.

Kemp, J. F. (1888), *Trans., N. Y. Acad. Sci.*, **7,** 55–56; cited in *Econ. Geol.*, **19,** 709, 1924.

——, (1924), The pegmatites: *Econ. Geol.*, **19,** 697–723.

Kessler, F. C. (1941), Geology of the Royal Gorge Area: *Rocks and Minerals*, **16,** 51–53.

Kuznezova, E. (1931), Materials for the study of pegmatite veins of the Dzirul Massif, Transcaucasia: *Bull., United Geol. Prosp. Serv., U.S.S.R.*, **98,** 1–19.

Landes, K. K. (1932), The Baringer Hill, Texas, pegmatite: *Am. Mineral.* **17,** 381–390.

——, (1933), Origin and classification of pegmatites: *Am. Mineral.*, **18,** 33–56, 95–103.

——, (1935), Colorado pegmatites. *Am. Mineral.*, **20,** 319–333.

——, (1939), Minerals of Eight Mile Park, Colorado: Abstr. *Am. Mineral.*, **24,** 188.

Loughlin, G. F., and Koschmann, A. H. (1935), Geology and ore deposits of the Cripple Creek District, Colorado: *Proc., Colo. Sci. Soc.*, **13,** 219–435.

Lovering, T. S. (1929), Geologic history of the Front Range, Colorado: *Proc., Colo. Sci. Soc.*, **12,** 59–111.

Mathews, E. B. (1894), The granites of the Pikes Peak area: *Bull., Geol. Soc. Am.*, **6,** 471–473.

——, (1900), The granitic rocks of the Pikes Peak Quadrangle: *Jour. Geol.*, **8,** 214–240.

Mohr, H. (1930), Der Nutzglimmer. Borntraeger Bros., Berlin. 275 pp.

Olson, J. C. (1942), Mica-bearing pegmatites of New Hampshire: *U. S. Geol. Surv., Bull.* **931-P.**

PAGE, LINCOLN R., HANLEY, J. B., AND HEINRICH, E. WM. (1943), Structural and mineralogical features of beryl pegmatites: Abstr. *Econ. Geol.*, **38,** 86–87.

PECORA, WILLIAM T. (1942), Nepheline syenite pegmatites, Rocky Boy Stock, Bearpaw Mountains, Montana: *Am. Mineral.*, **27,** 397–424.

PHILLIPS, A. H , AND HESS, H H. (1936), Metamorphic differentiation at contacts between serpentinite and siliceous country rocks: *Am. Mineral.*, **21,** 344–345.

POWERS, WILLIAM E. (1935), Physiographic history of the Upper Arkansas River Valley and the Royal Gorge, Colorado: *Jour. Geol.*, **43,** 184–199.

SCHALLER, W. T. (1911), Natramblygonite, a new mineral: *Am. Jour. Sci.*, **31,** 48–50.

——, (1912), Natramblygonite from Colorado: *U. S. Geol. Surv., Bull.* **509,** 101–103.

——, (1914), Mineralogical Notes, Series 3. *Jour., Wash. Acad. Sci.*, **4,** 354–356.

——, (1916), The amblygonite group of minerals-fremontite (natramblygonite). The crystallography of fremontite: *U. S. Geol. Surv., Bull.* **610,** 141–144.

——, (1925), The genesis of lithium pegmatites: *Am. Jour. Sci.*, **10,** 269–279.

——, AND HENDERSON, E. P. (1926), Purple muscovite from New Mexico: *Am. Mineral.*, **11,** 5–16.

SCHOUTEN, C. (1934), Structures and textures of synthetic replacements in "open space": *Econ. Geol.*, **29,** 611–658.

SCHWARTZ, G. M. (1925), Geology of the Etta spodumene mine: *Econ. Geol.*, **20,** 646–659.

SEKANINA, JOSEPH (1933), Contributions to the mineralogy of Moravian pegmatites: *Publ. Fac. Sci. Univ. Masaryk*, No. **180.**

SHAINEN, VINCENT E. (1946A), The Branchville, Connecticut, pegmatite: *Am. Mineral.*, **31,** 329–345.

——, (1946B), The Branchville, Connecticut, pegmatite: a correction in terminology: *Am. Mineral.*, **31,** 598–599.

SCHAUB, B. M. (1937), Contemporaneous crystallization of beryl and albite vs. replacement: *Am. Mineral.*, **22,** 1045–1051.

SMITH, W. C., AND PAGE, L. R. (1941), Tin-bearing pegmatites of the Tinton District, Lawrence County, South Dakota: *U. S. Geol. Surv., Bull.* **922**-T.

SPURR, JOSIAH E., GARREY, GEORGE H., AND BALL, SYDNEY H. (1908), Economic geology of the Georgetown Quadrangle, Colorado: *U. S. Geol. Surv., Prof. Paper* **63.**

STERRETT, DOUGLAS B. (1913), Mica in Idaho, New Mexico, and Colorado: *U. S. Geol. Surv., Bull.* **530,** 375–390.

——, (1923), Mica deposits of the United States: *U. S. Geol. Surv., Bull.* **740,** 49–56.

STOLL, W. C. (1945), Preliminary report on mica and beryl pegmatites in Idaho and Montana: *U. S. Geol. Surv.* Part I, 10–14.

TIEJE, A. J. (1923), The red beds of the Front Range in Colorado: a study in sedimentation: *Jour. Geol.*, **31,** 192–207.

U. S. Geol. Survey. (**1935**), Geologic map of Colorado. Ed. by George W. Stose.

VAN HISE, CHARLES R. (1904), A treatise on metamorphism: *U. S. Geol. Surv., Mono.* **47,** 720–728.

VLASSOV, K. A. (1946), Classification of granite pegmatites according to their texture and genesis: *C. R. (Dokl.) Acad. Sci., U.S.S.R.*, **53,** 831–834.

VOGT, J. H. L. (1926), Magmas and igneous ore deposits. Part I. *Econ. Geol.*, **21,** 207–233.

WALCOTT, CHARLES D. (1891), Preliminary notes on the discovery of a vertebrate fauna in Silurian (Ordovician) strata: *Bull., Geol. Soc. Am.*, **3,** 153–172.

WASHBURNE, CHESTER W. (1908), The Canon City coal field, Colorado: *U. S. Geol. Surv., Bull.* **381,** pt. 2, 341–378.

WILLIAMS, ALBERT (1883), Mica: *U. S. Geol. Surv., Min. Res.* **1882,** 583–584.

WOLFE, C. W., AND HEINRICH, E. WM. (1947), Triplite crystals from Colorado: *Am. Mineral.*, **32,** 518–526.

ZIEGLER, V. (1913), Lithia deposits of the Black Hills: *Eng. Min. Jour.*, **96,** 1053–1056.

ALPHA-SILICON CARBIDE, TYPE 51R

Newman W. Thibault, *Norton Company, Worcester, Massachusetts.*

Abstract

The morphological and x-ray crystallography, including indexed powder diffraction data, optical properties, etching behavior and chemical analyses of a very rare modification of α-SiC, formerly designated type V, are given in detail. Referred to the smallest hexagonal cell, $a_0 = 3.073$ Å; $c_0 = 128.17$ Å. Formula weights in this cell = 51. Space group $= C_{3v}^5 - R3m$. Densities: observed = 3.218; calculated = 3.217.

Introduction

Twenty years ago Ott (1928) described a modification of silicon carbide containing 51 formula weights per hexagonal unit cell and designated it SiC, type V. Although a morphological study of the crystal could not be made, x-ray study by means of rotation and oscillation photographs established the following constants:

Hexagonal unit: $a_0 = 3.09_6$ Å; $c_0 = 129.0_8$ Å; $Z = 51$.
Rhombohedral unit: $a_{rh} = 43.1_5$ Å; $\alpha = 4° 06'$; $Z = 17$.

During the author's comprehensive study of the SiC types (Thibault, 1944) no crystals of this modification were encountered, but more recently a large, very well-developed specimen of this type was found quite by accident. Preliminary data on this crystal were given in a paper presented before the Crystallographic Society, March 1946 (Thibault, 1946). Ramsdell (1947) has published Weissenberg data obtained from x-ray photographs made of the same crystal, and has substantiated the structure which he had previously deduced (Ramsdell, 1946) from Ott's original data.

Professor Ramsdell has also suggested a more logical method of designating the different modifications. This consists of the number of formula weights in the hexagonal unit cell (rhombohedral types being referred to the hexagonal unit) followed by the letter "H" or "R" depending upon whether the unit cell is hexagonal or rhombohedral. This method of notation appears to be quite satisfactory and is followed in the present paper.

Quite independently Zhdanov and Minervina (1945*a*, *b*, *c*) determined the same structure using Ott's original data.

Optical Properties

The crystal upon which the present paper is based is illustrated by Fig. 1. It was approximately 18×10×5 mm., being attached to a dense mass of SiC at the 18×5 mm. section.

Although macroscopically jet black, a plate cut about 1 mm. thick parallel to the c-axis showed the following pleochroism: ϵ = medium blue; ω = dark blue. Therefore absorption: $\omega > \epsilon$.

Indices of refraction were determined by using sulfur-selenium melts and a black crystal of α-SiC, type 6H, as control. As nearly as could be determined by the method used, ω was the same as that of the control, namely, about 2.63 for the essentially Li-light transmitted by the melt.

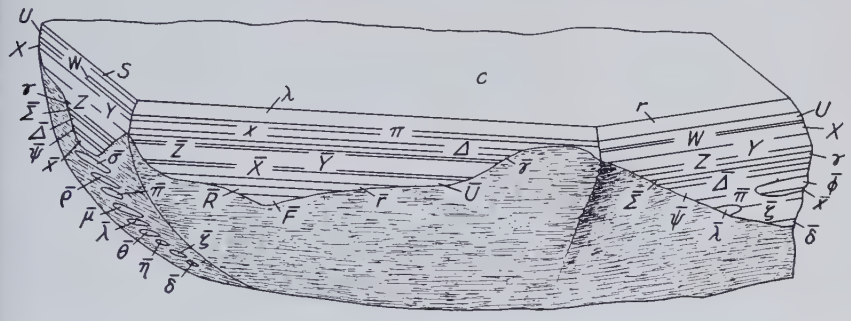

FIG. 1. Alpha-SiC, type 51R (formerly type V).

The index ϵ could not be determined, but it was greater than 2.66. The interference figure was uniaxial positive.

MORPHOLOGICAL CRYSTALLOGRAPHY

Fortunately the crystal was extremely well-developed, containing 76 well-established and 5 somewhat uncertain faces; it was, moreover, entirely free from intergrowths with any of the other α-SiC types.

Table 1 gives the complete morphological data for type 51R; Table 2 includes an angle table, while Table 3 lists the uncertain forms. Although showing rhombohedral-like face development with different series of forms in alternate pyramid zones, these series were entirely different from any of the other SiC types, only the basal pinacoid and the first order pyramids r–$\bar{r}$ and x–$\bar{x}$ being equivalent to forms found on any of the other types.

The observed axial ratio offering the greatest simplification of form indices and yielding simple arithmetical series of forms characteristic of crystals with rhombohedral lattices was 41.699. This is well within experimental error rationally related to the axial ratio of type 6H by a factor of $8\frac{1}{2}$. Because the $c:a$ value of type 6H was determined with great precision, and because the axial ratio of all the other types have also been rationally related to type 6H within experimental error, $4.9070 \times 8\frac{1}{2}$ or 41.710 is accepted as the axial ratio of type 51R.

TABLE 1. MORPHOLOGICAL DATA, α-SiC, TYPE 51R (FORMERLY TYPE V)

Form	Number Times Observed	Quality	Angle Between Form and Base		
			Measured Range	Weighted Average	Calculated Value
c 0001	1	A	—	—	0° 00′
F 1.0.$\bar{1}$.43	1	E	48° 17′	48° 17′	48° 14½′
$\bar{F}$ 0.1.$\bar{1}$.$\bar{4}\bar{3}$	1	C	48° 14½′	48° 14½′	
$\bar{R}$ 0.1.$\bar{1}$.$\bar{4}\bar{0}$	1	C	50° 18′	50° 18′	50° 17½′
r 1.0.$\bar{1}$.34	2	C-D	54° 45½′–54° 49′	54° 47½′	54° 47′
$\bar{r}$ 0.1.$\bar{1}$.$\bar{3}\bar{4}$	2	B-C	54° 44′ –54° 47½′	54° 46′	
S 1.0.$\bar{1}$.31	2	C-D	57° 15′ –57° 16′	57° 15½′	57° 14′
T 1.0.$\bar{1}$.28	1	C	59° 52′	59° 52′	59° 49½′
U 1.0.$\bar{1}$.25	3	C-D	62° 34½′–62° 35½′	62° 35′	62° 34′
$\bar{U}$ 0.1.$\bar{1}$.$\bar{2}\bar{5}$	2	A-C	62° 33′ –62° 34′	62° 33½′	
V 1.0.$\bar{1}$.22	1	D	65° 28′	65° 28′	65° 27′
W 1.0.$\bar{1}$.19	3	C-E	68° 25′ –68° 32′	68° 28′	68° 28′
$\bar{W}$ 0.1.$\bar{1}$.$\bar{1}\bar{9}$	1	E	68° 28′	68° 28′	
X 1.0.$\bar{1}$.16	3	B-C	71° 37½′–71° 40′	71° 38½′	71° 37½′
$\bar{X}$ 0.1.$\bar{1}$.$\bar{1}\bar{6}$	2	C-D	71° 30′ –71° 38′	71° 35′	
Y 1.0.$\bar{1}$.10	2	C-D	78° 21′ –78° 24′	78° 22′	78° 16′
$\bar{Y}$ 0.1.$\bar{1}$.$\bar{1}\bar{0}$	2	B	78° 13′ –78° 18½′	78° 16′	
Z 10$\bar{1}$7	3	B-C	81° 39½′–81° 53′	81° 45′	81° 44′
$\bar{Z}$ 01$\bar{1}$7	2	B-C	81° 42½′–81° 44′	81° 43′	
γ 10$\bar{1}$1	3	C	88° 46½′–88° 49′	88° 47½′	88° 48½′
$\bar{\gamma}$ 01$\bar{1}\bar{1}$	2	C	88° 46′ –88° 49½′	88° 48′	
$\bar{\delta}$ 1.0.$\bar{1}$.$\bar{5}\bar{0}$	2	C-E	43° 54½′–43° 56½′	43° 56′	43° 55½′
$\bar{\zeta}$ 1.0.$\bar{1}$.$\bar{4}\bar{4}$	2	B-E	47° 36′ –47° 41′	47° 37′	47° 35′
$\bar{\eta}$ 1.0.$\bar{1}$.$\bar{4}\bar{1}$	1	D	49° 35′	49° 35′	49° 35½′
$\bar{\theta}$ 1.0.$\bar{1}$.$\bar{3}\bar{8}$	1	C	51° 44½′	51° 44½′	51° 43½′
λ 0.1.$\bar{1}$.35	2	C	54° 00′	54° 00′	53° 59½′
$\bar{\lambda}$ 1.0.$\bar{1}$.$\bar{3}\bar{5}$	2	E	53° 59′ –54° 06′	54° 02½′	
$\bar{\mu}$ 1.0.$\bar{1}$.$\bar{3}\bar{2}$	1	D	56° 22½′	56° 22½′	56° 24′
π 0.1.$\bar{1}$.26	2	C	61° 38′ –61° 40′	61° 39′	61° 38½′
$\bar{\pi}$ 1.0.$\bar{1}$.$\bar{2}\bar{6}$	3	B-D	61° 33′ –61° 38′	61° 35½′	
$\bar{\rho}$ 1.0.$\bar{1}$.$\bar{2}\bar{3}$	1	C	64° 25′	64° 25′	64° 28½′
σ 0.1.$\bar{1}$.20	1	E	67° 21′	67° 21′	67° 27′
$\bar{\sigma}$ 1.0.$\bar{1}$.$\bar{2}\bar{0}$	1	B	67° 25′	67° 25′	

TABLE I—*Continued*

Form	Number Times Observed	Quality	Angle Between Form and Base		
			Measured Range	Weighted Average	Calculated Value
x 0.1.$\bar{1}$.17	2	B-D	70° 33′ –70° 38′	70° 36′	70° 33½′
$\bar{x}$ 1.0.$\bar{1}$.17	3	C-E	70° 27½′–70° 30′	70° 29′	
$\overline{\phi}$ 1.0.$\bar{1}$.$\overline{14}$	1	E	73° 50½′	73° 50½′	73° 47½′
$\overline{\psi}$ 1.0.$\bar{1}$.$\overline{11}$	3	C-E	77° 03′ –77° 06′	77° 04½′	77° 08′
Δ 01$\bar{1}$8	2	D	80° 33½′–80° 35½′	80° 34½′	80° 34′
$\bar{\Delta}$ 10$\bar{1}$8	3	B-C	80° 30′ –80° 36′	80° 33½′	
$\overline{\Sigma}$ 10$\bar{1}\bar{2}$	3	C-E	87° 35½′–87° 41′	87° 38½′	87° 37½′

TABLE 2. α-SiC, TYPE 51R (FORMERLY TYPE V), ANGLE TABLE

Hexagonal $-R$; ditrigonal pyramidal $-3m$

$a:c=1:41.710$ $\alpha=4°\,07'$

$p_0:r_0=48.163:1$ $\lambda=119°\,57'$

Lower	Upper		ϕ	ρ	A_1	A_2
	c	0001	—	0° 00′	90° 00′	90° 00′
$\bar{F}$	F	1.0.$\bar{1}$.43	+30° 00′	48° 14½′	49° 45½′	90° 00′
$\bar{R}$		1.0.$\bar{1}$.40	+30° 00′	50° 17½′	48° 13½′	"
$\overline{r}$	r	1.0.$\bar{1}$.34	"	54° 47′	44° 58′	"
	S	1.0.$\bar{1}$.31	"	57° 14′	43° 16′	"
	T	1.0.$\bar{1}$.28	"	59° 49½′	41° 31½′	"
$\bar{U}$	U	1.0.$\bar{1}$.25	"	62° 34′	39° 46′	"
	V	1.0.$\bar{1}$.22	"	65° 27′	38° 01½′	"
$\bar{W}$	W	1.0.$\bar{1}$.19	"	68° 28′	36° 20′	"
$\bar{X}$	X	1.0.$\bar{1}$.16	"	71° 37½′	34° 43½′	"
$\bar{Y}$	Y	1.0.$\bar{1}$.10	"	78° 16′	32° 01′	"
$\bar{Z}$	Z	10$\bar{1}$7	"	81° 44′	31° 01′	"
$\bar{\gamma}$	γ	10$\bar{1}$1	"	88° 48½′	30° 01½′	"
$\bar{\delta}$		0.1.$\bar{1}$.50	−30° 00′	43° 55½′	90° 00′	53° 04½′
$\bar{\zeta}$		0.1.$\bar{1}$.44	"	47° 35′	"	50° 15½′
$\bar{\eta}$		0.1.$\bar{1}$.41	"	49° 35½′	"	48° 44½′
$\bar{\theta}$		0.1.$\bar{1}$.38	"	51° 43½′	"	47° 10′
$\bar{\lambda}$	λ	0.1.$\bar{1}$.35	"	53° 59½′	"	45° 31½′
$\bar{\mu}$		0.1.$\bar{1}$.32	"	56° 24′	"	43° 50′
$\bar{\pi}$	π	0.1.$\bar{1}$.26	"	61° 38½′	"	40° 21′
$\bar{\rho}$		0.1.$\bar{1}$.23	"	64° 28½′	"	38° 36′
$\bar{\sigma}$	σ	0.1.$\bar{1}$.20	"	67° 27′	"	36° 53½′
$\bar{x}$	x	0.1.$\bar{1}$.17	"	70° 33½′	"	35° 15′
$\bar{\phi}$		0.1.$\bar{1}$.14	"	73° 47½′	"	33° 44′
$\bar{\psi}$		0.1.$\bar{1}$.11	"	77° 08′	"	32° 24½′
$\bar{\Delta}$	Δ	01$\bar{1}$8	"	80° 34′	"	31° 19′
$\bar{\Sigma}$		01$\bar{1}\bar{2}$	"	87° 37½′	"	30° 05′

Table 3. Uncertain Forms, α-SiC, Type 51R (Formerly Type V)

Form	No. Times Observed	Angle Between Form and Base Observed	Calculated
$\overline{T}$ 0.1.$\bar{1}$.$\overline{28}$	1	59° 12′	59° 49½′
10$\bar{1}$4	1	85° 50′	85° 15′
1.0.$\bar{1}$.$\overline{47}$	1	45° 31′	45° 42′
10$\bar{1}$5	2	83° 45′ 83° 57½′	84° 04½′

Etching Figures

Small chips removed from the crystal were etched both by immersion in a borax melt at red heat for about 2 hours, and by partial chlorination at about 1200° C. followed by removal of the resulting carbon by oxidation.

In both cases the etch figures were very similar in appearance to those formed on α-SiC, types 15R, 21R, and 33R (Thibault, 1944), and the same symmetry elements are indicated. The crystal class of type 51R is thus ditrigonal-pyramidal, or $3m$ of the hexagonal system. The single basal pinacoid observed on the 51R crystal is the upper form, in conformity with the arbitrary decision made in this respect when the other types were studied in detail.

Chemical Analyses and Measured Density

After the crystal had been studied optically and morphologically, additional small pieces were chipped off the upper base (each chip including basal pinacoid and first order pyramid faces) for equi-inclination Weissenberg and powder diffraction studies. Then the remainder of the crystal was crushed in a steel mortar until it all passed a 200 mesh screen. After ignition in an inclined tube furnace at 900° C. in oxygen for 15 minutes to remove any free carbon which might have been present, the sample was treated with HF-HNO_3 to remove any SiO_2 or free Si as well as iron introduced by powdering the sample. An x-ray powder photograph of a portion of the sample so prepared showed exactly the same pattern as obtained from the chips. There was, therefore, no morphological or x-ray evidence of the presence of any other SiC modification.

Mr. R. M. Rebert, Norton Worcester laboratories, determined the density, d at 30°/4° C. = 3.218, using a 5 cc. pycnometer, and xylene as the displacing liquid. This is the same density as he previously obtained from light green crystals of α-SiC, type 6H (Thibault, 1944).

Mr. Rebert then analyzed the sample according to the method outlined by Lamar (1939). In the following table this analysis is compared with a spectrographic analysis of a portion of the same sample as reported by

Mr. W. M. Hazel, Norton Chippawa laboratories, and with the analysis of light green, type 6H, crystals as previously reported.

	α-SiC, type 51R			α-SiC, type 6H
Element	Spectrographic Analysis	Quantitative Analysis	Theoretical	(Thibault, 1944)
Si	major	69.64%	70.03%	69.78%
C	not det.	29.91	29.97	29.99
Al	minor	0.05		0.01
Fe	minor	0.20		0.10
Ca	minor	0.16		0.16
Mg	minor	<0.01		0.01
Cu	faint trace	not det.		not det.
Ti	faint trace	not det.		not det.
Na	faint trace	not det.		not det.
B	faint trace	not det.		not det.
Total		99.96		100.05

Both analyses indicate a carbon content close to theoretical, the minor elements apparently substituting for Si in the structure. The higher content of iron and/or aluminum in type 51R is probably the cause of its black color compared with the transparent green of the type 6H crystals analyzed.

X-Ray Crystallography

Powder Diffraction Studies. In order to be certain that the sample used for powder diffraction studies was entirely type 51R it was prepared from chips removed from the crystal adjacent to the upper base where morphological study had indicated no intergrowth with any other α-SiC type. The chips were crushed in a steel mortar until all passed a 200 mesh screen, the magnetic removed with an Alnico hand magnet, and the sample further ground for some time in a boron carbide ("Norbide") mortar. For use with the Norelco Geiger-Counter *X*-ray Spectrometer a portion of the ground sample was flowed onto a glass slide using a few drops of dioxane as the liquid medium, no binder being employed. For use in the powder camera, a portion of the sample was mixed with a minute amount of library paste which itself gave no interfering pattern and extruded in the form of a rod approximately $\frac{1}{2}$ mm. in diameter using the technique described by Lukesh (1940).

Complete scans of nearly 90° (2θ) were made using the Brown recorder with chart travel of $\frac{1}{2}''$ per minute coupled to the Norelco spectrometer which was operated under the following conditions:

x-ray slit width	1 mm.
x-ray slit length	6 mm.
Geiger slit width	$\frac{1}{4}$ mm.
Geiger slit length	6 mm.
Amplitude	Maximum
Damping	Minimum
Time constant	5 seconds
Scanning speed	1° (2θ) per min.

Scans were made both with filtered copper and with filtered iron radiations. Although the former is to be preferred because of the greater intensity of the reflections and much more satisfactory recording of the weaker ones, the pattern obtained by the use of iron radiation was very useful because of better resolution of closely-spaced reflections. Figure 2 is a reproduction of the pattern obtained with filtered iron radiation of

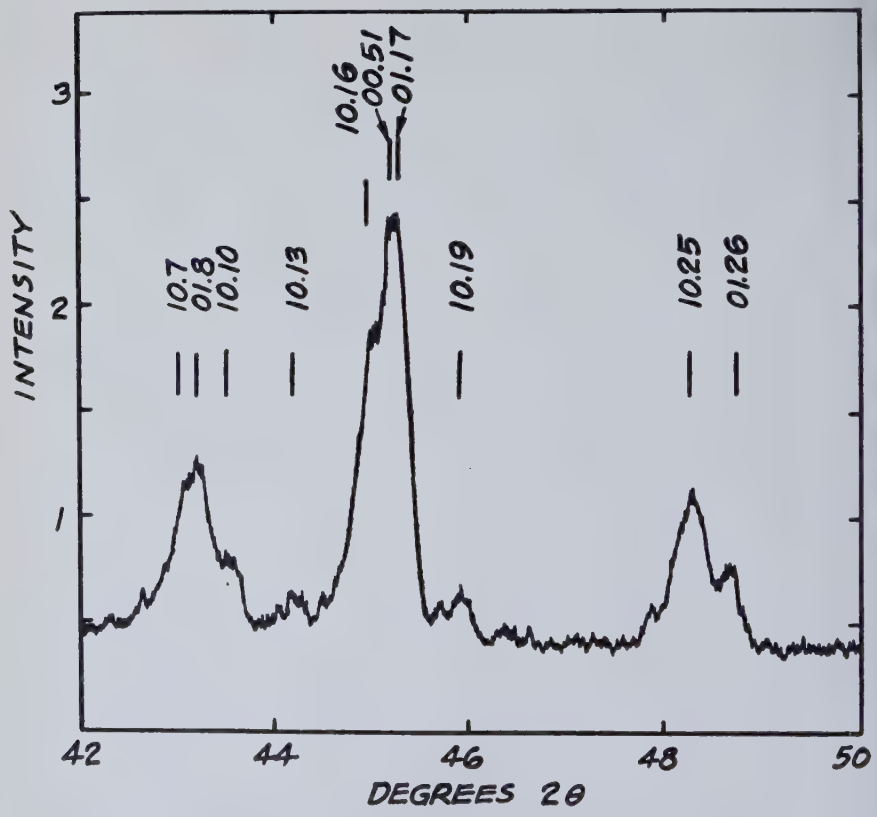

FIG. 2. Pattern obtained from α-SiC, type 51R, using Norelco x-ray spectrometer with filtered iron radiation. Interval: 42°–50° 2θ. *Calculated* positions of the reflections indicated by vertical lines.

the first few reflections in the powder pattern, the interval being $42° - 50°$ (2θ). Note the very excellent agreement between the observed position of the reflections as recorded and the calculated positions indicated by the vertical lines in the upper portion of the figure.

Regular powder photographs were made with the Norelco one radian camera using filtered copper radiation and a collimated beam approximately $\frac{1}{2}$ mm. in diameter. The specimen was rotated but not translated during exposure. Figure 3 is a reproduction of the powder pattern obtained, the portion covered by the scan of Fig. 2 being indicated by the arcs drawn adjacent to the photograph.

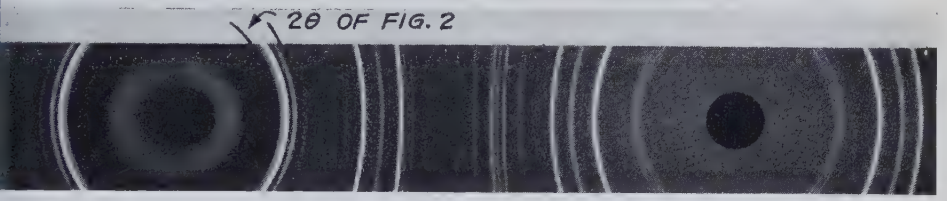

FIG. 3. *X*-ray powder photograph of α-SiC, type 51R. CuK_α radiation. Camera diameter about 57.3 mm. Portion included in Fig. 2 indicated by the arcs.

Data obtained from the various powder diffraction studies are given in Table 4. Values are for the $CuK\alpha_1$ reflections where resolved, otherwise for $CuK\alpha_1$ and α_2. For 2θ up to 90°, the intensity data were derived largely from the spectrometer curves made with filtered copper radiation. Here the strongest reflection was arbitrarily designated 10, the weakest, 1. Reflections not observed on the spectrometer curves, but visible on the powder photographs were assigned intensity values of <1. For 2θ greater than 90°, intensity data were derived from the powder photographs. The reflections were indexed by correlation with Weissenberg exposures, *a*-axis rotations, zero and first levels. Although indexing of the reflections offered little difficulty in the forward reflecting position, considerable uncertainty was often present in the back reflection because of the great number of planes which might contribute to the powder pattern. In many cases where the reflections from two or more planes are practically coincident, it is often impossible to determine whether some of the possible planes actually contributed to the observed reflections. Such cases are indicated by question marks in Table 4. The calculated values for $d_{hk.l}$ were derived from $a_0 = 3.073$ Å, $c_0 = 128.17$Å,* the accepted hexagonal unit cell dimensions of type 51R. The rhombohedral unit cell is $a_{rh} = 42.76$ Å, $\alpha = 4°07'$.

* To be consistent with the earlier work on SiC, the cell dimensions are given in Å, although they are actually kX units.

TABLE 4. POWDER DIFFRACTION DATA FOR α-SiC, TYPE 51R, (FORMERLY TYPE V)

"Line" No.	Intensity	*hk.l*	Equipment*	$d_{hk\,l}$ (Å)	
				Observed	Calculated
1 1a	5	10.7 01.8	G, Fe G, Fe	2.630 2.625	2.634 2.625
2	2	10.10	G, Fe	2.604	2.606
3	2	10.13	G, Fe	2.567	2.569
4	3	10.16	G, Fe	2.526	2.526
5	10	00.51 01.17	G, Fe	2.511	2.513 2.510
6	2	10.19	G, Fe	2.478	2.476
7	1	10.22	G, Cu	2.422	2.421
8	4	10.25	G, Fe	2.362	2.362
9	3	01.26	G, Fu	2.343	2.342
10	1	01.32	G, Cu	2.214	2.217
11	2	10.34	G, Cu	2.173	2.174
12	2	01.35	G, Cu	2.152	2.152
13	1	01.41	G, Cu	2.026	2.026
14	1	10.43	G, Cu	1.984	1.985
15	<1	10.58	P, Cu	1.704	1.700
16	1	01.59	G, Cu	1.685	1.683
17	1	10.61	G, Cu	1.650	1.649
18	<1	10.64	P, Cu	1.596	1.600
19	2	10.67	G, Cu	1.553	1.555
20	5	01.68 11.0	G, Cu	1.538	1.538 1.537
21	<1	10.70	P, Cu	1.510	1.509
22	<1	10.73	P, Cu	1.459	1.466
23	2	10.76	G, Cu	1.426	1.425
24	2	01.77	G, Cu	1.414	1.411
25	1	01.83	G, Cu	1.328	1.335
26	5	02.16 10.85 11.51 20.17?	G, Cu	1.313	1.313 1.312 1.311 1.310
27	1	01.86	G, Cu	1.302	1.300
28	1	02.25	G, Cu	1.290	1.288
29	1	20.26	G, Cu	1.287	1.285
30	1	00.102 02.34?	G, Cu	1.256	1.257 1.255
31	1	20.35	G, Cu	1.253	1.251
32	<1	02.43 10.94	P, Cu	1.214	1.215 1.214
33	1	20.59	G, Cu	1.137	1.135
34	<1	02.61	P, Cu	1.125	1.124
35	1	02.67	G, Cu	1.095	1.092
36	1	20.68	G, Cu	1.090	1.087
37?	<1	02.70	P, Cu	1.073	1.077
38	1	02.76	P, Cu	1.042	1.045
39	1	20.77	P, Cu	1.037	1.039

TABLE 4—(*continued*)

"Line" No.	Intensity	*hk.l*	Equipment*	$d_{hk.l}$ (Å)	
				Observed	Calculated
		10.118			1.006
		12.8?			1.004
40	1	21.10?	P, Cu	1.001	1.003
		01.119			.998
		02.85			.998
		21.16			.998
41	2	12.17	P, Cu	.995	.997
		20.86			.993
		21.25			.987
42	1	12.26	P, Cu	.984	.986
		10.121?			.984
		11.102			.973
43	2	21.34	P, Cu	.971	.972
		12.35			.970
44	<1	02.94	P, Cu	.952	.952
45	1	10.127	P, Cu	.942	.944
46	1	01.128	P, Cu	.936	.937
47	<1	12.59	P, Cu	.913	.913
48	<1	21.61	P, Cu	.906	.907
49	<1	21.64	P, Cu	.898	.899
50	1	21.67	P, Cu	.889	.890
		10.136			.888
51	4	30.0	P, Cu	.886	.887
		12.68			.887
52?	<1	01.137	P, Cu	.882	.883
		21.70			.882
53	2	21.76	P, Cu	.864	.864
54	2	12.77	P, Cu	.861	.861
55	<1	02.118	P, Cu	.841	.841
		10.145			.839
		00.153			.838
56	5	30.51	P, Cu	.837	.837
		20.119			.837
		21.85			.837
57?	<1	12.86	P, Cu	.832	.834
		02.121?			.829
58	<1	02.124	P, Cu	.816	.816
		12.92			.816
59	<1	21.94	P, Cu	.809	.809
60	2	12.95?	P, Cu	.805	.806
		02.127			.804
61	2	20.128	P, Cu	.801	.800
62	<1	20.131	P, Cu	.787	.788
63	1	20.134	P, Cu	.777	.777

* Equipment used: G = Norelco Geiger-Counter *X*-ray Spectrometer; P = Photographic method, 1 radian camera; Fe = filtered iron radiation; Cu = filtered copper radiation.

Weissenberg Photographs. Professor L. S. Ramsdell kindly made zero and first level, *a*-axis rotation Weissenberg exposures of the type 51R crystal. A number of planes which are common to most of the α-SiC modifications are indexed in Fig. 4, the zero level, *a*-axis rotation Weissenberg which has also been reproduced by Ramsdell (1947).

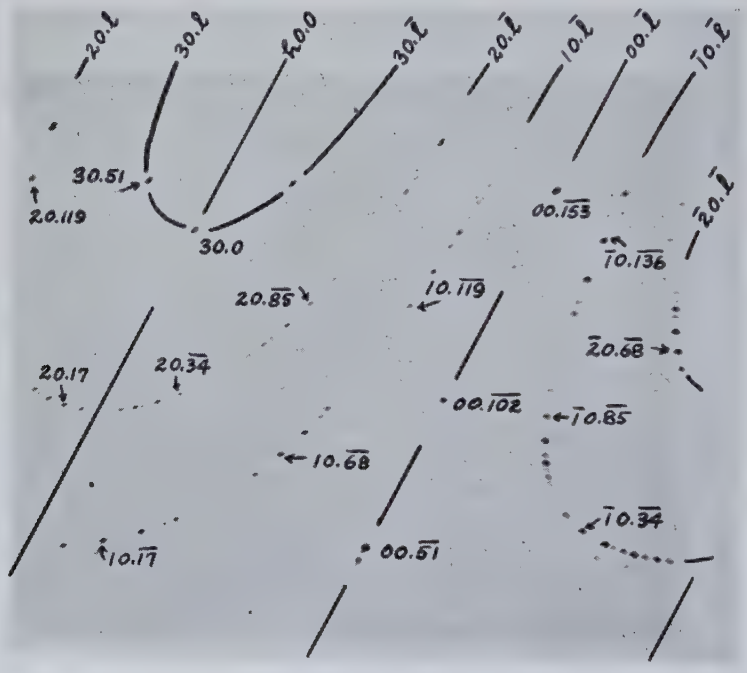

FIG. 4. Equi-inclination Weissenberg photograph of α-SiC, type 51R; *a*-axis rotation, zero level.

The space group of type 51R is obviously the same as that of the other rhombohedral types, $C_{3v}^5 - R3m$, and the calculated density is 3.217, in good agreement with the observed density of 3.218.

ACKNOWLEDGMENTS

The author is indebted to Miss Pauline Krukonis for making many of the calculations necessary in the course of the study, and to Norton Company for permission to publish the paper.

REFERENCES

All published papers on the crystallography of SiC which have appeared since the author's previous work (Thibault, 1944) as well as the articles cited in the present paper are included here.

Donnay, J. D. H. (1943), The morphology of carborundum: *Trans. Royal Soc. Canada*, **37,** sec. 4, 43–47.

Lamar, M. O. (1939) in Furman, N. H., Scott's Standard Methods of Chemical Analysis, Fifth Edition, vol. 1, pp. 813–816. N. Van Nostrand Co., Inc., New York, N. Y.

Lukesh, J. S. (1940), An improved technique for mounting powdered samples for x-ray diffraction: *Rev. Sci. Inst.*, **11,** 200–201.

Ott, H. (1928), Eine Neue Modifikation des Karborunds (SiC): *Festschrift "Arnold Sommerfelds,"* 208–214. S. Hirzel, Leipzig.

Ramsdell, L. S. (1944), The crystal structure of α-SiC, type IV: *Am. Mineral.*, **29,** 431–442.

Ramsdell, L. S. (1945), The crystal structure of α-SiC, type VI: *Am. Mineral.*, **30,** 519–525.

Ramsdell, L. S. (1946), The crystal structure of α-SiC, type V (abstract): *Am. Mineral.*, **31,** 205.

Ramsdell, L. S. (1947), Studies on silicon carbide: *Am. Mineral.*, **32,** 64–82.

Thibault, N. W. (1944), Morphological and structural crystallography and optical properties of silicon carbide: *Am. Mineral.*, **29,** 249–278; 327–362.

Thibault, N. W. (1946), Crystallography of the seven modifications of silicon carbide (abstract): *Am. Mineral.*, **31,** 512.

Zhdanov, H. (?), and Minervina, Z. (1945*a*), X-ray investigations of carborundum: *Acta Physicochim. U.R.S.S.*, **20,** 386–394.

Zhdanov, G., and Minervina, Z. (1945*b*), On the superperiodicity in carborundum crystals: *Jour. Phys.* (*U.R.S.S.*), **9,** 244–245.

Zhdanov, G. S., and Minervina, Z. V. (1945*c*), Analysis of the crystal structure of SiC V (51-layered packing): *Compt. Rend.* (*Doklady*) *Acad. Sci. U.R.S.S.*, **48,** 182–184.

—— (1947), Crystal structure of SiC VI and geometrical theory of silicon carbide structures: *J. Exptl. Theoret. Phys.* (*U.R.S.S.*), **17,** 3–6.

A DIRECT READING ANALYTICAL SPECTROSCOPE*

Frederick K. Vreeland[1]

Abstract

A system of spectroscopic analysis is described which eliminates measurement of wave lengths and reference to tables by direct comparison of the spectrum of the sample with master spectra of the several elements. Master films are built into a spectroscope having an optical system that projects two continuous spectra adjacent to the spectrum of the sample, and the master films are illuminated in their true colors for comparison line by line with the observed spectrum. Elimination films select out the lines of major constituents so the lines of other constituents are apparent for comparison with identification films. The master spectra are classified by index charts.

The spectroscope operates on 115 volts alternating current. The sample is placed on a dispensable refractory hearth adjustably mounted below a horizontal arc. Progressive heating permits successive excitation of the spectra of the component elements and facilitates their identification.

Applications to specific examples of mineral analysis are given.

Introduction

In the May–June, 1947, issue of *The American Mineralogist* Messrs. Peterson, Kauffman and Jaffe, of the U. S. Bureau of Mines, published a paper setting forth the advantages to the mineralogist of the spectroscope as a simple, direct and positive means of determining the constituent elements of a mineral sample.[2]

That paper was timely and appropriate. The present writer has used the spectroscope for this purpose for many years and found it indispensable. The purpose of the present paper is to describe a greatly simpified technique of spectroscopic analysis which is believed to be novel, and an apparatus especially designed for making this technique available to mineralogists and to those who want to get a result quickly and positively without the intricate and exacting process of measuring spectrum lines and searching through tables to decipher them.

This result is accomplished by the use of master standard spectra of the several elements, recorded on films and built into the spectroscope, where they are compared directly with the observed spectrum of the sample.

The instrument thus reads directly in terms of the constituent elements of the sample, without measurements or tables, without the time-

* Letter describing the apparatus and photograph of a direct reading analytical spectroscope, Model No. 3, mailed Aug. 26, 1947. Complete text of manuscript, mailed April 27, 1948.

[1] President, Vreeland Corporation; Laboratory, Mill Valley, California.

[2] *Am. Mineral.*, **32**, 322–335 (1947).

consuming process of photographic recording, and without the necessity of specialized training in spectroscopic technique. The apparatus is self-contained and includes everything necessary for making an analysis. It is designed for operation on an alternating current of 115 volts, without the use of motor-generators or other auxiliary apparatus, so that it may be plugged into an ordinary electric power outlet. It is light and portable enough to be carried in a car for field tests.

The Apparatus

The apparatus used is shown in Fig. 1. *A* is an arc holder, with a dispensable refractory hearth on which the sample is placed. *S* is a switch for turning the arc on and off. *C* is an eyepiece by which the spectrum is magnified and viewed. *D*, *D*, are films on which the master spectra are recorded, placed on both sides of the observed spectrum for direct comparison. *E*, *E*, are knobs for turning the spools on which the master spectrum films are wound.

All the rest is inside the box where the operator can forget it. The optical system is simple. The parts are rigidly mounted on pedestals on a substantial base casting and do not require adjustment. The spectrum is formed by a concave reflection grating of short focus, which not only makes the apparatus compact and simple, but forms a spectrum of great brilliance which is sensitive to elements present in small amounts. The focal length was chosen to give resolution sufficient for the separation of any elements likely to be found in mineralogical work, including minor constituents in irons which, as every spectroscopist knows, require care and precision when the ordinary spectroscopic methods are used.

Referring to Fig. 1, it will be noted that the points of the carbon electrodes of the arc are arranged in a horizontal plane, not vertically as in the usual spectroscopes and spectrographs. The sample is not placed in a hollow of the electrode, as is customary, but on a dispensable refractory hearth below the electrodes. The hearth adjacent to the electrodes has the effect of conserving and concentrating the heat of the arc. The hearth has a vertical adjustment for height, which permits control of the rate of "burning" of the sample, so that the spectra of the several component elements may be excited progressively and studied one by one instead of being all mingled together in confusion.

The alternating current in the arc is stabilized by a fixed ballast which does r ot require adjustment. For exceptional samples of highly refractory material an additional ballast is provided and snapped on by a switch, giving higher temperature in the arc. The optical system is designed to bring the spectrum of the sample to a focus in a curved band 3 mm. wide in the slot *B* between the films *D*, *D*, across which the characteristic lines

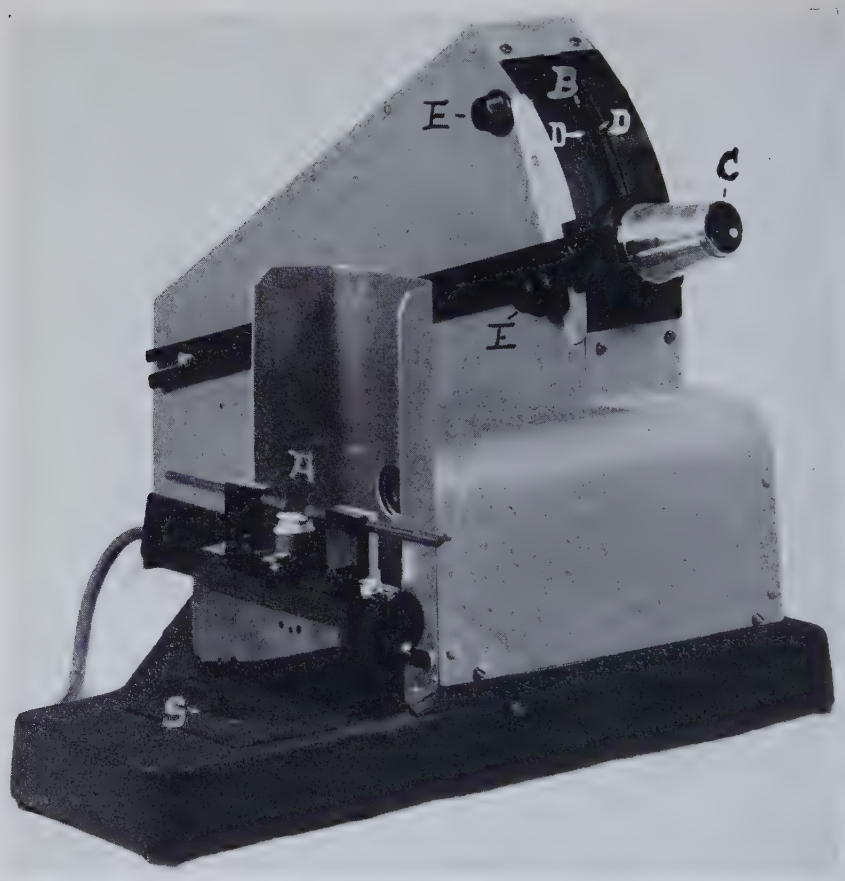

Fig. 1. The Direct Reading Analytical Spectroscope.
A. Arc holder with hearth.
B. Spectrum slot.
C. Eyepiece.
D, D. Master films.
E, E. Film control knobs.
S. Starting switch.

of the component elements appear, like rungs of a ladder, magnified by the eyepiece *C*. The lines are seen in the full brilliance of their colors against a dark background, free from dimming by any continuous spectrum.

The optical system also projects at the same time two continuous spectra, on opposite sides of the line spectrum of the sample and immediately adjacent to it. The films *D*, *D*, carrying the master standard spectra are

arranged parallel to and on opposite sides of the spectrum of the sample, and are illuminated by the two continuous spectra. The master standard films are photographic positives, so that the lines of the standards, each illuminated by the correct part of the spectra, appear in their true spectral colors. They may thus be compared directly with the corresponding lines of the observed spectrum. When the spectrum of the sample and the standard are matched the lines appear continuous and unbroken across the spectrum of the sample and the master film, so that any departure from the standard is immediately apparent.

By this means, not one but all the lines characteristic of an element can be matched against the standard with a precision greater than could be expected by the measurement of the wave lengths of the lines, one by one, by any feasible scale. By the multiple coincidences of all the lines of the spectrum of an element, its identification is assured with precision and positiveness. If there are any lines in the spectrum that do not match, they are recognized at once as belonging to another element or elements, which are thus marked for identification in their turn.

The matching of the standard to the spectrum is assured by using the two *D* lines of sodium as a datum, to which the film is adjusted by means of the knobs *E*, *E*. The *D* lines are recorded on each master standard film and indicated by a marker and, since the *D* lines appear in practically every observed spectrum, the adjustment of the standard to this datum is easy. The *D* lines are exceedingly sensitive and are produced by less than 0.001% of sodium in the sample or the carbons.

Analytical Procedure

A sample is taken, in the amount of something like 25 milligrams, powdered in a mortar and placed on a hearth. The hearth is dispensable. A fresh hearth is used for each sample. Several refractory materials have been found suitable for hearths. For most mineralogical work slips of porcelain may be used if the determination of aluminum or titanium is not required. The china clay used in most porcelains contains a substantial amount of titanium. For exacting work hearths especially made of a purified material are preferable. Hearths of graphite are useful for highly refractory samples.

With the sample in place on the hearth, which is lowered, the switch *S* is turned on and the carbon points brought into contact, then separated, drawing an arc. The hearth is then raised gradually until spectrum lines are seen through the eyepiece. This gradual heating of the sample is a valuable feature, since the several elements vary greatly in their response to excitation. Mercury and antimony appear immediately and are soon volatilized and disappear. The alkalis, sodium, potassium, lithium, etc.,

appear quickly. In some combinations they inhibit the excitation of other elements until they are gone. The heavy metals appear with various degrees of heating. Zinc and cadmium appear soon. The metals of the platinum group require strong heat. The rare earths are slow to appear.

Applying the heat gradually by raising the sample slowly into the arc makes it possible to develop the spectra of the several components successively and pick them out one by one, without confusion. When a pattern of spectrum lines appears, if it is not recognized by the observer, reference is made to an index chart on which all the spectra of the master standards are recorded. When the desired pattern is found on the chart the corresponding master film is rolled into place by the knobs *E*, *E*, and its lines matched against the lines of the spectrum. The identification of that element is then complete and positive. Other components are likewise identified one by one, as they appear, by their line patterns.

This simple system of identifying elements by the patterns of their spectrum lines is in marked contrast with the laborious process usually employed of measuring the wave lengths of individual lines and looking them up in tables. It saves much time, labor, and specialized study. It is more positive and more accurate.

No two elements have the same spectral pattern. Their patterns are distinctive in arrangement and in color, and once learned they can usually be identified by inspection. The comparison of the observed pattern with its master film makes the identification complete. It is like fitting a key into a lock. Each notch of the key corresponds to a tumbler of the lock. So with the spectrum. Each coincidence of a line of the spectrum with an immediately adjacent standard line is highly accurate in itself. When such coincidences are multiplied the possibility of error is eliminated.

The Master Films and Index Charts

The character of the master films may be understood by reference to the index charts used as a guide to the selection of the desired identification film. Figure 2 is a reproduction of one of the index charts. This chart shows the most significant line groups in the spectra of 16 more important metals. The spectra are arranged in the order of the positions of the prominent line patterns in the spectrum, ranging, for this chart, from the violet to the yellow; lead, with its strong violet line, being first on the left and molybdenum, with its yellow triplet, being last on the right.

It will be apparent at once that each element has its own distinctive pattern of lines. It will be noted also that there are certain resemblances as well as differences between the several patterns. The most conspicuous pattern of all, which everybody knows, is the brilliant yellow doublet of

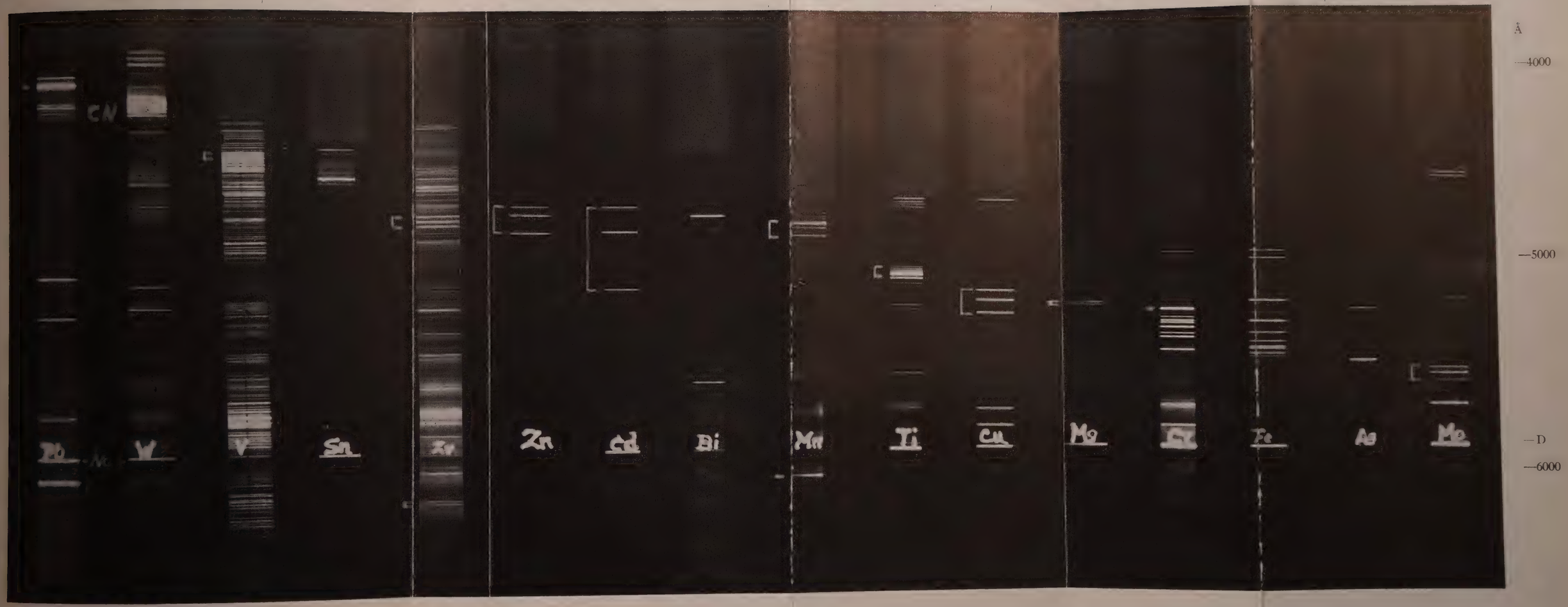

FIG. 2. Index chart of the identification films of 16 metallic elements. Prominent line groups are indicated by brackets.

sodium, the *D* lines of Fraunhofer. These lines, used as the datum for orienting the spectra, are recorded on every master film. They are indicated by the letters identifying the element on each of the films. Sodium has also several weaker doublets, one in the green, one in the red and one in the blue, which are not strong enough to appear in this chart. Potassium likewise, which is listed on another index chart, has a pair of strong lines in the deep red and another pair in the high violet. Aluminum is noted for its several doublets in the ultra violet.

There are physical reasons for these and other line groups in the arrangement of the electrons in the atom, but that is outside the scope of this discussion. We shall find it convenient to use the patterns empirically for identifying the elements.

Referring again to the chart, Fig. 2, it will be noted that there are several groups of three lines, differing in spacing and in color. Zinc (spectrum No. 6) has three bright blue lines. Copper (No. 11) has three similar lines, but they are a vivid green. Cadmium (No. 7) has three blue lines with a wider spacing. Molybdenum (No. 16) has a closer group of three yellow lines. Magnesium (No. 12) has a still closer group of three green lines. Manganese (No. 9) has a triplet of red lines that appear in the reproduction as a single broadened line but are clearly resolved by the instrument into the three components. Manganese has also a vivid group of blue lines. Chromium (No. 13) has a close green triplet with a separation of only 1.5 and 2.4 Å, which shows in the figure as a broadened bright line. It is resolved by the instrument and is the first group to appear when there is a trace of chromium present. When chromium is present in larger amounts the pattern of other green lines appears below the close triplet. Zirconium (No. 5) has a spectrum of many lines, but it is readily distinguished by a group including a bright green triplet, and by another still brighter triplet in the red.

These and other similar groups are valuable because they can be seen at a glance and are unmistakable. They are especially useful in detecting their elements from complex samples. As they flash in and out with variations in the light of the arc they are immediately distinguished as separate from the surrounding lines, and comparison with the master film establishes their identification.

This is an outstanding advantage of the present system of visual analysis over the conventional method of spectrography, where everything is jumbled together and has to be laboriously unscrambled.

Other elements have quintuplets. Titanium (No. 10) has such a group of five blue-green lines, almost equally spaced, which are immediately evident. Vanadium (No. 3) has a closer violet quintuplet of 5 Å spacing

FIG. 3. Identification Spectrum, I, and Elimination Spectrum, E, of iron.

that readily distinguishes its otherwise complex spectrum. Every spectroscopist knows the famous ultra-violet quintuplet of magnesium. The triplet of magnesium here employed is equally distinctive.

Some elements have distinctive pairs of lines more widely spaced. Silver (No. 15) has a green line and a yellow line. The latter has a weaker component 6 Å below it. Bismuth (No. 8) has a wide pair, one blue and the other yellow. Lead (No. 1) has a green pair, not so strong as its outstanding violet line. Tungsten (No. 2) has a closer green pair, besides stronger violet lines.

These and other distinctive line groups and *raies ultimes* are charted on a graduated scale included in the film of master spectra, as a supplementary guide to the master films and index charts, and as a guide for finding suspected elements in the spectrum.

There remains the spectrum of iron, No. 14. Iron has one of the most intricate of metallic spectra. The ordinary working tables of the spectroscopist list some 2500 lines of iron, whose wave lengths are determined with an accuracy of one part in a million or better and are used by spectroscopists as a standard of reference. Its lines are closely spaced over the entire range of the visible and ultra-violet spectrum.

For the purpose of our identification film the number used is reduced to about 25 prominent lines that are visible when iron is present in small amounts. One of these, a strong green line of $\lambda = 5{,}371.493$ Å, is visible when a small trace of iron is present in a sample, and six others near it form a distinctive pattern that is readily identified when any substantial amount of iron is present. Larger amounts bring out a group of blue lines and still larger amounts a group of red lines. Thus identification of iron and a rough estimate of the amount present is readily made by inspection.

When iron is a major constituent, innumerable fine lines appear. To pick out the lines of other constituents of an iron mineral by the conventional method of wave length measurements is a highly exacting problem. By the present method of master standards an elimination film is used. This is shown on a larger scale at *E* in Fig. 3, though much of the fine detail is lost in reproduction. The identification film of Fig. 2, No. 14 is shown on the same scale next to it, at *I*. The elimination film is mounted on one side of the spectrum and the identification film on the other side. By matching the lines of the elimination film against the lines of the sample, any lines that do not match are at once apparent as belonging to a different element and are identified by matching against the appropriate identification film.

Similar identification films of other elements are included so that complex spectra including many elements may be analyzed.

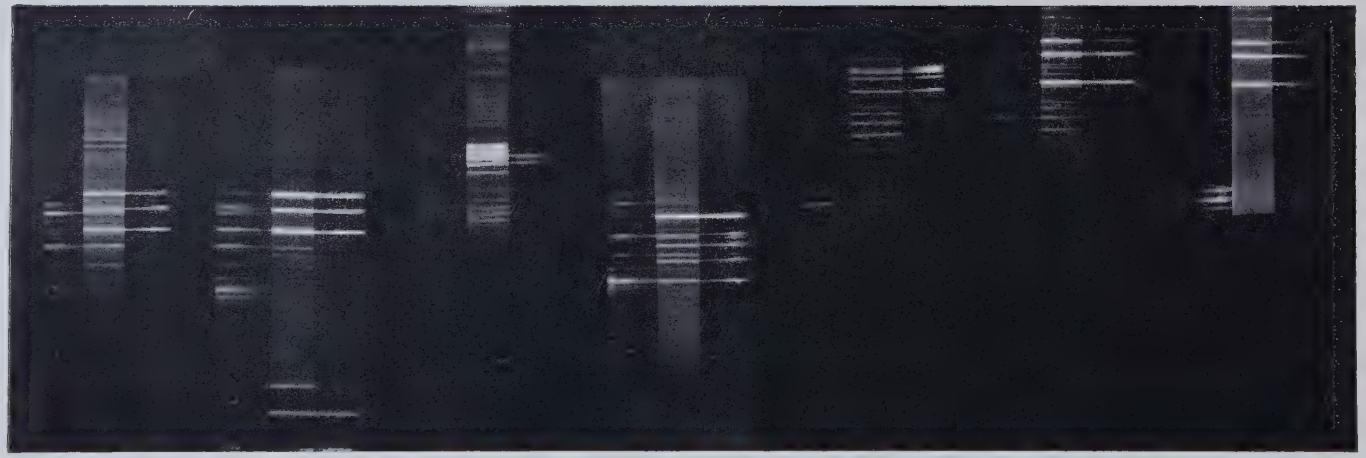

G F E D C B A

FIG. 4.—Spectra of four iron minerals matched against master films. Photographed as seen by observer.

A, B, C—Three aspects of franklinite.

A—Early phase. Zn matched by identification film, right.

B—Later phase. Zn matched right, Fe left, Mn unmatched, weak.

C—Final phase. Mn matched right, Fe left, Zn finished.

D—Chromite. Cr matched right, Fe left.

E—Ilmenite. Ti matched right, Fe not yet developed.

F—Chalcopyrite. Cu matched right, Fe (weak) left.

G—Chalcopyrite, later phase. Cu matched right, Fe left, Ti visible and unmatched.

The procedure in practice is illustrated for several iron minerals in Fig. 4. Each of the figures, A, B, C, D, E, F, G, is a photograph of a part of the spectrum of a sample, made with a camera whose lens was substituted for the eye piece of the spectroscope. The photographs are limited in scope and detail because of the curvature of the field.

A, represents the spectrum of franklinite at the beginning of the "burning." Zinc only has been excited at this time and its three brilliant blue lines are seen matched against the identification film of zinc at the right of the spectrum. The elimination film of iron is shown in part at the left but its lines are not matched in the spectrum. The iron spectrum has not been developed.

B, shows the spectrum of the same sample as it appeared a little later. The zinc lines are still bright. The spectrum of iron is partly developed and its lines are matched against the lines of the iron film on the left. Intermingled with the zinc lines are five other blue lines that do not match either film and so are known as belonging to another element.

C, shows the final stage. The zinc lines have almost disappeared and the five other blue lines, now stronger, are matched against the film of Mn and thus identified. The iron spectrum is well developed and its lines matched against the film on the left.

D, shows the spectrum of chromite. The pattern of chromium green lines is well developed and matched against the film on the right. The spectrum of iron is still weak but the lines that are visible are matched against the iron film on the left.

E, shows the spectrum of ilmenite. The pattern of titanium is well developed including not only the conspicuous blue-green quintuplet, matching the film on the right, but also other less sensitive lines that are not included in the identification film. Titanium is thus shown to be a large constituent. The iron spectrum is not yet developed.

F, shows the spectrum of chalcopyrite in an early stage, with the copper spectrum matched at the right, including its three green lines and two yellow lines in full strength. The iron spectrum is beginning to appear.

G, shows a later stage. The copper lines are weaker and the iron stronger. Titanium is visible faintly as a small constituent.

Without going into unnecessary detail, it may be said that index charts similar to Fig. 2 are made with the elements arranged in groups having natural affiliations, such as the alkali elements, Li, Na, K, Rb, Cs; the elements of the calcium group, Mg, Ca, Sr, Ba; the elements of the platinum group, Ru, Rh, Pd, Os, Ir, Pt; the rare earths elements, etc.

This arrangement is convenient since the elements of each group are often associated in minerals and also because the spectra of the several groups have certain general characteristics in common. The alkali ele-

ments, with their single valence electron, have relatively simple spectra with very strong lines, and are quick to appear. The elements of the calcium group, with two valence electrons, have more complex spectra, with strong lines and slower to develop.

The elements of the transitional group, including the metals shown in Fig. 2 and the metals of the platinum group, are not so readily generalized, but each has a distinctive line pattern.

Gallium, indium, and thallium each have individual lines of outstanding brilliancy. Silicon and beryllium have visible arc lines but they are not strong. These elements are best determined in the ultra-violet. The rare earth elements, with their incomplete *N* shells having different numbers of electrons, are in a class by themselves spectroscopically, as they are chemically. They have spectra of many lines that are slow to develop by which they may be recognized as a group. Since they are practically always mixed in nature, their separate determination by the conventional methods is difficult. By the present method, the elimination films weed out at a glance the lines of the more common elements, such as cerium and lanthanum, leaving the lines of the other constituents clearly marked for identification.

Of the elements of negative valency, P, As, S, Se, Te, F, Cl, Br, I do not produce lines in the visible arc spectrum that are favorable for identification. Some of them, notably fluorine, produce molecular bands that are useful for this purpose, but it is not the purpose of this paper to go into that rather specialized field except for certain examples of unusual interest to mineralogists.

Molecular Band Spectra

One element that is common in minerals, aluminum, has its most prominent lines high in the violet, near the limit of visibility, but it has also a characteristic molecular band spectrum that is useful in identifying it. Like other molecular bands, this consists of many fine lines whose spacing is concentrated toward a series of band heads, which are sharply defined limits of the bands. The element is recognized by the pattern of these band heads on the master film, as in the case of line spectra.

The principal lines of boron are high in the ultra-violet but it also has a band spectrum by which it is identified. Fluorine does not form a line spectrum by arc excitation, but CaF has a brilliant band spectrum in the yellow and red. When F is present without Ca, a little of a calcium compound mixed with the sample produces the band spectrum and shows the presence of fluorine.

The bright bands shown on some of the spectra in Fig. 2, on the violet end, are molecular bands of CN, formed by the combination of carbon of

the electrodes with nitrogen of the air. The fine structure is lost in the reproduction but the pattern of band heads can be seen.

There are many other band spectra that are of interest to specialists but they may usually be disregarded in the analysis of minerals.

Conclusion

The spectroscope here described is designed primarily for qualitative analysis. It is specialized for that purpose. The use of master standards for direct comparison with the visible spectrum, combined with the feature of progressive excitation which causes the elements to appear in succession, greatly facilitates the determination of the constituent elements of the sample, whether simple or complex.

It does not pretend to be a quantitative instrument. However, it is adapted for the semi-quantitative estimation of the relative amounts of the elements present in a sample, by comparison of the spectrum with the identification films and the elimination films, as indicated in the case of iron in Fig. 3.

In general it may be said that a major constituent should show all the lines of the elimination film; a minor constituent, the strongest of those lines; a small percentage, the lines of the identification film; and a trace, only the most prominent lines. These four classes may differ, roughly, by a factor of ten. One may thus distinguish between essential components of a mineral, minor constitutents or isomorphous substitutions, and impurities.

The system is especially adapted to finding the minor constituents of a complex sample. It is useful for the detection of titanium in irons, silver in galena, barium in feldspars, manganese in calcite, hafnium in zircon, cesium, rubidium and thallium in lepidolite, etc; also in such problems as the relation of impurities to color and fluorescence.

It is useful in prospecting for the immediate examination and selection of numbers of samples, and as a guide to detailed assays. In this field it is a great time and labor saver, as well as a guide to the assayer or chemist. It has an advantage over an assay in its ability to locate the presence of an element in small, selected parts of a specimen without destroying the specimen. In the study of rocks, it is not unusual to detect as many as ten or a dozen elements in a single sample.

This system is not a substitute for precise chemical or spectrographic analyses. The writer has made some contribution in the latter field. It is believed, however, that it fits in a niche that is all its own and is not occupied by any system otherwise available.

THE USE OF BECKE LINE COLORS IN REFRACTIVE INDEX DETERMINATION

R. C. Emmons and R. M. Gates, *University of Wisconsin, Madison, Wisconsin.*

Abstract

The dispersion of immersion liquids is generally much greater than that of most minerals of the same refractive index. Colors appear in the Becke line when the liquid and mineral dispersion curves intersect. The colors produced offer a guide to the wave length for which the liquid and mineral have the same refractive index. From the Becke line colors the refractive index of the mineral for the *D* (589 mμ) line can be estimated with accuracy better than $\pm .002$.

Immersion liquids customarily used are selected among other things for their low dispersion (1). The purpose of such a selection is to give the sharpest possible Becke line with white light, meaning one without a pronounced color fringe. Outlined here is a method employed for many years at the University of Wisconsin according to which the detailed appearance of the Becke line colors is used to extend the accuracy and applicability of the method. Specifically, not only do the colors of the Becke line close the gaps between liquids but they also serve to give an extrapolation which enables the operator to estimate the values of proximate indices in related extinction positions.

Becke line colors are explained by the difference in slope between the liquid and mineral dispersion curves and their point of intersection (Fig. 1). In this figure, the liquid and *Y*-ray of the mineral agree in refractive index for wave length 550 mμ. For the shorter wave lengths the liquid is higher in refractive index than the *Y*-ray and for the longer wave lengths the liquid is lower in refractive index than the *Y*-ray. Hence, for the wave lengths shorter than 550 mμ the Becke line will move toward the liquid and for the longer wave lengths the Becke line will move toward the mineral by the customary raising of the microscope tube. But the amount of apparent movement of the Becke line depends as always on the refractive index difference and the refractive index difference is greater for the extremes of wave length. This yields the spectral spread usually observed in the Becke line. If the slope of the dispersion curve of the liquid should agree with that of the mineral, there is, of course, no color in the Becke line. To the extent that the slope of the liquid dispersion curve is greater than that of the mineral a spread appears in the Becke line colors—the spread being greater with a greater slope difference. In general, the lower the mineral and liquid refractive indices, the more nearly the slopes of the dispersion curves empirically agree. And correspondingly, although the dispersion curve slope for minerals usually

increases with an increase in refractive index, the slope increase for liquids is much greater. Hence, colors appear more clearly and more discretely in the Becke line in the study of minerals of high refractive index, when liquid immersion media are being used. Further, in the region of average refractive indices (1.55) the Becke line colors consist ordinarily of yellow

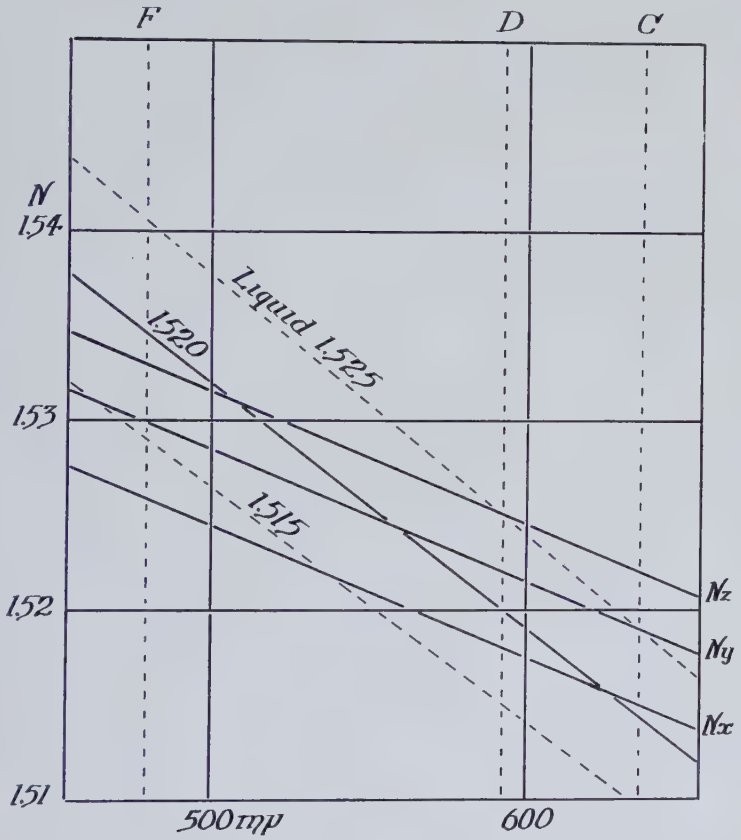

FIG. 1. THE RELATIONSHIP BETWEEN THE DISPERSION CURVES OF MICROCLINE AND APPROPRIATE IMMERSION MEDIA. The overlap in the range of visible light is sufficient to permit all three indices of the average mineral to be determined in one mount in white light.

and blue whereas in the higher values (1.70) an almost complete spectrum can usually be seen. This is to be explained by the principles outlined above. Namely, when the difference in the slopes of the two dispersion curves is sufficient, the spread in the spectral colors is strong enough to overcome blending of colors which takes place in the lower index range.

The refractive index spread acquired by a liquid through its dispersion is also brought out in Fig. 1. The preferred liquid for the mineral would, of course, be liquid 1.520. Also plotted in Fig. 1 in dashed lines are liquids 1.525 and 1.515. Both of these adjacent liquids overlap the dispersion curves of this, an average mineral. For desirable accuracy the refractive index values for any such mineral curves can be satisfactorily estimated essentially without extrapolation through this dispersion curve overlap. The gaps between liquids are literally closed. In the lower refractive index ranges (± 1.40) suitable liquids have not been found to accomplish this—the dispersion curve slopes of liquids and minerals are too nearly equal.

The accuracy of a given refractive index determination by this method depends mainly on two things, (1) how close to the chosen wave length (usually 589 mμ) is the point of intersection of the liquid and mineral dispersion curves, and (2) how effectively the operator can use the available colors of the Becke line. For best results, aiming toward accuracy, two determinations should be made in adjacent liquids on one mineral refractive index curve thereby establishing its slope. Knowing the slope and assuming the slope of other rays of the same mineral to be essentially the same, then any point of intersection at any wave length on another refractive index curve, such as *X* or *Z* in Fig. 1, makes it possible to estimate those indices for the *D* line by drawing their curves parallel to the one in which two determinations are made. That is, it is not necessary to make any determinations for the *D* line itself by mixing liquids. It is desirable, however, to plot results on some such graph as that of Fig. 1, though with practice and for routine work the experienced operator does not do it. Also, the refractive index values of the liquid for other reference wave lengths such as *F* and *C* should be given on the bottle, the value for the *D* line being the liquid reference or tag.

To illustrate the application of the method four cases may be described.

1. In the case of Fig. 1 in which the liquid and the *Y*-ray of microcline agree in refractive index near the middle (550 mμ) of the visible spectrum, the colors of the mid spectrum do not appear since they undergo little refraction at the solid-liquid interface. The colors for the extreme wave lengths are refracted and therefore appear as narrow fringes. Since the slopes of the two dispersion curves are not greatly different at this position on the refractive index scale, these colors are only modestly spread and are therefore blended with adjacent colors of the spectrum. The effect is that of medium yellow and medium blue appearing on opposite sides of the interface.

2. The liquid and the *Z*-ray of microcline (Fig. 1) agree in refractive index in the blue region of the spectrum. The colors of the Becke line here

are rich blue or violet on one side of the interface and a very pale yellow on the other. Since the dispersion curves intersect in the blue, all colors on the violet side are segregated and can produce only a rich blue or violet color. On the other hand, the colors composing the yellow fringe consist of a large part of the spectrum and yield therefore a very pale yellow line.

3. Similarly, the liquid and the *X*-ray of microcline agree in refractive index in the red region of the spectrum and yield for the same reasons a yellowish brown or even a red fringe on one side of the interface and a very pale blue on the other side.

Since the standard record in determinative tables is preferably given for the *D* line, the refractive index of the mineral and liquid may be said properly to agree when the color fringes are rich yellow and pale blue. A brown or red fringe indicates that the mineral is lower than the recorded (*D* line) refractive index of the liquid. Similarly, fringes of medium yellow and medium blue or still more, pale yellow and rich blue indicate that the refractive index of the mineral is higher than that of the liquid. With practice the approximate difference between the refractive indices of mineral and liquid can be well enough estimated that for minerals of average birefringence, such as the feldspars, the refractive indices of more than one ray can be determined from a single mount. In instructing beginning students especially, great emphasis should be placed on the proper recognition of shades of color of the Becke line and their use in the extrapolation of refractive index values.

4. When the dispersion curves differ more strongly in slope as has been pointed out for the minerals of higher refractive indices, the application of the method is both easier and more accurate (Fig. 2). Since for high refractive indices the Becke line may show an almost complete spectrum, it is usually possible to recognize the matching color by scanning the colors seen. A part of the spectrum appears always on one side of the interface and another part on the other side. Between these little or no color is seen but can be readily named. It is the matching color for which the mineral and liquid agree in refractive index. The matching color is best seen when the grain is well below focus. These ideal conditions are quite commonly met even in the very low refractive index range when the mineral dispersion curve has a lower relative slope than that illustrated in Fig. 1.

Should there be any doubt in the recognition of the matching color, a further observation may be made. On raising the focus according to standard Becke line procedure the colors on one side of the interface move toward the mineral and on the other side move toward the liquid. By observing the colors nearest the interface and on both sides of it, the match-

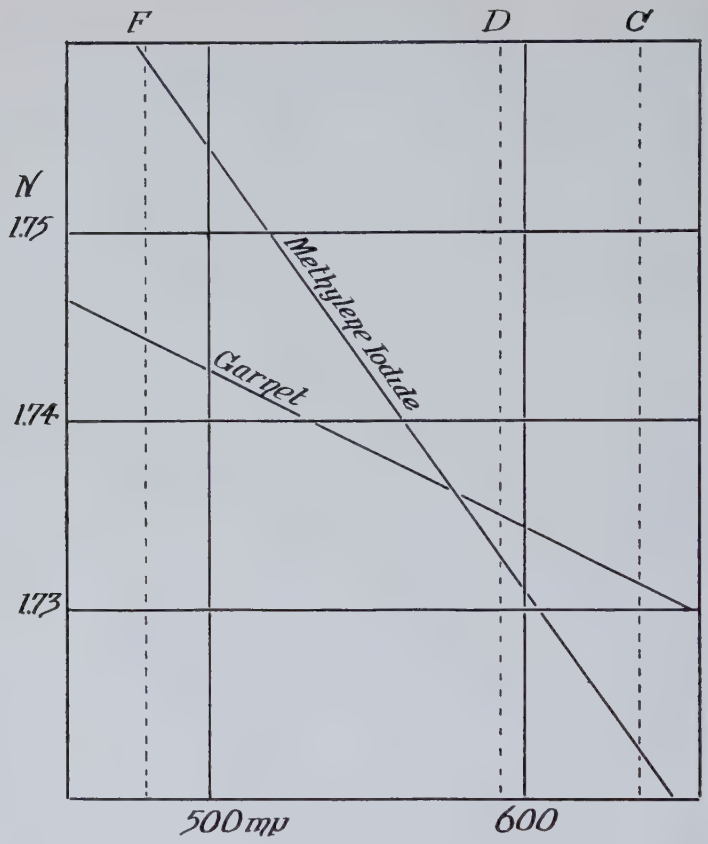

FIG. 2. THE RELATIONSHIP BETWEEN THE DISPERSION CURVES OF GARNET AND METHYLENE IODIDE. This shows the benefits which accrue to a mount in a liquid of relatively high dispersion.

ing color is revealed as lying between them. The greater the slope difference between liquid and mineral dispersion curves, the more accurate is this observation. It essentially fails below 1.50 as stated earlier.

The liquids of standard sets of immersion media ordinarily include α-chloronaphthalene, α-iodonaphthalene, and methylene iodide, all of which have highly satisfactory dispersion. Low dispersion is usually encountered in the liquids in the all important 1.50 to 1.60 range and below it. We have nothing to offer by way of improvement below 1.50. However, ethyl salicylate which is miscible in all proportions with both mineral oil and α-chloronaphthalene may be used to the exclusion of mineral oil above 1.521 and with mineral oil below 1.521. Its dispersion is .021 ($N_F - N_C$) and that of α-chloronaphthalene is .030. This gives

liquids of excellent dispersion above 1.52 and a fair dispersion for 1.50. Fortunately, most work is done in the refractive index range above 1.50. The details are:

Liquid	R.I. (D, 24° C.)	N_F(486 mμ)–N_C(656 mμ)
Methylene iodide and sulfur	1.775±	.0369
Methylene iodide	1.738	.0369
α-iodonaphthalene	1.710	.0368
α-chloronaphthalene	1.633	.030
Ethyl salicylate	1.521	.021
Mineral oil	1.48	.0125

H. Winchell (2) recently published an ingenious diagram for the determination of 2V. The diagram is very helpful also in speeding up routine immersion work by the use of uncentered interference figures. When an optical symmetry plane is vertical (a straight and centered isogyre) and a recognized optical direction appears in the field in such a way that its angle with the microscope axis may be measured, the available refractive indices may be used to learn critical rays by calculations or graphical extrapolation. The calculation is covered elsewhere (3). This detail is most useful when the recognized direction (bisectrix or optic axis) is near the margin of the field making an angle with the microscope axis of about 25 degrees.

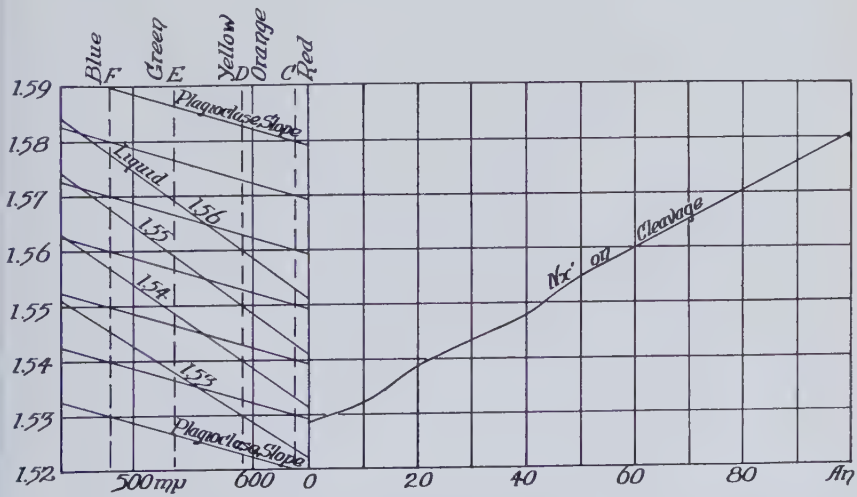

FIG. 3. TSUBOI'S PLAGIOCLASE DETERMINATION METHOD ADAPTED TO WHITE LIGHT. The Hartman scale is substituted for the uniform scale originally used by Tsuboi. The dispersion curves of the recommended immersion media are added. Tsuboi's two $N_{x'}$ curves for 001 and 010 have been averaged.

Another advantage accrues to the use of colors in the Becke line in the determination of feldspars by means of Tsuboi's curve (4)—probably the most used feldspar curve of all. As originally drawn, the curves are intended for data obtained from the use of monochromatic light but are quite amenable to use with white light. In Fig. 3 is one of Tsuboi's curves averaged and his feldspar dispersion curves to which have been added some dispersion curves of the liquids in a specific immersion set (ethyl salicylate and α-chloronaphthalene). The procedure is simple and rapid. As outlined above, determine the approximate wave length at which the Becke line colors are divided and locate this value on the abscissa scale. Follow vertically to the intersection of this value with the dispersion curve for the liquid being used. From this point follow the Tsuboi procedure, namely, follow the feldspar dispersion curve to the *D* line and from there horizontally to the mineral "index cleavage" curve in the right hand portion of the diagram. The abscissa gives the anorthite content as determined by Tsuboi. Although four liquids cover the plagioclase curves, actually two liquids, 1.540 and 1.550, cover all common plagioclases. The Hartman wave length scale has been substituted in the figure for the uniform scale of Tsuboi's original diagram.

Perhaps the greatest value to be offered by the detailed use of the Becke line colors in selected immersion media of high dispersion lies in the avoidance of extra mounts and the mixing of liquids to secure a better agreement.

References

1. Larsen, E. S., and Berman H. (1934), The Microscopic Determination of Nonopaque Minerals: *U.S.G.S. Bulletin* **848.**
2. Winchell, Horace (1946), A chart for measurement of interference figures: *Am. Mineral.*, **31,** 43–50.
3. Emmons, R. C. (1943), The Universal Stage: *Geol. Society of America, Memoir* **8.**
4. Tsuboi, Seitaro (1923), A dispersion method of determining plagioclases in cleavage flakes: *Mineral. Mag.*, **20,** 108.

PROPERTIES AND CHEMICAL FORMULA OF FOURMARIERITE

Henri Brasseur,
Laboratoire de Cristallographie et d'Applications des Rayons X, Université de Liège, Belgium.

Abstract

A comparison of the optical properties of fourmarierite and becquerelite shows a similarity. This, combined with x-ray analysis, is used to deduce the chemical formula of fourmarierite.

Fourmarierite, a very rare uranium mineral, was first studied by Buttgenbach (1), who described it as orthorhombic with $a:b:c=0.883_{17}:1:0.811_5$ and specific gravity 6.046.

The chemical analysis of the mineral was made by Mélon (2). However, the sample used contained not only fourmarierite, but also some kasolite and chalcolite. From his results, Mélon concluded that the formula of fourmarierite should be $PbO \cdot 5UO_3 \cdot 10\ H_2O$. Later Schoep (3) made a new analysis which led him to the composition $PbO \cdot 4UO_3 \cdot 5H_2O$.

The optical properties deduced from Buttgenbach's and Schoep's descriptions and from measurements by Billiet, may be represented as $n_\alpha = 1.85$ along a axis, $n_\beta = 1.92$ along c, $n_\gamma = 1.94$ along b axis. Optically it is negative. Examined in convergent light with an immersion objective, a (100) cleavage lamella shows the poles of the optic axes at the edges of the field.

The absolute dimensions of the unit cell have been determined by Brasseur (5) who found $a = 14.52\ kX$, $b = 16.72\ kX$, $c = 14.07\ kX$, and pointed out that, assuming Buttgenbach's specific gravity value to be correct, the number of the molecules in the unit cell would be either 8.62 (from Schoep's formula) or 6.82 (from Mélon's formula).

Later Brasseur (6), comparing the optical properties of fourmarierite and becquerelite, suggested a possibility of checking the value of M/ρ (M, molecular weight; ρ, density). Although it was possible definitely to reject Mélon's formula, two erroneous facts led to a conclusion which should be corrected: First, the refractive indices used for becquerelite were those given by Billiet; it has been shown since that these values were incorrect and that the actual indices are:

$$\left.\begin{array}{l} n_\alpha,\ 1.725 \\ \text{or} \\ n_\alpha = 1.735 \end{array}\right\} 1.730 \qquad \left.\begin{array}{l} n_\beta = 1.825 \\ n_\beta = 1.820 \end{array}\right\} 1.822_5 \qquad \left.\begin{array}{l} n_\gamma = 1.830 \\ n_\gamma = 1.830 \end{array}\right\} \text{Schoep \& Stradiot (7), Larsen (8).}$$

Second, the specific gravity had been measured on poor crystals. Under the circumstances, it was decided to re-examine the formula of fourmarierite, taking new data into account.

Thanks to a gift from the "Union minière du Haut Katanga", it was possible to select 15 to 20 mg. of very pure fourmarierite. Using Berman's microbalance, the specific gravity was found to be (at 21° C.) $\rho = 5.755$, $\rho = 5.689$, $\rho = 5.777$. The mean of these values, 5.740 ± 0.051 (21° C.), should be the best value of the density ever given for fourmarierite.

New measurements were also made, by the same method, of the specific gravity of highly pure becquerelite of the same origin. The results obtained, $\rho = 5.125$, $\rho = 5.056$, $\rho = 5.090$, lead to a mean value 5.090 ± 0.035 (21° C.).

Measurements of the refractive indices of becquerelite were made by the prism method $(00\bar{1}):(101)$ in order to confirm the figures given by Schoep and Stradiot, and by Larsen. Three different prisms were used.

Goniometric Angle	Prism Angle	Index parallel to b		Index perpendicular to b	
		578 mμ	541 mμ	578 mμ	541 mμ
132°47′	47°13′	1.816	1.840	1.792	1.809
132°50′	47°10′	1.826	1.840	1.805	1.811
133°15′	46°45′	1.823	1.837	1.798	1.812
Mean Values		$1.82_2 \pm 0.006$	$1.83_9 \pm 0.002$	$1.79_8 \pm 0.007$	$1.81_1 \pm 0.002$

Values obtained for the index n_β parallel to b (for $\lambda = 578$ mμ) are seen to be in good agreement with those published by Schoep and Stradiot, and by Larsen. As to the values obtained for the index perpendicular to b, they give only a check for the accuracy of the measurements of n_α and n_γ and agree better with $n_\alpha = 1.735$.

In order to make the calculations possible, it was necessary to redetermine the formula of becquerelite, taking into account the new value of the specific gravity. The dimensions of the unit cell of becquerelite had been previously determined by Billiet and de Jong (9), who found for this orthorhombic mineral: $a = 13.9$ kX, $b = 12.55$ kX, $c = 14.9$ kX. Our values differ from these by an amount smaller than the experimental error ($\cong 0.5\%$). Accordingly, calculations can be made using these figures. Three formulas have been proposed: $2UO_3 \cdot 3H_2O$ (I), $3UO_3 \cdot 5H_2O$ (II), $UO_3 \cdot 2H_2O$ (III). Formula I leads to 12.81 (i.e. $12 + 6.75\%$) molecules per cell; formula II leads to 8.46 (i.e. $8 + 5.75\%$) molecules per cell; formula III leads to 24.90 (i.e. $24 + 3.75\%$) molecules per cell. The space group being V_h^{16}, the cell cannot contain either 13 or 25 molecules. There seems to be little doubt that the real formula is nearer $UO_3 \cdot 2H_2O$ than either of the other two.

Using this formula and assuming the coordination of oxygen round the uranium atom to be the same in becquerelite and fourmarierite, calculations lead to the following refractivities. From becquerelite, $I_{UO_3-\beta \cong \gamma} = 20.4$

and $I_{UO_3-\alpha} = 18.0_3$. These values have been used for the following calculations (see (6)), in which $R\rho/M = (n^2-1)/(n^2+2)$, where R is the molecular refractivity; M, the molecular weight; ρ, the density; and n, the refractive index.

Formula	$R_{\beta\simeq\gamma}$	M	$\frac{R}{M}$	ρ	$\frac{R}{M}\rho$	$n_{\beta\simeq\gamma}$	R_α	$\frac{n_\alpha^2-1}{n_\alpha^2+2}$	n_α
$PbO \cdot 4UO_3 \cdot 5H_2O$	112.43	1457	.0772	5.63	.435	1.82			
$PbO \cdot 4UO_3 \cdot 6H_2O$	116.49	1475	.0789	5.70	.450	1.86			
$PbO \cdot 4UO_3 \cdot 7H_2O$	120.55	1493	.0806	5.77	.465	1.90	110.95	.429	1.805
$PbO \cdot 4UO_3 \cdot 8H_2O$	124.61	1511	.0823	5.84	.481	1.94_5	115.01	.444	1.840
$PbO \cdot 4UO_3 \cdot 9H_2O$	128.67	1529	.0841	5.91	$.497_5$	1.99			

It can be seen, from these results, that the most probable formula for fourmarierite should be either $PbO \cdot 4UO_3 \cdot 7H_2O$ or $PbO \cdot 4UO_3 \cdot 8H_2O$. The first one is in good agreement with the measured density but leads to somewhat low values for the indices; the second one is in good agreement with the values of the refractive indices, but gives too high a value for the density.

Whether the formula of fourmarierite should be $PbO \cdot 4UO_3 \cdot 7H_2O$ or $PbO \cdot 4UO_3 \cdot 8H_2O$ cannot be decided from the foregoing results. However, it may be noticed that there is a close similarity between becquerelite and fourmarierite. Both are orthorhombic, optically negative, and the dimensions of the unit cell are, respectively, $a = 13.9$ kX, $b = 12.55$ kX, $c = 14.9$ kX for becquerelite, $a = 14.5$ kX, $b = 16.7$ kX, $c = 14.07$ kX for fourmarierite. This suggests the possibility that the number of oxygen atoms in fourmarierite be 4/3 of the number of oxygen atoms in becquerelite. As the number of oxygen atoms in becquerelite is 120, the corresponding number in fourmarierite would be 160, which points to the formula $PbO \cdot 4UO_3 \cdot 7H_2O$.

In conclusion, I would like to express my thanks to the Union minière du Haut Katanga for providing the necessary fourmarierite and becquerelite samples.

References

1. Buttgenbach, H., *Ann. Soc. Géol. Belgique*, **47,** C 41 (1923–1924).
2. Melon, J., *Ann. Soc. Géol. Belgique*, **47,** B 200 (1923–1924).
3. Schoep, A., *Ann. Musée du Congo Belge*, (1) **1** (II), p. 19 (1930).
4. Billiet, V., *Bull. Soc. franç. Minér.*, **40** (1926).
5. Brasseur, H., *Bull. Soc. Roy. Sc. Liège*, **10,** 369 (1941).
6. Brasseur, H., *Bull. Soc. Roy. Sc. Liège*, **15,** 523 (1946).
7. Schoep, A., and Stradiot, S., *Am. Mineral.*, **32,** 347 (1947).
8. Larsen, E. S., *U. S. Geol. Survey, Bull.* **848.**
9. Billiet, V., and de Jong, W. F., *Natuurw. Tijds.*, **17,** 157 (1935).

A SURVEY OF INORGANIC PIEZOELECTRIC MATERIALS

Paul H. Egli, *Crystal Section, Naval Research Laboratory, Washington 20, D.C.*

Abstract

An exhaustive survey of inorganic piezoelectric materials was made in an effort to develop improved crystals, particularly for underwater sound gear. The field of water-soluble materials was covered thoroughly enough that further prospecting appears unprofitable. The results of this survey, together with all major surveys by previous investigators, are presented in a single table. Sufficient data are presented, concerning the piezoelectric activity of each of the materials investigated to indicate whether they justify further investigation for various applications.

Introduction

This survey was undertaken in an effort to provide improved materials for piezoelectric applications, particularly for underwater sound gear, a goal which influenced both the selection of materials to be investigated and the extent to which each material was studied. The essential properties required for sonar gear are maximum sensitivity, chemical and mechanical stability, and high dielectric breakdown strength.

On this basis, water-soluble inorganic materials represented the most promising field for investigation. In selecting the individual compounds for study, previous surveys were of little value because of obvious errors, discrepancies between different investigations, and lack of quantitative data. Moreover, there were no well established principles by which the piezoelectric activity of a particular compound could be even roughly predicted. Certain generalizations appeared reasonable, but there were no data to confirm them and the possibility of exceptions could not be ignored. For example, it seemed likely that activity would be greatest when there was a large difference in electrochemical potential between constituent ions. It was also suggested that hydrogen bonding, or largely ionic coupling, were necessary; but existing data were not sufficient to confirm these hypotheses.

Attempts were completely unsuccessful to establish firm relationships by which piezoelectric activity could be predicted on the basis of carefully investigating a small series of type compounds. Thus it became necessary to make an exhaustive survey, eliminating from consideration only those compounds which were unsuitable for other reasons, e.g., poor chemical stability.*

* As a result of the survey, the factors which influence piezoelectric activity can be outlined somewhat more confidently and will be discussed in a paper to be released shortly by S. Zerfoss et al.

Test Procedure

The efficiency and reliability of the investigation depended as much on developing new techniques for detecting and measuring piezoelectricity as on the ability to grow crystals. The general goal was to be able to make tests on as small specimens as possible in order to save growing time.

A "click" test, using a modification of a circuit by Giebe and Scheibe was used for the first indication of activity. In general, well-formed crystals down to 100 mesh can be tested on this device. The *NRL* design of this apparatus has proved highly reliable and free of spurious responses so that a click is positive evidence of piezoelectric activity. Moreover, the loudness of the click is a rough quantitative measure of activity. Several other factors including Q (internal mechanical and electrical losses), dielectric, and elastic constants contribute to the magnitude of the click; but the variability of these factors between most crystals is relatively small so that the piezoelectric coupling is the dominating variable.

Absence of any response is less positive proof of lack of piezoelectric activity because the indication may be swamped out on very weak materials by a low Q or by high conductivity. Usually, however, these difficulties can be easily identified by a characteristic sizzling noise so that for all practical purposes the click test is reliable.**

For more quantitative data, a dynamic test procedure was adopted which depends on accurate measurement of the resonant and antiresonant frequencies of the specimen. A low capacity crystal holder and the associated circuits were perfected to the point where reasonably accurate data can be obtained on well shaped specimens as small as 2 mm. cubed. The results of these tests on small crystals have proved in every case to be within 25% of precise measurements on full sized specimens.†

Basis for Selecting the Materials Included in Survey

The first step in compiling the list of materials to be investigated was an exhaustive search through the literature for all inorganic compounds which had ever been reported as having a symmetry structure which permits piezoelectric activity. All such compounds were considered even

** A complete report on the important factors in this test procedure and the design of the *NRL* device has been described. See "An Improved Apparatus for Detecting Piezoelectricity" by Ralph G. Stokes, *Am. Mineral.*, **32**, 670–677 (1947).

† The complete procedure and a description of the equipment were presented in an article entitled "The Approximate Determination of Piezoelectric Properties by Measurements on Small Crystals" by Elias Burstein, published in *The Review of Scientific Instruments*, **18**, 317–327 (1947).

if the more recent structure investigations indicated a non-piezoelectric class.

To this list were added all the compounds that had previously been tested by anyone regardless of their reported results. On the basis of modern symmetry data, many of these compounds would not be considered, but they were included in order that all available information be available from one source.

Finally, to complete the list, it was realized that errors in symmetry classification had caused omissions just as it had caused many non-piezoelectric materials to be included. In the course of the investigation as generalizations were developed concerning the type of chemical formulas which were likely to be piezoelectric, all available compounds of these types were considered, regardless of symmetry data.

Before a material was investigated, a search was made for all available information concerning its properties. On the basis of this information, many compounds were eliminated because of some factor which prevented their having any possible practical application. For example, a long list of sulfides and oxides was eliminated because of high conductivity, and another large group was eliminated because they were chemically unstable at temperatures within usual operating ranges. Many insoluble materials, particularly if naturally occurring, were eliminated because several recent surveys of minerals have failed to discover any compound of value, and synthesis would be excessively expensive.

If, however, a compound was of possible help in confirming some general principle in relating activity to composition and structure, it was investigated regardless of possible practical value. Thus, it seems unlikely that any further prospecting among water-soluble inorganic materials would be profitable.

Description of Results

All compounds which it was thought reasonable to consider are listed alphabetically in Table 1. The first column lists the reported symmetry classifications. No effort was made to check the classifications which are from many sources, and wherever the symmetry listed conflicts with the test for piezoelectricity, it seems certain that the symmetry class is incorrect. In cases where more than one classification is shown, the order in which they are listed is not intended to infer which is most likely. When two classes are listed which differ only by a center of symmetry, the test for piezoelectricity indicates which is more likely correct. The principal reason for including the reported symmetry is for convenience in considering possible applications. For example, the modes of vibration of certain classes are not suitable for high frequency oscillator applica-

tions even though some of the crystals in that class may be strongly piezoelectric.

The second column indicates the results of previous investigators by number as listed in the bibliography. Only the six principal surveys by previous investigators are listed, but these cover essentially all past work. Less than a dozen other references were located, each of which referred to a single compound. The remaining compounds were new to *NRL* with the exception of the well known developments of $BaTiO_3$ and the isomorphs of *ADP*.*

The third column lists the results of *NRL* tests. An adjective description is the result of click tests. A k value refers to the piezoelectric coupling coefficient. This is a measure of the interaction between the electrical and mechanical behavior of the crystal, and forms a useful "figure of merit" for most applications. In a few cases, the k given is an approximate value obtained by test of a small specimen of unknown orientation, but for the most part, it represents confirmed data for the strongest activity along the various axes. Repeated observations on many materials indicated that a material classified as "moderate" by the click test had a coupling coefficient of approximately 0.1, which it is generally agreed is the minimum necessary to be usable for any application. Thus, any material with less than a moderate response can confidently be regarded as having no practical value, and a response of "moderate" or better indicates that further consideration is justified. The data included are not intended to be sufficient for evaluating possible applications but do narrow the list which must be more thoroughly investigated. For example, a material with a k of less than 0.2 could offer no advantage over the present crystals used for underwater sound gear. Materials with k as low as 0.1 can be considered for high frequency oscillator control, providing they are in symmetry classes having desirable modes of vibration.

A number of materials are listed which were not investigated at *NRL*. Some of these compounds are obviously not piezoelectric—by well confirmed symmetry data—but are included so that no material considered in previous surveys is omitted. Other compounds are included which are reported to be in a symmetry class that allows piezoelectricity but have not been tested at *NRL* or by previous investigators. The reason for this lack of attention is described in the final column. Comments are also included for some of the materials tested to indicate a limiting factor in

* It was later found that a number of these compounds had also been tested by H. Jaffe of the Brush Development Company. For example, $LiSO_4 \cdot H_2O$, valuable for its strong hydrostatic response, was being developed under the company code name *LH*.

TABLE I. CRYSTALS INVESTIGATED FOR PIEZOELECTRICITY

Chemical Compound	Schoenfliess Symbol for Reported Structure	Previous Investigation	NRL Investigation	Practical Limitations
Ag_3AsO_3	T_d		V. Weak	Unstable
Ag_3AsO_4	T_d			Unstable
Ag_3AsS_3	C_{6v}	+1		Insol.-Decomp.
$AgBrO_3$	D_{4h}, V_d		Neg.	
AgCl	O_h	−5	Neg.	
AgCN	C_{3v}		Mod.	Hygroscopic
$AgClO_3$	V_d		Neg.	
$AgClO_4$	T_d<208° C.			
Ag_2HgI_4	V_d		Neg.	
AgI	T_d, C_{6v}	+5, −3	Neg.	
$AgIO_3$	Rhomb?	+5	Mod.	Insol.-Decomp.
$AgK(CN)_2$	D_3d	−4, −5		
$AgNO_2$	D_{2h}		V. Weak	Hygroscopic
$AgNO_3$	V, C_{2v}	−3, −4	Neg.	
Ag_3PO_4	O_h, T_d		V. Weak	
$AgTl(NO_3)_2$			Neg.	
$AlAsO_4$	V_d			Req. hydrothermal synthesis
$AlCl_3$	D_3			Deliquescent
AlF_3	D_3			Hygroscopic
$Al(PO_3)_3$	T_d			
$AlPO_4$	D_3		Mod.	
AuI_3	C_3			Unstable
$BAsO_4$	S_4, V_d, D_{6h}			Non piezo. symmetry most likely
BPO_4	S_4, V_d, D_{6h}			Non piezo. symmetry most likely
$BaBr_2 \cdot 2H_2O$	C_{2h}	−5	Neg.	
$Ba(BrO_3)_2 \cdot H_2O$	C_{2h}		Neg.	
$BaCdCl_4 \cdot 4H_2O$	C_i	−5		
$BaCl_2 \cdot 2H_2O$	C_{2h}	−5	Neg.	
$Ba(ClO_3)_2 \cdot H_2O$		−5	Neg.	
$Ba(CNS)_2$			Neg.	
$BaFe(CN)_6 \cdot 6H_2O$		−5	Neg.	
$Ba(NO_2)_2 \cdot H_2O$		+5	Weak	Unstable
$Ba(NO_3)_2$	T, T_h	−1	Neg.	
$BaPt(CN)_4 \cdot 4H_2O$	C_{2h}	−5		
$BaSO_4$	V_h	−5		
$BaS_2O_6 \cdot 2H_2O$		+6	Mod.	

TABLE I—*Continued*

Chemical Compound	Schoenfliess Symbol for Reported Structure	Previous Investigation	NRL Investigation	Practical Limitations
$BaTiO_3$			Active	
BeO	C_{6v}			
BeS	T_d, V_{4h}, V_d			Decomposes
$BeSO_4 \cdot 4H_2O$	V_d		k~0.1	
$Bi(CNS)_3$	C_{6v}		Neg.	
$BiCl_3 \cdot 3SC(NH_2)_2$	C_3		V. Weak	
BiI_3	C_3			Insol.-Decomp.
$BiKF_4$			Neg.	
$BiKI_4$			Neg.	
Bi_2O_3	V_d, T, C_2			Insol.-Inverts
CaF_2	O_h	−5	Neg.	
$CaPd(CN)_4 \cdot 5H_2O$	D_2	−5		
$CaPt(CN)_4 \cdot 5H_2O$	D_2	−5		
$CaSO_4 \cdot 2H_2O$	C_{2h}	−5	Neg.	
CdF_2	O_h	−5		
CdI_2	D_{3d}, C_{6v}	−5	Neg.	
$CdKI_3$			Neg.	
CdS, Se, Te	C_{6v}, T_d			Conductivity
$CdSO_4 \cdot xH_2O$	C_{2h}		Neg.	
CeF_3	D_{6m}, D_6			Insol.
Ce_2O_3	D_3			
$Ce_2(SO_4)_3 \cdot 8H_2O$	C_i		Neg.	
$Ce(NH_4)_2(NO_3)_5 \cdot 4H_2O$			Strong	Conducts-Deliquescent
$Co(CNS)_2 \cdot 3H_2O$	C_{2h}, C_{2v}		Neg.	
$CoCl_2$	C_{3v}			Deliquescent
$Co(NH_3)_w(NO_3)_x(NO_2)_y(SO_4)_z$	D_2, D_{2h}		Neg., V. Weak	Large series of complexes, all relatively unstable
CoS, Se	D_{6h}, C_{6v}			Conductivity
$CoSO_3 \cdot 6H_2O$	C_3		Mod.	Unstable
$Cr_2(SO_4)_3$			Neg.	
$CsNO_3$	C_{3v}		Weak	
$Cs_2S_2O_6$	D_6		V. Weak	
CuBr	T_d			Unstable

TABLE I—*Continued*

Chemical Compound	Schoenfliess Symbol for Reported Structure	Previous Investigation	NRL Investigation	Practical Limitations
$CuCl$	T_d	+3	k=0.12	Unstable
CuF	T_d			Hydrolyses
Cu_2HgI_4	D_{2d}		Neg.	
CuI	T_d			Unstable
$CuK_2Cl_4 \cdot 2H_2O$	D_{4h}		Neg.	
$CuNaCl_3 \cdot xH_2O$			Neg.	
$CuSO_4 \cdot 3H_2O$	C_s		Weak	Hygroscopic
$CuSeO_3 \cdot 2H_2O$	D_2		Neg.	
$CuSeO_4 \cdot 5H_2O$	C_i		Neg.	
$CuSO_4 \cdot 5H_2O$	C_i		Neg.	
$FeNH_4Cl_4$			Neg.	
$Fe(NH_4)_3F_6$	T, T_d, O_h, C_{2v}			Hygroscopic
$Fe(NH_4)_2(SO_4)_2$	D_3		Neg.	
$FeSO_4 \cdot (NH_4)_2SO_4 \cdot 6H_2O$	C_{2h}	−5		
$FePO_4$	D_3			Req. hydrothermal synthesis
FeS	C_{6v}			Conductivity
GeO_2	D_3			
GeS_2	C_{2v}			
HIO_3	V	+2	k=0.3	Hygroscopic
$HgBr_2$	C_{2v}		Neg.	
$HgCN$	V_d			Unstable
$Hg(CN)_2$	V_d	+2, +3	Weak	
$Hg(CNO)_2$		+3		Unstable
HgI_2	C_{2v}, C_{4h}	−5	Mod.	
HgS	T_d	+2, +3		Conductivity
ICN	$D_{3d}, D_3, C_3, C_{3v}, C_{3i}$	+3, +5		
In_2O_3	D_3			
$IrCl_4$		−5		
$KAl(SO_4)_2 \cdot 12H_2O$	T_h	−3		
KBr	O_h	−3	Neg.	
$KBrO_3$	C_{3v}, D_3	+2, +3	k=0.23	
$KB_5O_8 \cdot 4H_2O$	C_{2v}		Mod.	
$KClCrO_3$	C_{2h}		Neg.	

TABLE I—*Continued*

Chemical Compound	Schoenfliess Symbol for Reported Structure	Previous Investigation	NRL Investigation	Practical Limitations
KCN	T, O_h		Neg.	
KCNO	D_{4h}	−5	Neg.	
$KCe(NO_3)_5 \cdot 1\frac{1}{2}H_2O$	C_{2v}		Neg.	
$KCd(NO_2)_3$		+5		Unstable
$K_2Cd(NO_2)_4$	V_h	−5		
$KClO_3$	C_{2h}		Neg.	
$KClO_4$	V_h, T_d		Neg.	
$K_3Cu(CN)_4$	D_3		Quest.	
K_2CrO_4	V_h	−3	Neg.	
$K_2Cr_2O_7$	C_i	−2, −4, −3, −5	Neg.	
KD_2PO_4	V_d	+		
$K_3Fe(CN)_6$	C_{2h}	−3	Neg.	
$K_4Fe(CN)_6 \cdot 3H_2O$	C_{2h}	−3	Neg.	
KHF_2	D_{4h}			Unstable
KH_2AsO_4	V_d	+1, +2	$k \sim 0.1$	
KH_2PO_4	V_d	+1	$k = 0.11$	
$K_2Hg(CN)_4$	O_h	−5		
$K_3Hg(NO_2)_5 \cdot H_2O$	V_h	−5		
KIO_3	Perov.		Mod.	
KIO_4	C_{4h}		Neg.	
$K_2La(NO_3)_5 \cdot 1\frac{1}{2}H_2O$	C_{2v}		Weak	
$KLiSO_4$	C_6	+2	$k = 0.04$	
$KLiSeO_4$	C_6	+6		
$KMgPO_4 \cdot 6H_2O$	C_{2v}			Insol.-Decomp.
$K_3Na(SO_4)_2$	D_{3d}		Neg.	
$K_3Na(CrO_4)_2$			Neg.	
KNH_4SO_4			Neg.	
$K_2Ni(SO_4)_2 \cdot 6H_2O$			Neg.	
KNO_2	C_3		V. Weak	
KNO_3	V_h, C_{3v}	−3	Neg.	
K_2PdCl_4	V_d			Symmetry quest.
$K_2S_2O_3 \cdot 1\frac{2}{3}H_2O$	C_{2v}		V. Weak	
K_2SO_4	V_h	−3		
$K_2S_2O_6$	D_3	+6	Mod.	
$K_2S_4O_6$	C_s		Slight	
$K_2S_2O_8$	C_i			Unstable
K_2SnCl_6	O_h		Neg.	
K_2TeO_3			Neg.	
K_2TeO_4	V_h		Neg.	
K_2TlCl_6(?)		−5		
$K_2Zn(CN)_4$	O_h	+5		Inactive structure proven

TABLE I—*Continued*

Chemical Compound	Schoenfliess Symbol for Reported Structure	Previous Investigation	NRL Investigation	Practical Limitations
LaF_3	D_6			
La_2O_3	D_3			
$Li_2BeF_4 \cdot H_2O$	C_{3i}	−4		
$LiClO_3$			Neg.	
$LiClO_4 \cdot 3H_2O$	C_{6v}		Mod.	
$LiI \cdot 3H_2O$	C_{6v}		Quest.	
$LiIO_3$	D_6		Mod.	
$LiKSO_4 \cdot CrO_4$(?)	C_6	+6		
$LiKSO_4 \cdot MoO_4$(?)	C_6	+6		
$LiNH_4SO_4$	V_h		Neg.	
$LiNaCO_3$	D_{3h}		Mod.	
$LiNaSO_4$	C_{3v}	+6	$k=0.04$	
$LiNa_3(CrO_4)_2 \cdot 6H_2O$	C_{3v}			
$LiNa_3(MoO_4)_2 \cdot 6H_2O$	C_{3v}	+6		
$LiNa_3(SO_4)_2 \cdot 6H_2O$	C_{3v}			
$LiNa_3(SeO_4)_2 \cdot 6H_2O$	C_{3v}	+6		
$LiRbSO_4$	C_6			
$Li_2SO_4 \cdot H_2O$	C_2	+1	$k=0.35$	
$Li_2SeO_4 \cdot H_2O$	C_2	+6	Weak	
$Mg(NH_4)_2(SO_4)_2 \cdot 6H_2O$	C_{2h}		Neg.	
$Mg(ClO_4)_2 \cdot 6H_2O$	C_{2v}			Hygroscopic
$MgCrO_4 \cdot 7H_2O$	V		V. Weak	
$MgSO_3 \cdot 3H_2O$	C_{3v}		Weak	
$MgSO_3 \cdot 6H_2O$	C_3		$k=0.06$	
$MgSO_4 \cdot 7H_2O$	V	+1	$k=0.06$	
$NaBrO_3$	T	+2, +3	$k=0.04$	
$Na_2Ca(CO_3)_2 \cdot 2H_2O$	C_{2v}	+6	V. Weak	
$Na_2CO_3 \cdot H_2O$	C_{2v}		Mod.	
NaCN	C_{2v}		V. Weak	
NaCNO	C_{3v}			Unstable
$NaClO_3$	T_h	+1	$k=0.03$	
$NaClO_4$	T_h, T_d		Neg.	
$Na_4Fe(CN)_6 \cdot 12H_2O$(?)		−5		
$Na_2Fe(CN)_5NO \cdot 2H_2O$		−5	Neg.	
$NaH_2AsO_4 \cdot H_2O$	D_2			
$Na_2HAsO_4 \cdot 7H_2O$			Neg.	
$NaH_2PO_4 \cdot H_2O$	D_2		$k=0.05$	
$NaIO_3$	V_h	−5	Neg.	
$NaIO_4$	C_{4h}	+6, −5	Neg.	
$NaIO_4 \cdot 3H_2O$	C_3	−5	Neg.	

TABLE—*Continued*

Chemical Compound	Schoenfliess Symbol for Reported Structure	Previous Investigation	NRL Investigation	Practical Limitations
$Na_2Mg(CO_3)_2$	C_3		Slight	
$NaNH_4HPO_4 \cdot 4H_2O$	C_{2h}	−5	Neg.	
$NaNO_2$	C_{2v}		Weak	Deliquescent
$NaNO_3$	D_{3d}	+6	Neg.	
$Na_2S_2O_8$			Neg.	
$Na_2S_2O_3 \cdot 5H_2O$	C_{2h}		Neg.	
$Na_3SbS_4 \cdot 9H_2O$	T	+1		Conductivity
Na_2SeO_3			Neg.	
Na_2SeO_4	V_h		Neg.	
$NaSiO_3 \cdot 5H_2O$			Slight	
$Na_2WO_4 \cdot 2H_2O$	V_h		Neg.	
$Nd(BrO_3)_3 \cdot 9H_2O$	C_{6v}	−5		
NdF_3	D_6			
Nd_2O_3	D_3, D_3d			
$(NH_4)_3AlF_6$	T			Unstable
$NH_4B_5O_8 \cdot 4H_2O$	V_h		Weak	
NH_4Br	O_h		Neg.	
NH_4CdCl_3	D_{2h}		Neg.	
NH_4CdBr_3			Neg.	
NH_4CdI_3			Neg.	
NH_4Cl	O_h	−3	Neg.	
$2NH_4Cl \cdot CuCl_2 \cdot 2H_2O$	D_{4h}	−5		
NH_4ClO_2	C_{4v}			Unstable
NH_4ClO_4	V_h, T_d	−5	Neg.	
$(NH_4)_2CrO_4$	C_6, C_{6h}	−5	Neg.	
$(NH_4)_2Cr_2O_7$	C_{2h}		Neg.	
NH_4F	C_{6v}	+5		Hydrolyses
$NH_4H_2AsO_4$	V_d		$k=0.24$	
$NH_4H_2PO_4$	V_d		$k=0.30$	ADP
$(NH_4)_6H_7(MoO_4)_6$	C_{2h}	−5	Neg.	
NH_4IO_3	C_{4h}	+5	Neg.	
$NH_4MgAsO_4 \cdot 6H_2O$	C_{2v}			Vap. Pres.
$NH_4MgPO_4 \cdot 6H_2O$	C_{2v}			Vap. Pres.
NH_4NO_3	T, V_d, V_h		Neg.	
$(NH_4)_2PtCl_6$	O_h	−5		
$(NH_4)_2SnCl_6$	O_h		Neg.	
$(NH_4)_2SiF_6$	O_h	−5		
$NiCa(CN)_4 \cdot 5H_2O$	D_2			
$Ni(NH_4)_2(SO_4)_2 \cdot 6H_2O$	C_{2h}		Neg.	
$NiNO_3 \cdot 6H_2O$	C_{2h}	−5		

TABLE I—*Continued*

Chemical Compound	Schoenfliess Symbol for Reported Structure	Previous Investigation	NRL Investigation	Practical Limitations
NiS	C_{3v}			Conducts
$NiSO_3 \cdot 6H_2O$	C_3		Mod.	
$NiSO_4 \cdot 6H_2O$	D_4	+1	$k=0.06$	
$NSO_4 \cdot 7H_2O$	V	+2	Weak	
NiSbS	T			
$PbBr_2$	V_h	−5		
$PbCl_2$	V_h		Neg.	
$Pb(CNS)_2$		−5		
$Pb_3(Fe(CN)_6)_2 \cdot xH_2O$			Neg.	
$PbMoO_4$	C_4, C_{4m}, C_6	−2, −4, −3		Insol.
$Pb(NO_3)_2$	T, T_h	−1	Neg.	
$PbS_2O_6 \cdot 4H_2O$	D_3			
$RbB_5O_8 \cdot 4H_2O$			Mod.	
$RbClO_4$	V_h, T_d			
$Rb_4Fe(CN)_6 \cdot 2H_2O$	C_1			
$RbNO_3$	C_{3v}	+5	Weak	
$Rb_2S_2O_6$	D_3		V. Weak	
SbI_3	C_3			Hydrolyses
Sb_2O_3	O_h	−5		
ScF_3	D_3			
SiC	T, C_{3v}	−2, −3		
SiO_2	D_3		$k=0.1$	Quartz
$Sr(ClO_3)_2$	D_{2h}, C_{2v}		V. Weak	
$Sr(IO_3)_2$			Neg.	
$Sr(NO_3)_2$	T, T_h	−1	Neg.	
$SrS_2O_6 \cdot 4H_2O$	D_3		Weak	
SrS_2O_6	D_3	+6	Mod.	Deliquescent
$TlClO_4$	V_h, T_d			
TlF	V_{2h}			Hydrolyses
V_2O_5	C_{2v}			Deliquescent
$ZnBeF_4 \cdot 7H_2O$		−3		
$ZnK_2(SO_4)_2 \cdot 6H_2O$	C_{2h}		Neg.	
$Zn(NH_4)_2(SO_4)_2 \cdot 6H_2O$	C_{2h}		Neg.	

TABLE I—*Continued*

Chemical Compound	Schoenfliess Symbol for Reported Structure	Previous Investigation	NRL Investigation	Practical Limitations
ZnO	C_{6v}	−2		
$Zn(OH)_2$	V			Gelatinous
$Zn_3(PO_4)_2 \cdot 4H_2O$	D_2			Insol.-Inverts
ZnS	T_d	+2, +3	$k=0.02$	
$ZnSO_4 \cdot 7H_2O$	V	+1, +2	$k=0.07$	

their value even though the piezoelectric activity is strong enough to be of interest.

ACKNOWLEDGMENT

The material investigated for this report required the combined efforts of both the chemists and physicists of the Crystal Section. Much of the early crystal growing was done by A. A. Kasper, with extensive contributions from G. Kennedy, W. S. Twenhofel, and C. Pelto. More recently this work has been done by S. Zerfoss with L. R. Johnson and I. I. Friedman. The piezoelectric measurements were under the direction of Paul L. Smith with assistance from W. Fry and originally performed by G. Mason. Improved techniques were devised by E. Burstein and instruments designed by R. Stokes.

REFERENCES

1. GIEBE, E., AND SCHEIBE, A., *Zeit. Physik*, **33,** 760 (1925).
2. ELINGS, S. B., AND TERPSTRA, P., *Zeit. Krist.*, **67,** 279 (1928).
3. HETTICH, A., AND SCHLEEDE, A., *Zeit. Physik*, **50,** 249 (1928).
4. GREENWOOD, G., *Zeit. Krist.*, **91,** 235 (1935).
5. HETTICH, A., AND STEINMETZ, H., *Zeit. Physik*, **76,** 688 (1932).
6. FLINT, E. E. (Trans.), *All-Union Sci. Research Inst. Econ. Mineral (USSR)*, No. **142,** 50–102 (1939).

Note: The first five references and a list of earlier works which they incorporate are available in a Scheibe, "Piezoelectrizität des Quarzes", Edwards Brothers, Inc., Ann Arbor, Mich. (**1945**).

SIMPLE GNOMONIC PROJECTOR FOR *X*-RAY LAUEGRAMS

Samuel G. Gordon, *The Academy of Natural Sciences of Philadelphia.*

Abstract

The indexing of Lauegrams requires transposition of the Laue spots (which are at tan 2θ) to tan θ (stereographic trace of plane pole in F-Laue, and gnomonic plane-pole in B-Laue) or to cot θ (gnomonic plane-pole of F-Laue). The geometry involved is simple: to the line through the Laue spot and the center of the Lauegram draw the unit circle (5 cm. radius for $D=5$ cm. in camera), tangent to the line at the center of the Lauegram. From the Laue spot draw a line through the center of the circle. Erect perpendiculars to this line, tangent to each side of the unit circle. It is easily proven that the intersections of these tangents with that of the tangent through the Laue spot and the center of Lauegram are the points required θ, and $90°\text{-}\theta$. A simple transporteur may be constructed by swivelling a carpenter's square to a straight-edge, such that the center of rotation is 5 cm. below the straight edge used to connect Laue spot and center of Lauegram; and the vertical arm moves tangent to it at the required distance. Such a device was described by Clark and Gross in 1937 for plotting $90°\text{-}\theta$. However, the vertical arm can be adjusted to any distance from the center of rotation, giving reductions to 4, 3, 2.5 or 2 cm. as desired. A shorter vertical arm, on the opposite side of the center is used for plotting θ. Since the device is simply an angle bisector, it can be used for converting gnomograms to stereograms.

Since the spots on an *x*-ray Lauegram are at tan 2θ, the indexing of the atomic planes which produced the spots is most rapidly done by making a projection of those planes. The advantage of using the gnomonic projection was long ago demonstrated by Wyckoff.[1] In the gnomonic projection the projected poles are at cot θ (Fig. 1). To facilitate the making of a gnomonic projection from a Forward Lauegram, Wyckoff designed a gnomonic ruler:[1] the position of a Laue spot was read on a scale to the left of the center of the Lauegram (2θ), and the same figure to the right of the center located the gnomonic projection of the pole of the atomic planes (at $90°\text{-}\theta$).

A gnomonic ruler which eliminated the scales was introduced by Clark and Gross[2] in 1937. As described below, modification of this ruler permits reduction of the scale of the projection in Forward Lauegrams, and the addition of another arm extends its usefulness to Back Lauegrams.

[1] Wyckoff, R. W. G., *Am. Jour. Sci.*, **50,** 317 (1920). The gnomonic projection was first used for Lauegrams by Rinne, in 1915 (*Ber. K. Sächs. Ges. Wiss. Leipzig* (Math.-phys. Klasse, **67,** 303, 1915). Wyckoff credits Frederick E. Wright for pointing out the advantage of the gnomonic projection over that of the "modified stereographic projection" introduced by W. L. Bragg (see below) in 1913.

[2] Clark, G. L., and Gross, S. T., *Science*, **17,** 272–273 (1937).

Figure 1 will serve as a key to the simple geometry involved in figures 2 to 5. X-rays (X) impinging upon a set of planes A–B at the reflecting angle will produce a Laue spot at FL (Forward Lauegram), at the Bragg angle 2θ. The pole of the normal to this set of planes is indicated on the spherical projection at AB, and the projection of this pole on the gnomonic plane is at G_{fl}. The problem is to project the position of G_{fl} on the Forward Lauegram from the Laue spot FL.

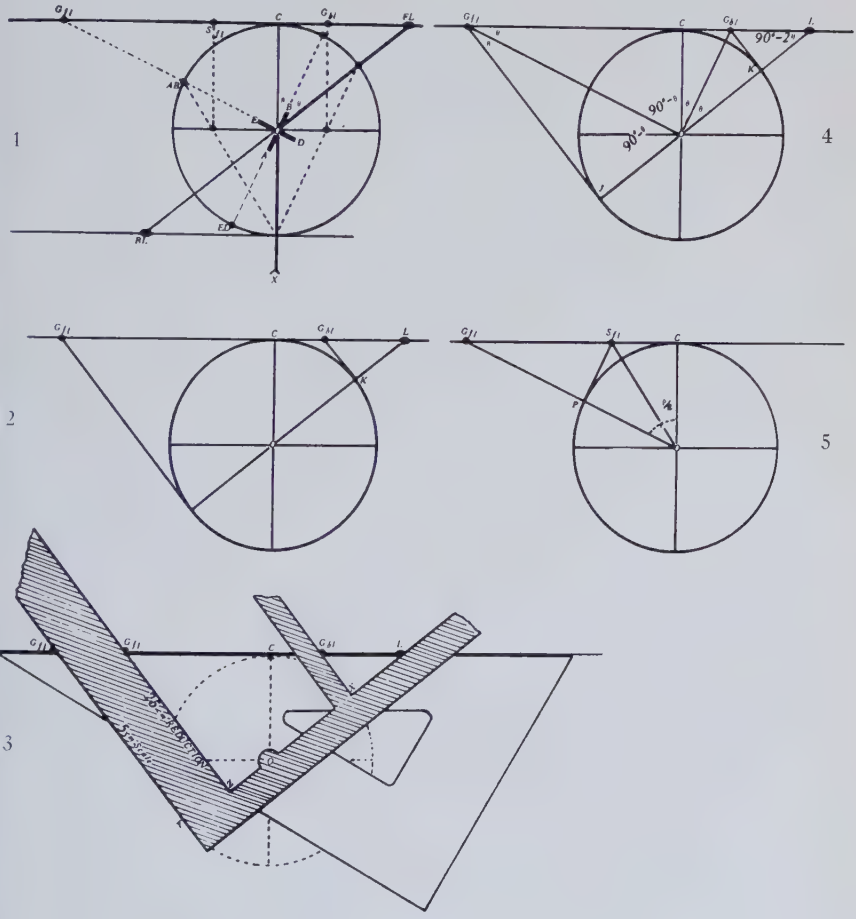

Another set of planes (drawn at right angles to the set A–B) is indicated by the letters E–D. They will produce a Back Laue spot at BL. The pole of the set of planes E–D in spherical projection is at ED, and the gnomonic projection of this pole projected to the upper plane will be at G_{bl}.

The problem is to project the position of G_{bl} on the Back Lauegram from the Laue spot BL. Note that, in this case θ is the angle X–D.

This figure, for completeness shows the position of the stereographic pole[3] of the set of planes A–B, and the stereographic projection of this pole upon the gnomonic plane at S_{fl}.

As indicated in Fig. 2, the graphic solution of this problem is quite simple. Draw a circle, with a radius equal to the distance from crystal to film, tangent to the line between the Laue spot (L) and the center of the Lauegram (C) at this center. Draw a line (LJ) from the Laue spot thru the center of the circle. Erect perpendiculars to this line tangent to the circle, at K and J. The intersection of these tangents, with the tangent (LC) in the gnomonic plane at the points G_{bl} and G_{fl} locate the projection of the poles of the planes of Fig. 1 in the Back Lauegram and the Forward Lauegram respectively.

This immediately suggests a simple projector, by means of which the gnomonic projection of the poles of the planes can be quickly located (Fig. 3). A straight edge, such as that of a draughtman's triangle can be used to connect the Laue spot with the center of the Lauegram: once a center point (C) has been scratched on the edge of the triangle. A square, which can be made from an ordinary carpenter's square, is pivoted to the triangle at a point (O) at right angles to the center point (C) on the edge of the triangle, at a distance (C to O) equal to the distance from crystal to film in the camera (usually 5 cm.). Upright arms are spaced so that their ruling edges (at X and Y) are the same distance from the pivot center, O. The horizontal arm of the square has a ruling edge Z–X which passes through the pivot center.

To use the instrument, the straight-edge of the triangle is placed with its center mark at the center of the Lauegram (or a tracing, or a copy made by pricking points through a print onto a sheet of drawing paper). The horizontal arm of the square is swung on its pivot at O until the ruling edge is upon the Laue spot, L.

The point G_{bl} on the right arm then is the projection of the pole of the planes responsible for the reflection in a Back Lauegram. In the case of

[3] This is the stereographic projection of the pole of the normal to the planes A–B, as used by morphological crystallographers. In the early days of x-ray crystallography the literature was ornamented by the "modified stereographic projection" introduced by W. L. Bragg in 1913 (*Proc. Roy. Soc.*, **A 89,** 248, 1913), in which, not the normal to the set of planes, but the projection of the trace of the reflecting planes upon the gnomonic plane was plotted: in Fig. 1, the point G_{bl} (trace of A–B) rather than S_{fl} was used in indexing. The zones of which appeared as festoons of spots (ellipses) on the Lauegram projected as circles tangent to the center of the Lauegram.

a Forward Lauegram, the point G_{fl} on the left arm is the projected pole. One can proceed very rapidly over a Lauegram in this fashion. It is convenient to slightly notch the center mark on the triangle: the drawing can be held down with a slightly protruding pin, and the triangle may then be pivoted about the Lauegram from one zone to another. The writer has found it preferable to work counterclockwise around a Lauegram, thus covering up Lauespots that have been projected.

It will be noted that the left arm in Fig. 3 has two ruling edges, one marked 5 cm. and the other 2.5 cm. reduction. The 5 cm. scale is based on a fundamental sphere with a radius of 5 cm. However, on this scale, many poles will lie at considerable distances from the center of the projection, if not beyond the limits of an ordinary sheet of drawing paper. The scale of the projection can be easily reduced by moving the ruling edge towards the pivot: thus a distance of Z to O of 2.5 cm. will produce a projection based on a fundamental sphere of 2.5 cm. This distance was chosen because it was easy to convert tables on hand (of tangents $\times 5$ cm.) to this scale by simply dividing by two. The scale can be made 2 or 3 cm. (or any other desired) by placing the left arm at such a distance from the pivot center at O (the distance, however, from O to C must be equal to the crystal to film distance).

The geometrical proof of Fig. 2 will be obvious from Fig. 4. It is based on the geometrical relation that from an external point only two tangents can be drawn to a circle; that these two tangents are equal; and further, that a line from the intersection of two tangents to the center of the circle bisects the angle between the two tangents.

Therefore $C-G_{bl}=G_{bl}-K=\tan\theta$; and $C-G_{fl}=G_{fl}-J=\cot\theta$.

Since the Lauespot is at 2θ, and it is desired to find θ in the Back Lauegram, the problem is simply one of bisecting this angle. It will be obvious also from Fig. 4, that the location of G_{fl} involves only the bisecting of angle C, J, G_{fl}.

The instrument shown in Fig. 3 is merely an angle bisector and is adaptable to any problem of this kind. One example will suffice (shown in Fig. 5): that of converting a gnomonic projection to a stereographic projection (or vice versa). The pole in gnomonic projection is at the angle ρ; the stereographic pole (upon the same plane) is at $\rho/2$. The angle can be bisected graphically by erecting a tangent at P. The point S_{fl} can be quickly located with the instrument by turning the drawing upside down, placing the center point at C, rotating the horizontal arm to G_{fl} and the point S_{fl} is at the intersection with the right vertical arm.

It may also be pointed out that it is not necessary to use the instrument for every spot in a zone: once two points are located in a zone, a straight

line can be drawn through them. All of the projected points from a festoon will then lie on this line: by connecting each Laue spot in the ellipse with the center of the projection (with a straight edge), then the intersection with the line through the zone will suffice to locate the projected pole.

My thanks are due to Mr. Ben Birchall of Philadelphia, who kindly made the instrument for me.

THE LIVINGSTON, OVERTON COUNTY, TENNESSEE, METEORITE*

STUART H. PERRY, *Associate in Mineralogy, U. S. National Museum*

AND

E. P. HENDERSEN, *Associate Curator, Mineralogy and Petrology, U. S. National Museum.*

This meteorite was brought to the attention of S. H. Perry in 1941 by Miss Creola M. Wisner of Livingston, Tenn., to whom the authors are indebted for this fragment of 165 grams. It is solid metal and little affected by oxidation.

The meteorite was found in 1937 by Sherman Smith on his farm about

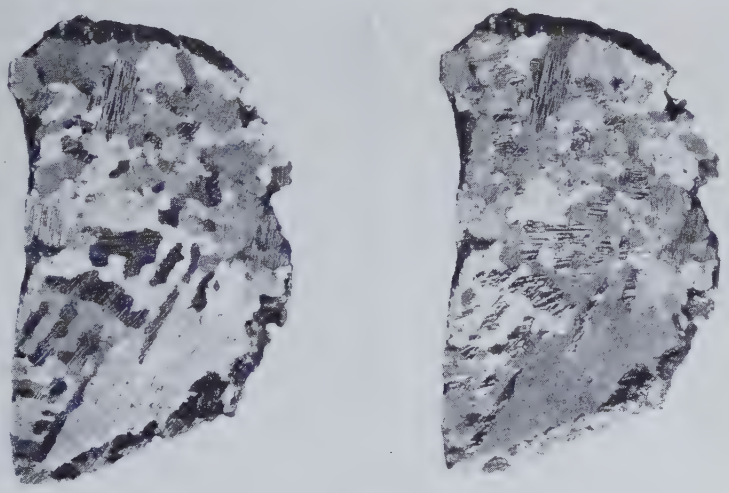

FIGS. 1 and 2. Two photographs ×2, with light from two different directions showing the diversely oriented sheen of the various kamacite areas.

two miles west of Monroe, a hamlet eight miles north of Livingston, the county seat of Overton County (Latitude 36° 25′ N. Longitude 85° 15′ W.).

The mass was described by Mr. Smith as shaped somewhat like a pancake, thicker in the center, 15 or 18 inches across, and weighing per-

* Published by Permission of the Secretary of Smithsonian Institution.

haps 30 pounds. It lay on the rocky bank of Eagle Creek, a considerable stream which flows through a narrow valley at that place. Mr. Smith took it to be a flat stone, but being surprised by its weight when he turned it over, took it to his house nearby where with some difficulty the fragment referred to was broken off with a hammer and chisel. A smaller piece of about 40 grams also broken off at that time is now in the collec-

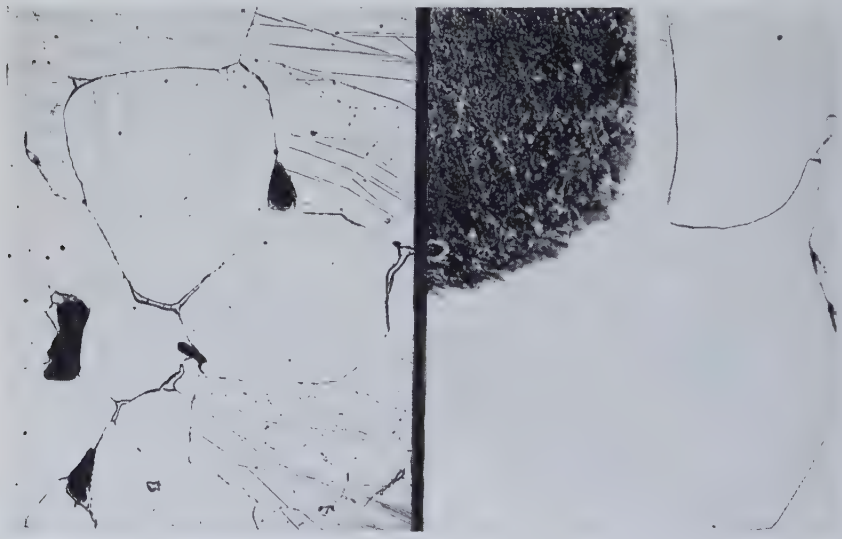

FIG. 3. Typical general microstructure. Irregular kamacite grains with Neumann lines; schreibersite bodies along a grain boundary; four areas of darkened taenite. Nital 15 seconds, ×58.

FIG. 4. Part of an area of darkened taenite with surrounding border of clear fully transformed taenite. There is no definite resolution of the dark core, in which light particles of taenite can be seen in a groundmass of dark gamma-alpha aggregate. Picral 30 seconds, ×572.

tion of S. H. Perry, but the larger of the two fragments was presented by Mr. Perry to the U. S. National Museum.

The meteorite lay for some time on the porch of the house but in the following year Mr. Smith moved to the other side of the creek valley and lost track of the iron. Later the house was moved to a new location some distance away and its site became part of a cultivated field. The spot was carefully searched by both Mr. Smith and Mr. Perry, but with no result. Mr. Smith believed that the iron was left there when the house was moved and became buried in the earth when the site of the house was put under cultivation.

The Livingston iron is a medium octahedrite, the bands of kamacite being sparingly developed and too irregular to permit satisfactory measurement. Much of the surface examined shows no octahedral pattern. The granular kamacite shows exceptional abundance of Neumann lines (Figs. 1 & 2).

The microstructure consists of irregular kamacite grains of varying size. The Neumann lines are diversely oriented, sometimes crossing grain boundaries with little or no change of direction. Irregular bodies of schreibersite are numerous along grain boundaries. The general macrostructure is shown in Figs. 1 and 2.

No plessite fields were observed, and no taenite lamellae, but taenite occurs abundantly in round irregular bodies, clear at the edges but with cores darkened because of incomplete transformation. While there is some appearance of acicular structure at the edges of the dark cores, these areas at high magnification are dense and obscure, but showing the clear separation of needles or particles of taenite and of alpha-gamma aggregate usually seen in darkened taenite.

A sample was removed from the 165 gram fragment and analyzed.

LIVINGSTON, TENN., METEORITE

E. P. Henderson, *Analyst.*

Fe	91.45
Ni	7.45
Co	.48
P	.25
S	trace
	99.63

Molecular ratio of $\frac{\text{Fe}}{\text{Ni}+\text{Co}} = 12.20$

THE DEGREES OF FREEDOM OF SIMPLE SYMMETRY OPERATIONS*

HENRI BADER, *Bureau of Mineral Research, Rutgers University, New Brunswick, New Jersey*

ABSTRACT

The geometrical dimensions of elements of symmetry, symmetry operations and symmetrical patterns are shown to be correlated. It is argued that the conventional elements of symmetry are strictly applicable only to three dimensional patterns, their use in defining one- and two-dimensional groups resulting in ambiguity. The specific elements of one- and two-dimensional groups are defined.

Point symmetry groups define the symmetry of the environment of a point (for instance, the center of an ideal crystal form) by means of elements of symmetry containing the given point. In defining *spacial* point symmetry groups, we use only five types of elements of symmetry, the center of symmetry (C_i), the plane of symmetry (C_s), axes of rotation (C_n), and axes of rotary-reflection (S_n) or axes of rotary-inversion (J_n). The latter two are interchangeable *complex* elements of symmetry. We will here consider only the three *simple* elements C_i, C_s, and C_n. These elements are symbols indicating the admissibility of specific symmetry operations. Thus C_i indicates the operation of inversion, C_s indicates reflection, and C_n indicates rotation through angles of $360°/n$. These elements, however, are more than mere symbols; they *control* the corresponding symmetry operation. This control can be expressed in the following law of degrees of freedom of simple symmetry operations.

$a+b=c$.
a = number of geometrical dimensions of the element of symmetry.
b = degrees of freedom (= dimensions) of the controlled symmetry operation.
c = number of geometrical dimensions of the pattern under consideration.

C_i is a (dimensionless) point. It controls the operation of inversion, consisting in moving points along lines passing through the center of symmetry. There is no restriction on the direction of these lines, therefore the operation of inversion has *three* degrees of freedom.

C_n is one-dimensional. In the operation of rotation, points are able to move only in planes normal to C_n; the operation of rotation has *two* degrees of freedom.

C_s is two-dimensional. The corresponding operation consists in the transfer of points from one side of the plane to the other. Visualizing the operation, we see that all points move along parallel lines normal to the

* Published by permission of the Director, Bureau of Mineral Research, Rutgers University.

plane of symmetry. The operation of reflection has only *one* degree of freedom.

Thus C_i, C_s, C_n, and the corresponding operations satisfy the law of degrees of freedom. That this law is not a truism becomes clear when we consider the symmetry of one- and two-dimensional patterns.

It is customary to define the two-dimensional *plane* point symmetry groups (for instance the symmetry of crystal faces) by means of the corresponding spacial point groups, all the elements of a group lying normal to the plane pattern. Only three types of groups fulfill this requirement, namely C_n, C_s, and C_{nv}. We cannot, however, legitimately exclude C_i. The law of degrees of freedom shows that this method of defining plane point symmetry groups is arbitrary, the arbitrariness residing in the choice of one additional dimension for the sake of convenience. We could quite as legitimately choose to define plane patterns in terms of the symmetry elements of four or more dimensional spaces. The inconsistency in the use of three dimensions to define the symmetry of two-dimensional patterns results in one ambiguity, namely the equivalence of C_i and C_2. Now the essence of inversion is the establishment of enantiomorphic equivalents, and that of rotation the establishment of congruent equivalents. Thus the equivalence of C_i and C_2 is inadmissible.

The discrepancy resulting from recourse to more dimensions than necessary is even more striking in the case of the one-dimensional *linear* point symmetry groups. There are only two such groups, one being asymmetric. In terms of spacial groups the other can be defined by any of three, in this case equivalent, elements, namely C_i, C_s, or C_2.

The above considerations are of no practical consequence; we shall continue to state crystal face symmetries in terms of spacial point symmetry groups. Theoretically, however, the law of degrees of freedom of symmetry operations is a useful concept. It states that in choosing elements of symmetry we may not transcend the geometrical dimensions of the pattern under investigation if we wish to avoid ambiguity. C_i, C_s, and C_n then, are specifically elements of symmetry of three-dimensional groups, not admissible in one- and two-dimensional groups.

The element of symmetry specifically representing the single symmetrical linear symmetry point group is obviously a point, as we must claim the one available dimension to provide the degree of freedom of the corresponding operation. This operation is a reflection, in virtue of the single degree of freedom. It is a reflection in a point and the controlling point of reflection may be symbolized as A_s. A_1 designates the asymmetric linear point symmetry group. The edges between crystal faces, for instance, belong either to the group A_1 or A_s.

Plane point symmetry groups define two-dimensional patterns. The

two possible specific elements of symmetry are the point rotation (B_n) and the line of reflection (B_s). The corresponding operations are rotation around a point (two degrees of freedom) and reflection in a line (one degree of freedom). The asymmetric group is given the symbol B_1. Thus plane point symmetry groups are restricted to B_1, B_n, B_s, and B_{ns}. These, of course, correspond to the Schoenflies symbols C_1, C_n, C_s, and C_{nv}.

The following figure shows the relations between the different elements of symmetry, the controlled operations, and the dimensions of the pattern.

Dimensions of Pattern	Name of Symmetry Groups	Dimensions of Element of Symmetry		
		0	1	2
1	Linear Point Symmetry Groups	Point of Reflection A_s ↗	—	—
2	Plane Point Symmetry Groups	Point of Rotation B_n ↗	Line of Reflection B_s ↗	—
3	Spacial Point Symmetry Groups	Point of Inversion C_i ↗	Line of Rotation C_n ↗	Plane of Reflection C_s ↗
		Operation of Inversion Three degrees of Freedom	Operation of Rotation Two degrees of Freedom	Operation of Reflection One degree of Freedom

Note: The figure suggests an interesting extrapolation, namely expansion downward and to the right into the domain of four- and more-dimensional spaces. Should the extrapolation be valid, then the elements of symmetry of four-dimensional space, for instance, would be as follows:

(1) Point of ?.
(2) Line of inversion.
(3) Plane of rotation.
(4) Three-dimensional space of reflection.

NOTES AND NEWS

NOTES ON THE RELIABILITY OF THE *X*-RAY DIFFRACTION SPECTROMETER FOR QUANTITATIVE MINERAL ANALYSIS*

HOWARD F. CARL**

The use of the Geiger-counter *x*-ray diffraction spectrometer for mineral identification and analysis is becoming more widespread as the convenience and reliability of this equipment are appreciated by more workers in the field. There is, consequently, increased interest in specific techniques employed when this instrument is used for quantitative mineral analysis.

A recent paper (1) by this author, discussing certain aspects of quantitative *x*-ray analysis and presenting a specific technique employing a Geiger-counter spectrometer for mineral-powder analysis, has been subject to a criticism (2), which appears quite unjustified in the light of the experience of the writer.

One point of this criticism was that by this technique, "considerable amounts of *colloidal* quartz, if mixed with other well-crystallized materials, could be present and yet elude measurement, especially if well-crystallized quartz were also to be found in the mixture." In all fairness to any method of *x*-ray diffraction analysis, it must be admitted that no technique developed for well-crystallized mineral powders would have much value in working with either colloidal or amorphous materials. Such limitations are certainly universally recognized.

Secondly, it was not intended to be implied that "variations in the *x*-ray output are more serious in the case of the photographic method than in that of the Geiger-counter spectrometer," as charged by Dr. Lonsdale. It was merely pointed out that, for short exposures, variations in total *x*-ray output may be *significant* when only one measurement per analysis (a film density), is made.

The main part of Dr. Lonsdale's criticism was devoted to an expression of disbelief in the linearity of response of the automatic recording spectrometer, except "over a very restricted portion of the graph" and a consequent limited usefulness for quantitative analysis was therefore inferred. It was also pointed out that, "The instrument ceased to record, even at highest sensitivity, at an intensity which was certainly more than 100 times the minimum intensity observable with a scaling circuit and mechanical impulse counter."

* Published by permission of the Director, Bureau of Mines, United States Department of the Interior.

** Physicist, College Park Branch, Metallurgical Division, Bureau of Mines, College Park, Maryland.

The technique described in the original paper is such that good linearity of response, or the lack thereof, is immaterial to the successful performance of quantitative analysis. A complete calibration of the equipment is obtained by determining standard working curves which incorporate in their development the characteristic response of all the

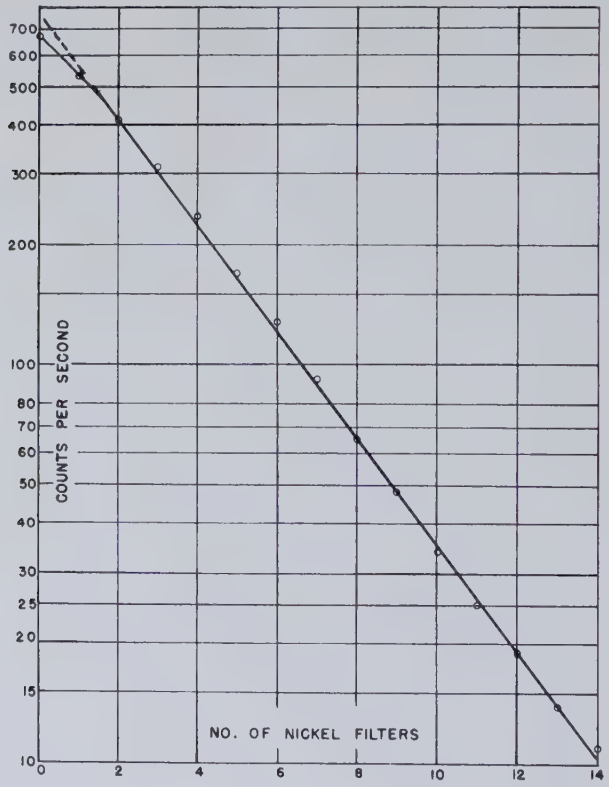

Fig. 1

elements of the apparatus. The only assumption necessary is that these responses remain constant during an analysis and can be standardized and hence reproduced from day to day. The sensitivity of the recording method is sufficient to obtain accurate data on as little as 1 to 5 per cent of a material, on about 2 per cent of quartz. Of course, scaling and mechanical counting would extend this lower limit to smaller values but at a sacrifice to the speed of analysis. Likewise the actual linearity of response of the equipment is excellent over most of the range of counting rate used. The following graphs illustrate this point.

Figure 1 presents a plot of counts per second, on a logarithmic scale, versus number of filters (nickel foil) superimposed in the diffracted beam. It indicates that, for rates between 10 and somewhat above 400 counts per second, the linearity of the Geiger-tube response is good. Figure 2 shows the excellent linearity of the recorder unit from 5 to 100 (full-scale) divisions. Inquiries to other investigators have revealed that this type of performance is typical of many x-ray diffraction spectrometer installations and is not an exceptional one.

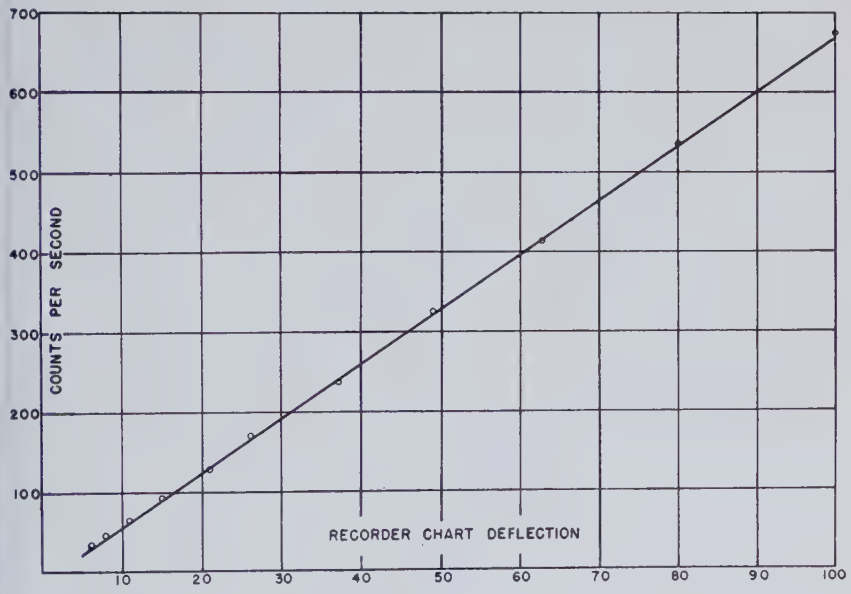

FIG. 2

Further work with this equipment has shown that the standard conditions under which the working curves were originally obtained are not so critical that changes, renewals, or readjustments in the component parts of the equipment will invalidate these curves to the extent of necessitating their complete redetermination. Within the limits of accuracy of analysis originally stated, plus or minus 10 per cent of the amount present, after such changes a readjustment of the coupling control sensitivity to give the original deflection for one or more of the standard samples, including the 100 per cent sample, has been found sufficient to reproduce satisfactorily the original working curves. That is, the installation of a new Geiger-counter tube, new electronic tubes, and a complete realignment of the spectrometer produced no material distortion

in these working curves. This indicates that the characteristic responses of the equipment were not appreciably altered by such changes.

Although there is theoretical evidence that scanning at a slower rate than, say, 1 R.P.M., should produce more reliable values of recorded intensities, in practice no significant difference has been observed between scanning rates of $\frac{1}{2}$ R.P.M. and 1 R.P.M. in the reproducibility of results. In other words, a slower scanning rate itself does not allow a reduction in either the number of intensity recordings on the same sample or in the number of sample mounts necessary. However, for many analyses, particularly those in which the concentration of the mineral is above 10 per cent or so, very satisfactory results have been obtained at the 1 R.P.M. rate with only three determinations of line height on three different mounts, instead of the usual five. The time for an analysis is reduced thereby from about 45 to about 30 minutes. On the other hand, with proper care at all stages of the technique, results good to about plus or minus 5 per cent of the amount present, when the mineral concentration was above 10 per cent, have been achieved on "ideal" samples. Such "ideal" samples are those having strong and isolated diffraction lines, no preferred orientations, and forming readily reproduced mounted surfaces.

References

1. Carl, Howard F., Quantitative mineral analysis with a recording *x*-ray diffraction spectrometer: *Am. Mineral.*, **32**, 508–517 (1947).
2. Lonsdale, Kathleen, Note on quantitative analysis by *x*-ray diffraction methods: *Am. Mineral.*, **33**, 90–92 (1948).

A NEW OCCURRENCE OF HELVITE*

A. E. Weissenborn,
U. S. Geological Survey, Spokane, Washington.

Helvite has been found in a zinc replacement deposit in limestone at the Grandview mine in the Black Range, Grant County, New Mexico. So far as is known, this mineral has not previously been found in a deposit of this type. The various types of occurrence and associations and the properties of helvite and the helvite group are described in a paper by Glass, Jahns, and Stevens.[1]

While mapping one of the replacement zinc deposits in limestone at the Grandview mine in the Swartz district, Grant County, New Mexico, the author collected a specimen of fluorite from a vug in the ore body. Subsequently tiny tetrahedrons of yellow helvite were discovered in the

* Published by permission of the Director, U. S. Geological Survey.

[1] Glass, J. J., Jahns, R. H., and Stevens, R. E., Helvite and danalite from New Mexico, and the helvite group: *Am. Mineral.*, **29**, 163–191 (1944).

specimen, in part incrusting the surface of the fluorite and in part embedded in it. Sphalerite was also present. Some of the crystals of helvite are nearly a millimeter across, and smaller ones form clusters of interlocked crystals. The clusters are no more than 2 to 3 millimeters across, and along with the single crystals, are scattered sparsely on the specimens, most commonly being on the fluorite crystals. Several tetrahedrons occur as inclusions in the transparent, colorless crystals of fluorite; other crystals are partly enclosed, having only sharp corners exposed above the surface of the fluorite crystals.

The yellow mineral was tentatively identified as helvite by John W. Adams of U. S. Geological Survey. Robert L. Smith confirmed the identification in the Geological Survey's laboratory in Washington. Further confirmation was made by the usual tests, by *x*-ray powder photographs, and by the staining process developed by Gruner.[2] The index of refraction, measured by Jewell J. Glass, is slightly variable, *n* ranging from 1.730 to 1.733. The relatively low index indicates that the mineral is essentially the manganese member [$(Mn, Fe, Zn)_4Be_3Li_3O_{12}S$] of the helvite group.

At the Grandview mine the ore occurs as replacements in the Ordovician Montoya limestone in small lenses, pods, and pipelike bodies along minor faults and fractures and at fault intersections. The ore minerals are sphalerite and galena with local rare concentrations of chalcopyrite. Associated minerals are garnet, epidote, serpentine, magnetite, fluorite, pyrite, quartz, calcite, and chlorite.[3] Traces of scheelite are visible under the mineralight. The limestone has been recrystallized and locally contains considerable garnet. No igneous rocks are exposed in the mine workings, but a small quartz monzonite intrusion crops out a short distance west of the mine, and two drill holes put down by the U. S. Bureau of Mines penetrated altered igneous rock about 100 feet to the west of, and slightly below, the nearest workings.

On a subsequent trip to the Grandview mine a number of specimens of ore, gangue, and country rock were collected. Helvite was identified in three of them, but it does not form as well-developed crystals as in the original material. Like the original specimen, the later ones were from vugs, and the helvite in all of the specimens was associated with fluorite and sphalerite.

The helvite at the Grandview mine apparently is not of economic importance, but similar deposits should be examined carefully for helvite. It closely resembles garnet and might easily be overlooked.

[2] Gruner, John W., Simple tests for the detection of the beryllium mineral helvite: *Econ. Geology*, **39**, 444–447 (1944).

[3] Griggs, R. L., and Ellison, S. P., Geology and ore deposits of the Swartz district, Grant County, New Mexico: Unpublished manuscript, U. S. Geological Survey.

BOOK REVIEWS

VORRÄTE UND VERTEILUNG DER MINERALISCHEN ROHSTOFFE. Ein Buch zur Unterrichtung für Jedermann, by Felix Machatschki, Springer-Verlag in Wien I, Mölkereibastei 5, **1948,** Printed in Austria. viii+191 pages, 6 figs. Heavy paper covers. Price $3.70.

In this little book Professor Machatschki, who is now at the University of Vienna, has summarized for his countrymen the essential facts about the distribution and reserves of mineral raw materials. The book is divided into three sections:—

I. The supply of mineral raw materials (17 pages).

II. Occurrence and origin of mineral raw materials (11 pages).

III. Important mineral raw materials and their distribution (150 pages).

The point of view is geochemical and geological throughout. The first two sections and a brief appendix on rocks serve to orient the general reader in this regard.

The author is rightly of the opinion that the usual sort of statistical material is of little value to the layman and where given for just a particular year, or a limited period, may be very misleading. Average production figures with some reference to peaks and fluctuations, a review of trends and reserves are much more enlightening than exact figures on the output of some particular mineral substance in each of a great number of countries. Accordingly the book contains but few tables and these are in part unusual. One table in section II lists those raw materials which show a very irregular distribution, being produced in important amounts in only one or two countries, and gives for each the leading producers and the percentage of the world total which their production constitutes. In another table in the same section a system of symbols is used to indicate the supply and reserve situation for 33 raw materials in 22 countries and regions.

In section III there is given for each raw material a statement of its mineralogical and geological occurrence, its uses, production, distribution and reserves. In this section there are many digressions, as where the use of topaz as a gem is mentioned in connection with the distribution of fluorine in minerals, and cross references bridge the unnatural barriers which arise in any classification. In many places the estimate of reserves is stated in terms of the expected time to exhaustion of known supplies. The statement of production by individual countries, especially Austria, is often related to the needs of that country or the importance of a particular material in its economy. All values are given in dollars.

The book is well printed on good paper, is nearly free from misprints and has an excellent, 12 page, index.

A. Pabst, *University of California, Berkeley, California*

THE PETROGRAPHY AND PETROLOGY OF SOUTH AFRICAN CLAYS
V. L. Bosazza

This paper was presented by Mr. Bosazza for the degree of Doctor of Science (Geology) to the Natal University College, University of South Africa and published by Percy Lund and Humphries, London W.C. 1. (reproduced from typewritten pages by the replica process); price £2-2-0.

Much of the paper is devoted to discussions of clays in general, and hence covers a much wider field than the title indicates. Part 1 (pp. 3–114) takes up ultimate chemical composition including minor constituents, size distribution, microscopic examination, mineral analysis, clay minerals, water in clays, and reactions between clay minerals and organic compounds. Part 2 (pp. 115–176) takes up methods of classification, and the various hydrates composing clays and related materials. Part 3 (pp. 177–276) discusses weathering, transportation, sedimentation, and clays formed under varying conditions. It also gives more details about South African clays than the preceding sections.

In this thesis with its broad and rather diffuse presentation, the author gives about 100 direct quotations, and about 330 citations. There are a few notable omissions of pertinent materials on soils and clays, but Mr. Bosazza has assembled a rather remarkable list of references, and these will be very useful to other workers in the field.

The list of subjects treated, and the comments and evaluations of cited or quoted material constitutes a very elaborate approach to the problems of soils and clays. The 300 available pages hardly give space for such an exhaustive treatment, and a completely objective presentation and evaluation of all this material would be a staggering task, the more so as the science of clays and soils is in a formative stage.

There are, however, some subjects which might well have been covered more fully. For instance, the chapter on "microscopic examination by various means" mentions the making of thin sections of clays, but there is no discussion of optical properties, particularly of indices of refraction and birefringence which commonly permit a definite determinations of a clay mineral; nor is physical form mentioned, a property which is commonly completely diagnostic of kaolinite.

Interesting and somewhat surprising is the correlation of the change in the character of certain South African clay materials with climatic changes, as continental drift in Permian time (citing DuToit), brought the African continent into a progressively warmer and warmer environments.

Mr. Bosazza presents many new chemical analyses, most of them made by him, and many careful size analyses of soil materials. Descriptions of modes of occurrence, of physical and of chemical properties of many South African clays are given, and data is presented about numerous deposits of younger clays in the Delta, Nile valley.

The paper will be read with interest by all those working with clays and soils, and it gives information which will be very useful to those concerned with the commercial possibilities of South African clays.

C. S. Ross, *U. S. Geological Survey**

* Published by permission of Director, U. S. Geological Survey.

POPULAR GEMOLOGY, by Richard M. Pearl, pp. xii+316, 115 illustrations' $5\frac{1}{2}''\times8''$. John Wiley and Sons, Inc., New York, and Chapman & Hall, Ltd., London, **1946.** Price $4.00.

Persons seeking general information concerning gems will find *Popular Gemology* very easy and entertaining reading. As the more detailed scientific aspects of gems are treated very briefly, those interested in securing specific data concerning the various physical, optical, and other important properties will need to consult the more comprehensive books in the field of gemology.

The various chapters have attractive titles: The Lure of Gems, Recognizing Gems, Faceted Gems, Cabochon and Carved Gems, Gems of the Silica Group, Gems With a Genealogy, and Man-Made Gems. In the timely chapter of Luminescent Gems the various types of luminescence are discussed, the gems that exhibit this phenomenon are listed, and the necessary equipment described and illustrated. There is a short selected bibliography. Thirty pages are devoted to a very comprehensive index.

The order in which the various gems are discussed is quite unusual. It is doubtful that it aids in maintaining the interest of the reader. Many important historical facts, as well as the industrial and commercial uses, are included in many of the descriptions of the individual gems.

The book is amply illustrated and is well printed on excellent paper. It should stimulate further reading and study. *Popular Gemology* is a worthwhile addition to the rapidly growing list of books devoted to the study of gems.

Edward H. Kraus, *University of Michigan*

MINERALOGICAL SOCIETY (LONDON)

A meeting of the Society was held Thursday, June 24, 1948, in the apartments of the Geological Society of London, Burlington House, Piccadilly, W.1 (by kind permission). The following papers were presented:

(1) The application of phase-contrast microscopy to mineralogy and petrology

By Dr. F. Smithson

Phase-contrast microscopy is applicable to the study of minerals in thin section or in the form of grains. Such features as definition of boundaries, roughness of surface, zoning, etc., are conspicuous in cases where they are indistinct with ordinary illuminations. With a single polarizer added, "twinkling" becomes noticeable in a number of weakly birefringent minerals and the definition of boundaries between certain minerals may be improved with suitable orientation of the polarizer. Using phase-contrast with crossed nicols, further clarification of rock-textures sometimes results. Phase-contrast methods are unsuitable for examining opaque particles.

Replacement of the phase plate by appropriate stops produces images of high contrast, which exhibit some features more clearly and others less clearly than the phase-contrast image.

(2) The lattice parameters and interplanar spacings of some artificially prepared melilites

By Dr. K. W. Andrews (communicated by Dr. F. A. Bannister)

Lattice parameters and interplanar spacings are provided for gehlenite, akermanite, and three members of the intermediate series of solid solutions corresponding to 25, 50, and 75 per cent replacement of 2 Al by Mg+Si. The a parameter increases and the c parameter decreases going from gehlenite to akermanite, whilst the axial ratio varies from 0.659_0 to 0.638_7. Interplanar spacings are recorded in Å units.

(3) The densest and least dense packings of equal spheres

By Mr. S. Melmore

Proofs are given that the closest packings are those with a density of 0.74; and that the most open, under the condition that the symmetry operations are transitive on the spheres, are those with a density of 0.056.

(4) On the definition of diorite, gabbro, and related rocks

By Mr. S. E. Ellis (communicated by Dr. W. Campbell Smith)

A study has been made of the frequency-distribution of silica-saturated rocks of the calc-alkali series according to variations in the ratios between groups of constituent minerals. On the basis of the results, quantitative mineralogical definitions of diorite, gabbro, anorthosite and allied types are proposed. Triangular diagrams are used to demonstrate that the modal types defined in this way correspond fairly closely with distinct ranges in chemical composition definable in terms of simple ratios between Niggli values.

(5) Pyroxene from the Squilver dolerite, South Shropshire

By Mr. F. G. H. Blyth

Chemical analyses of the pyroxene and of the rock containing it are given, and the composition and optical properties of the mineral are discussed.

(6) Ships' loadstones

By Mr. C. E. N. Bromehead

By the year 1200 the magnetic compass was familiar over much of Europe. Artificial magnets began to be made commercially in 1750. Between these dates loadstone, as such, was a valuable economic mineral, used to make or to re-magnetize all compass-needles. It soon became usual to mount a piece of the mineral with irons held against its poles, forming "ships' loadstones," examples of which are exhibited. The paper gives a general history of the subject, with references, etc.

(Titles and abstracts kindly submitted by G. F. Claringbull, *General Secretary.*)

NEW MINERAL NAMES

Sanmartinite

Victorio Angelelli and Samuel G. Gordon, Sanmartinite, a new zinc tungstate from Argentina. *Notulae Naturae Acad. Natural Sci. Philadelphia*, No. **205**, 7 pp. (1948).

Chemical Composition: The zinc analogue of wolframite, but the analyses and low G. indicate that about one-sixth of the W positions in the lattice are vacant, i.e., $RW_{0.83}O_{3.5}$, with R=Zn, Fe, Mn, Ca. Analysis by Horace Hallowell gave WO_3 72.62, ZnO 18.18, FeO 7.24, MnO 1.73, CaO 1.48, Insol. 0.24; sum 101.25% Two other preliminary analyses are given.

Crystallography: The minute crystals (of the order of 60μ) are monoclinic, tabular parallel to {100}. The forms noted were {100}, {010}, {110}, {112}, and {102}. Goniometric data gave $a:b:c=0.8255:1:0.8664$, beta 90°28′; p_0 1.0495, q_0 0.8664. μ 89°32′.

From x-ray powder data a_0 4.712, b_0 5.738, c_0 4.958 (not stated whether Å or kX units), $a_0:b_0:c_0=0.8212:1:0.8641$. X-ray powder data and photographs are given; they closely resemble those of wolframite.

Physical Properties: Masses are dark brown to brownish black in color, but microscopic crystals are reddish-brown with red reflections, and are more or less translucent. They resemble dark sphalerite. Luster resinous. Sp. gr. (determined by Judith Weiss) 6.697.

Occurrence: From a small, abandoned, prospect in Los Cerillos, 7 km. southwest of San Martin, Department of San Martin, Province of San Luis. Also reported to occur at other nearby localities. Occurs in a quartz vein 50–60 cm. wide that is intercalated between a light-colored granite and a pink pegmatite. Sanmartinite is associated with scheelite, which it appears to replace, quartz, tourmaline, and willemite.

Name: For the region, which, in turn, is named for the liberator of Argentina, José de San Martín.

Michael Fleischer

Wurtzite—4H, Wurtzite—6H, Wurtzite—15R

Clifford Frondel and Charles Palache, Three new polymorphs of zinc sulfide. *Science*, **107**, 602 (1948).

Three new polymorphs of ZnS were found in shrinkage cracks in clay ironstone concretions embedded in carbonaceous black shale of the lower Conemaugh formation at numerous localities in western Pennsylvania and eastern Ohio. These are named in the notation suggested by Ramsdell, *Am. Mineral.* **32**, 63 (1947) for silicon carbide, where the number refers to the formula weights per unit cell, and H and R refer to hexagonal and rhombodehedral forms. In this notation, wurtzite—2H is ordinary wurtzite.

	A_0(Å.)	C_0(Å.)	Cell contents	Space group
Wurtzite—2H	3.811	6.234	Zn_2S_2	*C6mc*
Wurtzite—4H	3.806	12.44	Zn_4S_4	*C6mc*
Wurtzite—6H	3.813	18.69	Zn_6S_6	*C6mc*
Wurtzite—15R	3.822	46.79	$Zn_{15}S_{15}$	*R3m*

M.F.

DISCREDITED MINERALS

Seelandite (=Epsomite)

HEINZ MEIXNER, Was ist Seelandit? *Ann. Naturhist. Museums Wien* **50**, 690–693 (1939).

Seelandite was described in 1891 as a hydrated magnesium aluminum sulfate containing 4.1% MgO and 10.5% Al_2O_3. It has been doubtfully grouped with pickeringite. Examination of material believed to be from the type locality shows it to be epsomite. It is thought that aluminum was reported erroneously because of failure to add NH_4Cl before precipitating with ammonia, thus causing precipitation of magnesium, reported as aluminum.

M.F.

Ralph E. Grim, petrographer of the Illinois State Geological Survey and authority in the field of clay minerals, has been appointed research professor of geology at the University of Illinois. He will teach graduate courses while carrying on his regular work with the Survey.

Included in the project grants from the Penrose Fund of The Geological Society of America, the following are of special interest to the mineralogist: Bronson Stringham, University of Utah, alteration studies of the copper ore body at Bingham, Utah; Thomas F. Bates, Pennsylvania State College, electron microscope study of the mineralogy and petrology of the clay minerals.

GEORGE BANTA PUBLISHING COMPANY, MENASHA, WISCONSIN, U.S.A.